Available on CMS information server

CMS NOTE 1997/088

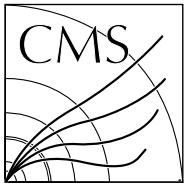

The Compact Muon Solenoid Experiment

CMS Note

Mailing address: CMS CERN, CH-1211 GENEVA 23, Switzerland

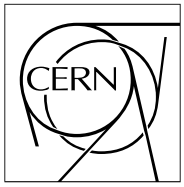

Occupancy studies for minimum bias and $b\bar{b}$ jet events with the V3 geometry of the CMS tracker

Thomas Kachelhoffer,
The CMS Tracker Layout Optimization Group

CERN, Geneva, Switzerland

Abstract

The V3 geometry of the CMS tracker is described by GEANT in the CMSIM software package. It is used to produce GEANT hits and reconstructed hits (clusters) generated by minimum bias (MB) events, with and without pile-up and by $b\bar{b}$ jets with 300 GeV transverse energy, also with and without pile-up. Resulting occupancies are described for all strip detectors of the CMS tracker. For $b\bar{b}$ jets, also local occupancy inside the core of the jet are described.

Contents

1 Status of simulation **3**

1.1 Global information . . . 3

1.2 Process involving generation of secondaries . . . 3

1.3 Values of GEANT cuts . . . 4

1.4 Information on MSGC simulation . . . 4

1.5 Information on silicon strip simulation . . . 6

2 Single Minimum Bias events studies with a 4 Tesla field **6**

2.1 Kinematics of single MB events . . . 6

2.2 GEANT hits per detector in single MB events . . . 7

2.3 Time distribution for single MB GEANT hits . . . 8

2.4 Reconstructed hits per detector in single MB events . . . 8

2.5 Cluster merging in single MB events . . . 9

2.6 Cluster splitting in single MB events . . . 9

3 Single Minimum Bias studies with a 2 Tesla field **10**

3.1 GEANT hits per detector in single MB events with a 2 Tesla field . . . 10

3.2 Reconstructed hits per detector in single MB events with a 2 Tesla field . . . 11

3.3 Cluster merging in single MB events with a 2 Tesla field . . . 12

3.4 Cluster splitting in single MB events with a 2 Tesla field . . . 12

4 Minimum Bias pile-up event studies with a 4 Tesla field **12**

4.1 GEANT hits per detector in MB pile-up events . . . 12

4.2 Reconstructed hits per detector in MB pile-up events . . . 13

4.3 Cluster merging in MB pile-up events . . . 13

4.4 Cluster splitting in MB pile-up events . . . 14

5 Single Minimum Bias events studies without δ rays generation **14**

5.1 GEANT hits per detector . . . 14

5.2 Reconstructed hits per detector . . . 15

5.3 Cluster merging . . . 15

5.4 Cluster splitting . . . 16

6 Single 300 GeV $b\bar{b}$ jet events studies **16**

6.1 Kinematics of $b\bar{b}$ jets . . . 16

6.2 GEANT hits per detector in $b\bar{b}$ jet events 16
6.3 Time distribution for $b\bar{b}$ GEANT hits 18
6.4 Reconstructed hits per detector in $b\bar{b}$ jet events 18
6.5 Cluster merging in $b\bar{b}$ jet events 18
6.6 Cluster splitting in $b\bar{b}$ jet events 19

7 Local studies inside single 300 GeV $b\bar{b}$ jet cores **19**
7.1 GEANT hits per detector in $b\bar{b}$ jet cores 19
7.2 Reconstructed hits per detector in $b\bar{b}$ jet cores 19
7.3 Cluster merging and splitting in $b\bar{b}$ jets core 20

8 MB pile-up events superimposed on 300 GeV $b\bar{b}$ jet studies **21**
8.1 GEANT hits per detector in "$b\bar{b}$ jets + MB pile-up" events 21
8.2 Reconstructed hits per detector in "$b\bar{b}$ jets + MB pile-up" events 22
8.3 Cluster merging in "$b\bar{b}$ jets + MB pile-up" events 23
8.4 Cluster splitting in "$b\bar{b}$ jets + MB pile-up" events 23

9 Local studies inside $b\bar{b}$ jets core superimposed on MB pile-up events **23**
9.1 GEANT hits per detector in $b\bar{b}$ jet core + MB pile-up events 23
9.2 Reconstructed hits per detector in $b\bar{b}$ jet cores + MB pile-up events 24
9.3 Cluster merging and splitting in $b\bar{b}$ jet cores + MB pile-up events 25

10 High P_t tracks and cluster merging effect **25**

11 Conclusion **26**

Liste of tables **27**

Appendix: tables **28**

Liste of figures **41**

Appendix: figures **44**

1 Status of simulation

The CMS software package CMSIM 112 is used with the V3 geometry. Minimum bias and $b\bar{b}$ jet events are generated by PYTHIA to produce the kinematics of primary tracks. Using GEANT, CMSIM follows all primary particles through all tracker detectors using a solenoidal magnetic field of 4 Tesla. It produces decays in flight and generates also secondaries from interactions with the tracker material. The primary pp vertices are smeared about the nominal position by a gaussian distribution in the 3 space dimensions. The σ of these distributions are 5.3 cm in z (beam direction) and 15 μm in the transverse x and y directions. All particles are stopped inside the CMS electromagnetic calorimeter or after 500 ns of flight to speed up the simulation procedure. This time of flight is calculates along the trajectories starting at the corresponding pp interaction point and includes some time delay from secondary interactions. CMSIM produces then the GEANT hits, i.e. intersection of particle trajectories with the detector elements, which are passed on to the digitization and cluster finder packages to produce the final reconstructed hits.

1.1 Global information

Some general features of the simulation are described in the following:

- 1000 single events are used for single minimum bias (MB) studies with production of GEANT and reconstructed hits.
- Part of these 1000 MB events are used to produce 20 CMS bunch crossings with pile-up. Each bunch crossing corresponds, on average, to a superposition of 18.75 single MB events for the silicon and twice more in the MSGC detectors.
- The total number of detectors (Silicon + MSGC) is 17334: 4872 Silicons and 12462 MSGCs.
- 50 single events are used with $b\bar{b}$ jet with 300 GeV transverse energy in the barrel region with production of GEANT and reconstructed hits.
- Pixel detectors are included in the geometry for material budget purposes only. They are not addressed in this note. All materials, like cables and mechanics, are also taken into account in the simulation, like described with the GEANT V3 geometry.

1.2 Process involving generation of secondaries

GEANT allows the user to choose between some mechanisms of production of secondaries as described below. The flags setting used here are shown in capital letters.

- DCAY = 1: decay in flight with generation of secondaries.
- MULS = 1: multiple scattering according to Molière's theory.
- PFIS = 1: nuclear fission induced by photons with generation of secondaries. The photon is stopped.
- MUNU = 1: muon-nucleus interactions with generation of secondaries. The muon is not stopped.
- LOSS = 1: continuous energy loss with Landau fluctuation and with generation of δ rays above DCUTE (see below).
- PHOT = 1: photo-electric effect with generation of secondaries. The interacting photon is stopped.
- COMP = 1: Compton scattering with generation of electrons.
- PAIR = 1: pair production with generation of e^+, e^-. The interacting γ is stopped.

- BREM = 1: bremsstrahlung with generation of γ.
- RAYL = 0: no Rayleigh effect.
- DRAY = 1: δ ray production with generation of e^-.
- ANNI = 1: positron annihilation with generation of photons. The positron is stopped.
- LABS = 1: generation of Cerenkov light with possible absorption of the photons.
- HADR = 1: hadronic interactions with generation of secondaries. The particle is stopped in case of an inelastic interaction, while it is not stopped in case of an elastic interaction.
- SYNC = 0: no synchroton radiation.

1.3 Values of GEANT cuts

The values of GEANT cuts used in this simulation are 10 times lower than the standard ones; they are listed below. These cuts can be different in some specific materials like the calorimeter when a parametrization of the shower is used.

- CUTGAM = 100 keV: cut for γ.
- CUTELE = 100 keV: cut for e^-.
- CUTNEU = 1 MeV: cut for neutral hadrons.
- CUTHAD = 1 MeV: cut for charged hadrons.
- CUTMUO = 1 MeV: cut for muons.
- BCUTE = 100 keV: cut for e^- bremsstrahlung.
- BCUTM = 100 keV: cut for μ bremsstrahlung.
- DCUTE = 100 keV: cut for electron δ rays.
- DCUTM = 100 keV: cut for muon δ rays.
- PPCUTM = 2.04 MeV: cut for e^+/e^- pairs created by μ.

Due to these cuts, all interactions with low energy neutrons ($\leq$ 1 MeV) and low energy photons ($\leq$ 100 keV) are not included, even in the sensitive volumes.

1.4 Information on MSGC simulation

Some features of the MSGCs used in the digitization and clusterization processes are described in the following:

- The pitch of the MSGC is 200 μm (512 channels per detector).
- The MSGC gas is Ne/DME in the ratio of 1:2; the mean gain is 3100 which gives a S/N ratio of 20 for pions at 3 GeV/c at normal incidence. Corrections according the Bethe-Bloch function are done for non MIPs. The number of primary e^- per track is 12.6 ± 3.5. These primary e^- can create some clusters again by ionization which gives a most probable value before amplification of 18.8 e^- and a mean value of 29 (see figure 4). The maximum arrival time of these e^- on the strip is 55 ns.

- The RMS total noise is 1600 e^- per strip.
- A balistic deficit of 70 % is applied to the signal.
- A deconvolution deficit of 78 % is applied after balistic deficit.
- Charge loss due to crosstalk: 6 % of the signal applied on each strip.
- Cluster finder characteristics:
  - The cut for a single strip charge is 1.8 σ above noise.
  - The cut for the seed strip charge is 3.5 σ.
  - No hole inside a cluster are accepted.

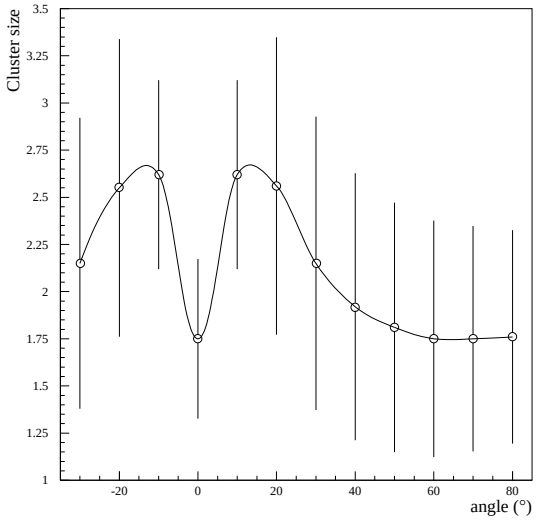

Figure 1: MSGC cluster size for π at 3 GeV/c (S/N = 20) vs incident angle.

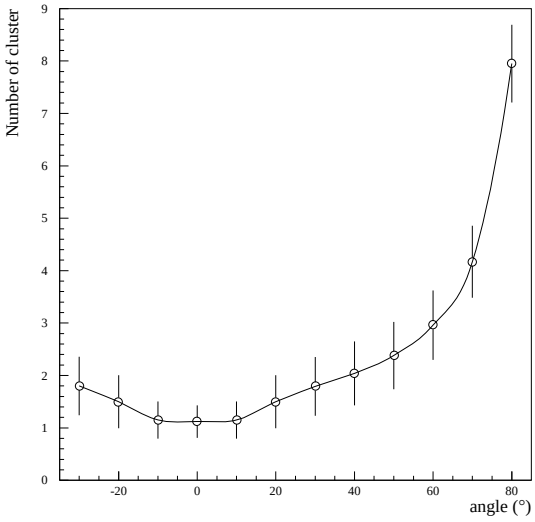

Figure 2: Number of clusters for π at 3 GeV/c vs incident angle for MSGCs.

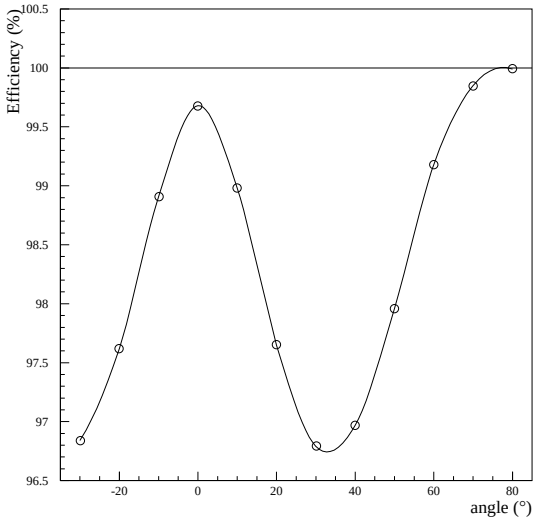

Figure 3: MSGC efficiency for π at 3 GeV/c vs incident angle.

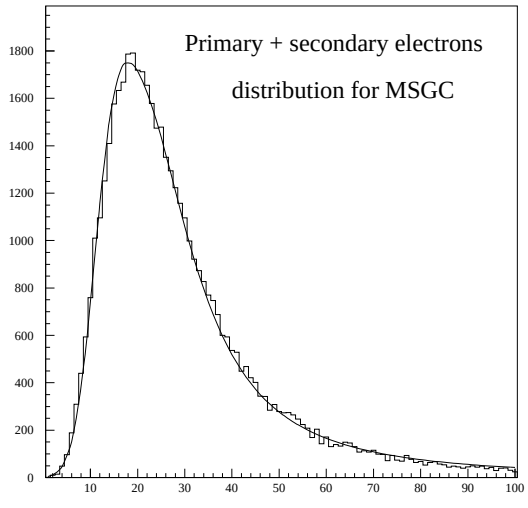

Figure 4: Number of primary plus secondary e^- before amplification in the MSGC.

The reconstructed hits are obtained after digitization and clusterization. This means that both thresholds of the cluster finder are applied at the level of the front end driver. So, all occupancies are given after applying these 2 thresholds.

Figure 1 shows the cluster size for π at 3 GeV/c as function of the incident angle of the track; the signal to noise ratio is 20 at normal incidence. The number of clusters per track is given in figure 2 and figure 3 gives the digitization and clusterization efficiency per track. Each point was calculated from 50000 single π.

1.5 Information on silicon strip simulation

Some features of the silicon strip detectors used in the digitization and clusterization process are as follow:

- The pitch of single sided detectors is 100 μm (512 channels per detector) and 67 μm for the $R-\phi$ view of double sided detectors (768 channels per detector).
- The stereo view is simulated by 256 strips per detector, but no attemp is made to simulate the double metal corrections.
- Cluster finder characteristics:
  - The cut for a single strip charge is 2 σ above noise.
  - The cut for the seed strip charge is 3 σ.
  - The cut for the overall cluster charge is 5 σ.

Like in case of MSGCs, all thresholds are applied at the level of the front end driver.

2 Single Minimum Bias events studies with a 4 Tesla field

2.1 Kinematics of single MB events

The following figures are obtained from charged and neutral primary tracks corresponding to 2000 single MB at the pp interaction point. No secondaries are included at this level, except for those produced by the generator (PYTHIA), like B mesons with very small flight path.

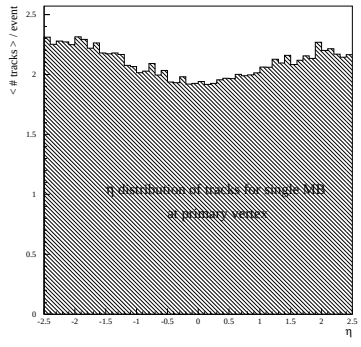

Figure 5: Pseudorapidity (η) distribution for single minimun bias events without P_t cuts. The bin size in η is 0.1.

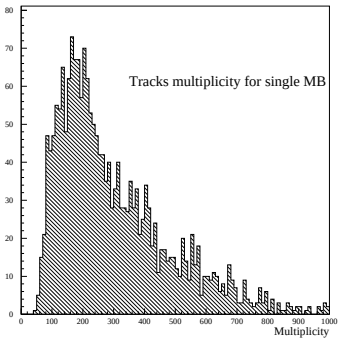

Figure 6: Primary track multiplicity distribution for single minimum bias events in the range $|\eta| \leq 5$ without P_t cuts.

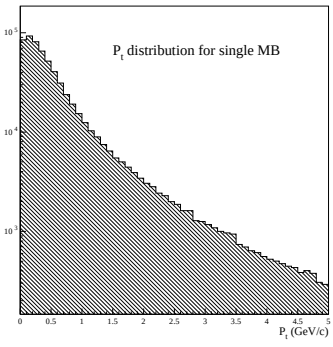

Figure 7: P_t distribution for primary tracks of $|\eta| \leq 5$ in single minimum bias events.

Figure 5 gives the average number of charged and neutral primary tracks emerging from the primary vertex for a pseudorapidity bin $\Delta\eta = 0.1$, in the acceptance range of the CMS tracker ($|\eta| \leq 2.5$); it is

about 2.095 ± 0.005 without P_t cuts (0.789 ± 0.003 for charged tracks), amounting to approximately 105 primary tracks (40 charged tracks) per single MB event at the pp interaction point ($-2.5 \leq \eta \leq 2.5$). The primary tracks are generated within $|\eta| \leq 5$ which gives a most probable number of primaries of about 200 (80 charged) per event as shown in figure 6. Figure 7 shows the corresponding P_t distribution for all primaries with $|\eta| \leq 5$. The mean P_t value is 0.60 GeV/c (0.64 GeV/c for charged particles).

2.2 GEANT hits per detector in single MB events

Table 1 shows the average number of GEANT hits per physical detector and per event for the different types of detectors (layers) as well as the corresponding RMS standard deviation.

Primary and secondary tracks cross, on average per event, 447.7 ± 0.7 detectors out of a total of 17334. 8.9 % of silicon strip detectors in the inner barrel layer and 0.46 % of MSGC detectors in the outermost barrel layer are crossed by one or more tracks.

Detector type	Ghits/det		% of hit detectors	Tot # of det	pitch (μm)
	$< \# >$	RMS			
Barrel Si-1	1.93	1.10	8.9 %	440	67
Barrel Si-2	1.86	0.99	5.8 %	580	”
Barrel Si-3	1.82	0.94	3.9 %	716	100
Barrel Si-4	1.83	1.03	2.7 %	856	”
Barrel MSGC-1	1.73	0.94	2.4 %	756	200
Barrel MSGC-2	1.74	0.99	1.8 %	846	”
Barrel MSGC-3	1.75	0.98	1.3 %	936	”
Barrel MSGC-4	1.75	0.99	0.97 %	1026	”
Barrel MSGC-5	1.78	1.14	0.77 %	1116	”
Barrel MSGC-6	1.81	1.17	0.59 %	1206	”
Barrel MSGC-7	1.83	1.34	0.46 %	1296	”
Fwd Si-1-SS	1.69	0.52	6.9 %	216	100
Fwd Si-2-SS	1.74	0.60	9.0 %	360	”
Fwd Si-3-SS	1.67	0.50	4.5 %	480	”
Fwd Si-1-DS	1.70	0.53	7.2 %	288	67
Fwd Si-2-DS	1.75	0.62	8.4 %	360	”
Fwd Si-3-DS	1.67	0.50	4.5 %	576	”
Fwd MSGC-1	1.62	0.41	2.5 %	840	200
Fwd MSGC-2	1.64	0.45	2.7 %	960	”
Fwd MSGC-3	1.63	0.41	1.9 %	1080	”
Fwd MSGC-4	1.63	0.41	1.5 %	1200	”
Fwd MSGC-5	1.62	0.39	1.2 %	1200	”

Table 1: GEANT hits per hit detector in single MB events.

The tracks produce on average 556.3 ± 0.7 GEANT hits per event in the silicon strip and MSGC detectors. This gives an average number of GEANT hits per detector ranging between 1.93 for the inner silicon barrel layer and 1.62 for the outermost MSGC forward ring. The mean value decreases for the silicon barrel due to the magnetic field when the radius increases. For the barrel MSGC, the number of GEANT hits per event is quit constant due to the production of secondaries. In the forward detectors, we clearly see the effect of the difference of η coverage of the different rings. For example, the second ring of forward silicon detectors is the largest one (in radius) and the occupancy in term of number of GEANT hits is higher. This effect explains also the higher percentage of detectors crossed by a track.

2.3 Time distribution for single MB GEANT hits

Figure 8 shows the time distribution of all GEANT hits per single MB event in a double logarithmic scale for all strip detectors of the CMS tracker. In figure 13 (appendix), the number of GEANT hits per event is presented as function of the time arrival at the barrel silicon detectors (hatched histogram) in addition to the histogram of figure 8. Figures 15 and 16 represent the same histograms but for the barrel MSGC detectors, figures 17 and 18 are for the forward silicon detectors and figures 19 and 20 are for the forward MSGC detectors.

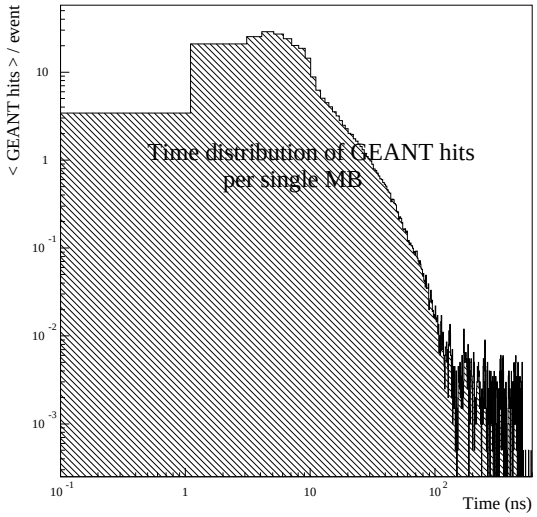

Figure 8: Time distribution of GEANT hits per event from single MB. The bin size is 1 ns. All silicon and MSGC detectors are included.

2.4 Reconstructed hits per detector in single MB events

Table 2 shows the analysis of reconstructed hits obtained after digitization and clusterization, for the different detector types. The "off-line" occupancy is defined by the ratio of the number of fired strips in a detector to the total number of strips for each detector type. A fired strip is a strip belong to a reconstructed cluster. Remember that this definition of occupancy applies only to detectors hit by a particle. Then, detectors without signals are not taken into account.

On average, 434.7 ± 0.7 silicon and MSGC detectors produce 700.6 ± 0.8 reconstructed hits per event after the digitization and clusterization process. The "off-line" occupancy is always below 1 % and the average number of detectors producing at least one reconstructed hit per event are compatible with the corresponding numbers for GEANT hits.

In the case of the silicon strip detectors, the mean number of reconstructed hits per detector is always lower than the corresponding number of GEANT hits. This may be due to the cluster merging effect. It should not be caused by an inefficiency of digitization as the numbers of detectors having a reconstructed or a GEANT hit are equal.

On the contrary, in the case of MSGCs, a given GEANT hit gives, after digitization and clusterization, more than one reconstructed hit on average due to cluster splitting. All these effects will be studied in more detail in the next sections.

The cluster sizes found for all detector types are in agreement with the test beam data, if we take into account the mean incident angle of the tracks (see table 18).

In appendix, figure 29 shows the "off-line" occupancy for the barrel detectors and figure 37 for the forward detectors. In figure 41 and 49 are plotted the corresponding cluster sizes.

Detectors type	Off-line occup		% of hit	Rhits/det		# of strips		Cluster
	$< \# >$	RMS	detectors	$< \# >$	RMS	$< \# >$	RMS	size
Barrel Si-1	0.83 %	0.95	8.9 %	1.26	0.74	6.04	5.73	4.79
Barrel Si-2	0.84 %	0.97	5.8 %	1.23	0.77	6.15	6.16	5.00
Barrel Si-3	0.96 %	0.99	3.9 %	1.14	0.55	4.91	4.41	4.31
Barrel Si-4	0.99 %	1.07	2.7 %	1.13	0.56	5.04	4.67	4.46
Barrel MSGC-1	0.94 %	0.78	2.3 %	2.55	2.15	4.89	3.94	1.92
Barrel MSGC-2	0.95 %	0.81	1.8 %	2.62	2.25	4.96	4.11	1.89
Barrel MSGC-3	0.95 %	0.85	1.3 %	2.62	2.22	4.93	4.27	1.88
Barrel MSGC-4	0.96 %	0.87	0.93 %	2.66	2.24	5.00	4.40	1.88
Barrel MSGC-5	0.96 %	0.82	0.74 %	2.65	2.23	4.94	4.00	1.86
Barrel MSGC-6	0.98 %	0.91	0.57 %	2.75	2.32	5.07	4.52	1.84
Barrel MSGC-7	0.96 %	0.85	0.44 %	2.71	2.36	4.99	4.29	1.84
Fwd Si-1-SS	0.61 %	0.66	6.9 %	1.09	0.36	3.24	2.90	2.97
Fwd Si-2-SS	0.62 %	0.56	8.9 %	1.13	0.43	3.28	2.63	2.90
Fwd Si-3-SS	0.62 %	0.56	4.5 %	1.07	0.30	3.29	2.55	3.07
Fwd Si-1-DS	0.52 %	0.61	6.8 %	1.13	0.50	3.78	4.34	3.35
Fwd Si-2-DS	0.52 %	0.52	7.9 %	1.17	0.49	3.80	3.87	3.25
Fwd Si-3-DS	0.52 %	0.52	4.2 %	1.10	0.35	3.84	3.73	3.49
Fwd MSGC-1	0.74 %	0.59	2.4 %	1.89	1.51	3.83	2.87	2.03
Fwd MSGC-2	0.78 %	0.65	2.6 %	2.01	1.61	4.04	3.19	2.01
Fwd MSGC-3	0.78 %	0.64	1.8 %	2.04	1.64	4.07	3.19	2.00
Fwd MSGC-4	0.79 %	0.64	1.4 %	2.10	1.65	4.11	3.14	1.96
Fwd MSGC-5	0.77 %	0.56	1.2 %	2.03	1.44	4.01	2.81	1.98

Table 2: Reconstructed hits per detector in single MB events.

2.5 Cluster merging in single MB events

For the MSGCs, the cluster size does not depend on the angle of the incident track due to the cluster splitting. For silicon detectors, a strong correlation between the incident ϕ angle and the cluster size is observed. If the angle increases, the cluster size also increases. There is also a strong correlation between ϕ and P_t for the primaries. For the secondaries, however no correlations exist.

Table 18 shows the most probable incident angle (ϕ) for primary tracks from single MB in different P_t ranges. In case of merged hits, it is the smallest of the two ore more values which is taken. The "?" symbol indicates that no primaries reach the detector, or that it has been impossible to determine the angle.

In table 19 is reported the effect of cluster merging effect for various P_t ranges. Merging is important for reconstructed hits for P_t below 0.3 GeV/c. At higher P_t, 8.6 % of reconstructed hits from tracks with $P_t > 1.2$ GeV/c are merged. Merging is due to low P_t tracks (all below 1.2 GeV/c). In conclusion, the merging effect is due to low P_t tracks from secondaries that affect the reconstructed hits generated by high P_t primary tracks.

2.6 Cluster splitting in single MB events

Table 20 presents the number of reconstructed hits per GEANT hit for various P_t ranges and for different layers. Cluster splitting strongly depends on the P_t of the track via its incident angle and affects more the MSGCs, due to the larger drift gap, than the silicon strip detectors. It is also more frequent for silicon detectors with a pitch of 67 μm compared to those with a pitch of 100 μm.

In the appendix, figure 55 shows the cluster merging effect for the barrel detectors in various P_t ranges and figure 63 for the forward detectors. In figure 67 and 75 the cluster splitting effect is illustrated in

various P_t ranges for the barrel and forward detectors respectively.

3 Single Minimum Bias studies with a 2 Tesla field

This study is to understand the difference between 2 values of the CMS solenoidal magnetic field. The standard studies are made with the field at the nominal value of 4 Tesla. The following study is made by dividing all component of the field vector by a factor 2. The nominal value becomes 2 Tesla. The statistic used here is 500 single minimum bias events.

3.1 GEANT hits per detector in single MB events with a 2 Tesla field

Primary and secondary tracks cross 464.1 ± 1.0 detectors out of 17334 per event. Table 3 shows the average number of GEANT hits per detector and per event for the different layers. These tracks produce on average 557.7 ± 1.1 GEANT hits per event in the silicon strip and MSGC detectors. This gives an average number of GEANT hits per detector ranging between 1.86 for the inner silicon barrel layer and 1.61 for the outermost MSGC forward ring.

Detectors type	Ghits/det		% of hit detectors	Tot # of det	pitch (μm)
	$< \# >$	RMS			
Barrel Si-1	1.86	0.97	7.4 %	440	67
Barrel Si-2	1.80	0.90	5.1 %	580	”
Barrel Si-3	1.77	0.87	3.8 %	716	100
Barrel Si-4	1.75	0.86	2.8 %	856	”
Barrel MSGC-1	1.67	0.71	2.7 %	756	200
Barrel MSGC-2	1.67	0.71	2.2 %	846	”
Barrel MSGC-3	1.69	0.75	1.7 %	936	”
Barrel MSGC-4	1.69	0.79	1.3 %	1026	”
Barrel MSGC-5	1.69	0.85	1.1 %	1116	”
Barrel MSGC-6	1.68	0.79	0.86 %	1206	”
Barrel MSGC-7	1.73	0.98	0.71 %	1296	”
Fwd Si-1-SS	1.69	0.52	5.7 %	216	100
Fwd Si-2-SS	1.74	0.61	8.0 %	360	”
Fwd Si-3-SS	1.66	0.48	4.4 %	480	”
Fwd Si-1-DS	1.71	0.57	6.2 %	288	67
Fwd Si-2-DS	1.74	0.58	7.5 %	360	”
Fwd Si-3-DS	1.68	0.57	4.4 %	576	”
Fwd MSGC-1	1.61	0.39	2.7 %	840	200
Fwd MSGC-2	1.62	0.41	3.0 %	960	”
Fwd MSGC-3	1.62	0.40	2.3 %	1080	”
Fwd MSGC-4	1.61	0.39	1.9 %	1200	”
Fwd MSGC-5	1.61	0.39	1.6 %	1200	”

Table 3: GEANT hits per hit detector in single MB events with a 2 Tesla field.

The comparison with a 4 Tesla field (see table 1 and 3) shows:

- A decrease of the number of GEANT hits per detector of the order of 4 % in the barrel region and no significant differences in the forward region.
- In the barrel region, the number of detectors crossed by a track changes by -17 % for the inner silicon layer and up to +4 % for the outermost. For the MSGCs, this number always increases by +13 % for the inner layer, and up to +54 % for the outer layer. We see the same effect in the

forward region, the changes are between -17 % and -2 % for silicon and between +8 % and +33 % for MSGC. The effect is more prononced at larger radius.

- The average number of GEANT hits per event is the same with a 2 Tesla or 4 Tesla field.

3.2 Reconstructed hits per detector in single MB events with a 2 Tesla field

On average, 451.4 ± 0.9 silicon and MSGC detectors produce 707.1 ± 1.2 reconstructed hits per event after the digitization and clusterization process. The "off-line" occupancy is always below 0.9 % (see table 4) and the average number of detectors producing at least one reconstructed hit per event are compatible with the corresponding number for GEANT hits.

The comparison with a 4 Tesla field (see table 2 and 4) shows:

- A decrease of the "off-line" occupancy of about -16 % in the barrel silicon, -9 % in the barrel MSGCs, -12 % in the forward silicon and -7 % in the forward MSGC detectors.
- A decrease of the number of reconstructed hits per detecor of about -4 % in the barrel silicon, -13 % in the barrel MSGCs and -10 % in the forward MSGC. In the forward silicon, it is not dependant of the field.
- The mean cluster size changes, on average, by -13 % in the silicon and +4 % in the MSGC detectors due to the difference of the ϕ incident angle.

Detectors	Off-line occup		% of hit	Rhits/det		# of strips		Cluster
type	$< \# >$	RMS	detectors	$< \# >$	RMS	$< \# >$	RMS	size
Barrel Si-1	0.71 %	0.76	7.4 %	1.21	0.70	5.24	4.83	4.33
Barrel Si-2	0.69 %	0.75	5.1 %	1.17	0.63	5.08	4.89	4.34
Barrel Si-3	0.83 %	0.76	3.8 %	1.12	0.49	4.27	3.67	3.81
Barrel Si-4	0.83 %	0.85	2.8 %	1.10	0.47	4.27	3.84	3.88
Barrel MSGC-1	0.85 %	0.72	2.7 %	2.22	1.91	4.46	3.64	2.01
Barrel MSGC-2	0.87 %	0.74	2.1 %	2.29	1.99	4.54	3.74	1.98
Barrel MSGC-3	0.85 %	0.68	1.6 %	2.25	1.85	4.44	3.43	1.97
Barrel MSGC-4	0.86 %	0.70	1.3 %	2.28	1.86	4.47	3.52	1.96
Barrel MSGC-5	0.87 %	0.73	1.0 %	2.32	1.99	4.54	3.69	1.96
Barrel MSGC-6	0.89 %	0.78	0.83 %	2.41	2.20	4.65	3.95	1.93
Barrel MSGC-7	0.91 %	0.87	0.69 %	2.43	2.10	4.70	3.98	1.93
Fwd Si-1-SS	0.54 %	0.50	5.7 %	1.10	0.34	2.87	2.46	2.61
Fwd Si-2-SS	0.56 %	0.50	7.9 %	1.13	0.43	2.95	2.36	2.61
Fwd Si-3-SS	0.56 %	0.50	4.4 %	1.07	0.30	2.95	2.23	2.76
Fwd Si-1-DS	0.45 %	0.57	5.8 %	1.15	0.57	3.13	3.70	2.72
Fwd Si-2-DS	0.45 %	0.42	7.0 %	1.17	0.46	3.20	3.16	2.74
Fwd Si-3-DS	0.46 %	0.48	4.1 %	1.11	0.43	3.31	3.36	2.98
Fwd MSGC-1	0.67 %	0.47	2.6 %	1.70	1.26	3.49	2.31	2.05
Fwd MSGC-2	0.70 %	0.54	2.9 %	1.77	1.32	3.65	2.64	2.06
Fwd MSGC-3	0.74 %	0.62	2.3 %	1.85	1.49	3.81	2.93	2.06
Fwd MSGC-4	0.73 %	0.56	1.8 %	1.86	1.40	3.81	2.78	2.05
Fwd MSGC-5	0.73 %	0.56	1.6 %	1.88	1.35	3.82	2.81	2.03

Table 4: Reconstructed hits per detector in single MB events with a 2 Tesla field.

In the appendix, figure 35 shows the "off-line" occupancy for the barrel detectors and figure 36 for the forward detectors. In figure 48 and 54 are plotted the corresponding cluster sizes.

3.3 Cluster merging in single MB events with a 2 Tesla field

Compared to single MB events with a 4 Tesla field, the cluster merging effect decreases in all P_t ranges. Averaged over all P_t, the decrease is about -12 % in the barrel region and -4 % in the forward part (see table 19 and 21). It is due to the lower occupancy.

3.4 Cluster splitting in single MB events with a 2 Tesla field

Compared to single MB events with a 4 Tesla field, the cluster splitting effect decreases in the whole P_t ranges. On average, without P_t cuts, the decrease is about -16 % for the MSGC and -3 % for the silicon detectors, except for the 2 inner barrel layers where it is -10 %. The decrease is most significant in the MSGC detectors due to the difference of incident angle of the track. (see table 20 and 22).

In the appendix, figure 61 shows the cluster merging effect for the barrel detectors and figure 62 for the forward detectors. In figures 73 and 74 is illustrated the cluster splitting effect for the barrel and forward detectors.

4 Minimum Bias pile-up event studies with a 4 Tesla field

4.1 GEANT hits per detector in MB pile-up events

Detectors type	Ghits/det		% of hit detectors	Tot # of det
	$< \# >$	RMS		
Barrel Si-1	3.63	2.32	81.0 %	440
Barrel Si-2	2.83	1.81	67.7 %	580
Barrel Si-3	2.40	1.45	54.7 %	716
Barrel Si-4	2.20	1.33	42.4 %	856
Barrel MSGC-1	2.34	1.45	60.7 %	756
Barrel MSGC-2	2.19	1.39	49.8 %	846
Barrel MSGC-3	2.08	1.33	39.7 %	936
Barrel MSGC-4	2.02	1.25	30.2 %	1026
Barrel MSGC-5	1.99	1.29	25.2 %	1116
Barrel MSGC-6	1.97	1.37	20.3 %	1206
Barrel MSGC-7	1.96	1.47	16.0 %	1296
Fwd Si-1-SS	2.68	1.36	74.7 %	216
Fwd Si-2-SS	3.14	1.67	83.2 %	360
Fwd Si-3-SS	2.28	1.09	59.4 %	480
Fwd Si-1-DS	2.74	1.42	76.0 %	288
Fwd Si-2-DS	3.08	1.68	81.1 %	360
Fwd Si-3-DS	2.28	1.08	58.9 %	576
Fwd MSGC-1	2.23	1.02	60.9 %	840
Fwd MSGC-2	2.30	1.09	63.1 %	960
Fwd MSGC-3	2.07	0.90	50.3 %	1080
Fwd MSGC-4	1.95	0.79	42.2 %	1200
Fwd MSGC-5	1.89	0.73	35.7 %	1200

Table 5: GEANT hits per detector in MB pile-up events.

For pile-up studies, a pp inelastic cross section of 80 mb is assumed. In the MSGCs, 2 bunch crossing are superimposed. This amounts to an average of 37.5 single minimum bias events together in the MSGC and half of it for the silicon strip detectors. This average number is obtained from a Poisson distribution. Per bunch crossing, 7988 ± 20 strips detectors out of 17334 are hit by one or more tracks on average. The tracks produce on average 14755 ± 27 GEANT hits per bunch crossing.

The most important effect of pile-up, in comparison with table 1 for single MB events, is the increase of the number of detectors hit by a track; it is of about 10 to 20 for silicon detectors and 20 to 35 for MSGCs. The increase of the GEANT hit number per detector, by a factor 1.5 on average, is only of secondary importance. The latter factor is higher for the inner layers and lower for the outer layers.

4.2 Reconstructed hits per detector in MB pile-up events

Per bunch crossing, 7790 ± 20 detectors out of 17334 have a total of 20345 ± 32 reconstructed hits. The "off-line" occupancy is defined, like before, as the number of fired strips in a detector divided by the total number of strip in this detector. The "on-line" occupancy is defined as the "off-line" occupancy times the number of hit detectors divided by the total number of detectors for the current layer. Except for the inner barrel silicon layer, all layers have an average "on-line", or global, occupancy below 1 % per bunch crossing.

Detectors	Off-line Occup		% of hit	Rhits/det		On-line Occup		Cluster
type	$< \# >$	RMS	detectors	$< \# >$	RMS	$< \# >$	RMS	size
Barrel Si-1	1.78 %	1.69	80.8 %	2.68	1.78	1.42 %	1.35	4.85
Barrel Si-2	1.41 %	1.45	67.5 %	2.05	1.47	0.94 %	0.99	5.01
Barrel Si-3	1.38 %	1.39	54.5 %	1.63	1.06	0.75 %	0.82	4.28
Barrel Si-4	1.25 %	1.28	42.1 %	1.44	0.83	0.51 %	0.53	4.42
Barrel MSGC-1	1.34 %	1.11	59.4 %	3.61	2.98	0.78 %	0.66	1.92
Barrel MSGC-2	1.25 %	1.09	48.6 %	3.39	2.87	0.60 %	0.54	1.91
Barrel MSGC-3	1.17 %	1.03	38.6 %	3.19	2.65	0.46 %	0.40	1.91
Barrel MSGC-4	1.14 %	1.03	29.2 %	3.14	2.68	0.37 %	0.29	1.89
Barrel MSGC-5	1.08 %	0.95	24.3 %	3.00	2.53	0.31 %	0.21	1.86
Barrel MSGC-6	1.09 %	1.01	19.5 %	3.02	2.60	0.29 %	0.16	1.87
Barrel MSGC-7	1.01 %	0.93	15.3 %	2.83	2.52	0.27 %	0.10	1.85
Fwd Si-1-SS	1.16 %	1.05	74.6 %	2.00	1.19	0.89 %	0.91	3.02
Fwd Si-2-SS	1.36 %	1.11	83.1 %	2.37	1.40	1.09 %	0.93	2.97
Fwd Si-3-SS	0.95 %	0.86	59.1 %	1.59	0.86	0.56 %	0.51	3.09
Fwd Si-1-DS	0.97 %	0.98	70.5 %	2.12	1.29	0.70 %	0.79	3.38
Fwd Si-2-DS	1.06 %	0.91	78.8 %	2.38	1.40	0.84 %	0.72	3.35
Fwd Si-3-DS	0.80 %	0.72	56.3 %	1.67	0.91	0.47 %	0.40	3.55
Fwd MSGC-1	1.11 %	0.90	59.4 %	2.79	2.17	0.64 %	0.54	2.05
Fwd MSGC-2	1.19 %	1.01	60.1 %	3.01	2.46	0.71 %	0.64	2.04
Fwd MSGC-3	1.06 %	0.89	48.9 %	2.76	2.25	0.51 %	0.44	2.00
Fwd MSGC-4	0.99 %	0.81	40.9 %	2.63	2.10	0.41 %	0.33	1.96
Fwd MSGC-5	0.94 %	0.72	34.9 %	2.48	1.89	0.34 %	0.24	1.97

Table 6: Reconstructed hits per detector in MB pile-up events.

The effect of pile-up is here the same as the one observed for the GEANT hits. The corresponding results are displayed in table 6. The cluster sizes do not vary with the addition of pile-up. In the appendix, figure 31 shows the "off-line" and "on-line" occupancy for the barrel detectors and figure 39 for the forward detectors. In figure 43 and 51 are plotted the corresponding cluster sizes.

4.3 Cluster merging in MB pile-up events

The merging effect between 2 or more tracks is only important when the lowest P_t track has $P_t < 0.3$ GeV/c (see table 23 and 19). Tracks with $P_t < 0.3$ GeV/c are very likely to be secondaries. The probability to merge one reconstructed hit coming from a track with $P_t > 1.2$ GeV/c and one other track is 9.7 % instead of 8.6 % in the absence of pile-up. In this case, most of the other merged tracks have a

low P_t (99 % are below 1 GeV/c). Globally, pile-up does not affect cluster merging. It seems that the merging effect comes from tracks and its secondaries produced nearby.

4.4 Cluster splitting in MB pile-up events

As for cluster merging, the cluster splitting effect does not depend on pile-up. It seems to be driven by the track incidence angle, which depends on the strength of the field (table 24, 20 and 18). It is than more important for the MSGCs, than for the silicon strip detectors. Cluster splitting is furthermore favored by the clustering algorithm requiring that all strips in a cluster be above threshold. For inclined tracks, the charge collected on a strip can be too small and the corresponding signal is lost. As no hole is permitted in a cluster by the MSGC clustering algorithm, the cluster splitting effect can be important.

In the appendix, figure 57 shows the cluster merging effect for the barrel detectors in various P_t ranges and figure 65 for the forward detectors. In figure 69 and 77 are given the cluster splitting effect in various P_t ranges for the barrel and forward detectors.

5 Single Minimum Bias events studies without δ rays generation

To understand the large rate of cluster splitting and cluster merging, especially for low P_t track, a simulation without δ rays production was performed.

5.1 GEANT hits per detector

Detectors type	Ghits/det		% of hit detectors	Tot # of det
	$< \# >$	RMS		
Barrel Si-1	1.71	0.68	8.9 %	440
Barrel Si-2	1.67	0.65	5.8 %	580
Barrel Si-3	1.65	0.66	4.0 %	716
Barrel Si-4	1.64	0.65	2.8 %	856
Barrel MSGC-1	1.67	0.76	2.5 %	756
Barrel MSGC-2	1.67	0.77	1.9 %	846
Barrel MSGC-3	1.67	0.78	1.4 %	936
Barrel MSGC-4	1.70	0.94	1.00 %	1026
Barrel MSGC-5	1.69	0.90	0.79 %	1116
Barrel MSGC-6	1.74	1.15	0.62 %	1206
Barrel MSGC-7	1.80	1.31	0.46 %	1296
Fwd Si-1-SS	1.58	0.36	6.6 %	216
Fwd Si-2-SS	1.61	0.40	8.6 %	360
Fwd Si-3-SS	1.56	0.30	4.5 %	480
Fwd Si-1-DS	1.58	0.33	6.9 %	288
Fwd Si-2-DS	1.60	0.39	8.2 %	360
Fwd Si-3-DS	1.56	0.30	4.4 %	576
Fwd MSGC-1	1.55	0.26	2.4 %	840
Fwd MSGC-2	1.57	0.32	2.6 %	960
Fwd MSGC-3	1.56	0.29	1.9 %	1080
Fwd MSGC-4	1.56	0.28	1.4 %	1200
Fwd MSGC-5	1.56	0.28	1.1 %	1200

Table 7: GEANT hits per detector in single MB events whitout δ rays production.

On average per single event, the 443.4 ± 0.7 detectors have 498.4 ± 0.7 GEANT hits (silicon strip and MSGC detectors). In table 7, the results without δ rays production are reported to be compared to the

results in table 1. There are 10 % less GEANT hits in the silicon and MSGC detectors compared to the simulation including δ rays.

5.2 Reconstructed hits per detector

The 430.4 ± 0.7 silicon and MSGC detectors give 688.7 ± 0.8 reconstructed hits per event. In table 8, the definition of occupancy is the same as for table 2. A comparison between the 2 tables shows that:

- For the silicon strip detectors, the "off-line" occupancy decreases by 10 % and the number of reconstructed hits per detector is the same. The cluster sizes are always lower.
- For the MSGC detectors, the "off-line" occupancy, the numbers of reconstructed hits per detector and the cluster sizes do not change.

Detectors	Off-line occup		% of hit	Rhits/det		# of strips		Cluster
type	$< \# >$	RMS	detectors	$< \# >$	RMS	$< \# >$	RMS	size
Barrel Si-1	0.77 %	0.84	8.9 %	1.24	0.80	5.63	5.26	4.54
Barrel Si-2	0.80 %	0.96	5.8 %	1.21	0.79	5.77	5.78	4.77
Barrel Si-3	0.92 %	1.00	4.0 %	1.14	0.62	4.67	4.23	4.10
Barrel Si-4	0.92 %	0.98	2.8 %	1.12	0.54	4.71	4.08	4.21
Barrel MSGC-1	0.94 %	0.82	2.4 %	2.58	2.20	4.90	4.09	1.90
Barrel MSGC-2	0.94 %	0.81	1.8 %	2.60	2.21	4.90	4.09	1.88
Barrel MSGC-3	0.94 %	0.83	1.3 %	2.60	2.20	4.88	4.13	1.88
Barrel MSGC-4	0.95 %	0.87	0.96 %	2.65	2.25	4.96	4.31	1.87
Barrel MSGC-5	0.94 %	0.83	0.76 %	2.60	2.20	4.88	4.20	1.88
Barrel MSGC-6	0.96 %	0.89	0.59 %	2.67	2.26	4.95	4.35	1.85
Barrel MSGC-7	0.96 %	0.84	0.44 %	2.73	2.36	5.02	4.26	1.84
Fwd Si-1-SS	0.57 %	0.54	6.6 %	1.07	0.31	3.04	2.65	2.84
Fwd Si-2-SS	0.57 %	0.51	8.6 %	1.10	0.35	3.02	2.34	2.75
Fwd Si-3-SS	0.59 %	0.53	4.3 %	1.06	0.24	3.15	2.44	2.97
Fwd Si-1-DS	0.49 %	0.64	6.5 %	1.12	0.53	3.52	4.30	3.14
Fwd Si-2-DS	0.49 %	0.53	7.6 %	1.14	0.49	3.50	3.56	3.07
Fwd Si-3-DS	0.52 %	0.60	4.1 %	1.08	0.36	3.77	4.04	3.49
Fwd MSGC-1	0.73 %	0.62	2.3 %	1.87	1.46	3.80	2.89	2.03
Fwd MSGC-2	0.76 %	0.67	2.5 %	1.97	1.63	3.96	3.24	2.01
Fwd MSGC-3	0.77 %	0.63	1.8 %	2.02	1.62	3.99	3.10	1.98
Fwd MSGC-4	0.77 %	0.67	1.4 %	2.04	1.59	4.01	3.15	1.97
Fwd MSGC-5	0.76 %	0.58	1.1 %	2.04	1.56	3.98	2.83	1.95

Table 8: Reconstructed hits per detector in single MB events whitout δ rays production.

In the appendix, figure 35 shows a comparison of the "off-line" occupancy for the barrel detectors from all types of event generation (single MB, MB pile-up, single MB without δ rays and $b\bar{b}$ jets with and without MB pile-up). Figure 36 gives such a comparison for the forward detectors. In figure 47 and 53 are shown the corresponding cluster sizes for the single minimum bias events without δ rays production.

5.3 Cluster merging

The comparison of tables 19 and 25 shows a decrease of the importance of cluster merging by about 8.5 % in the MSGC, 21 % in the barrel silicon detectors and 13 % in the forward silicon detectors. For the silicon strip detectors, the RMS values are strongly reduced. This effect is smaller for the MSGCs. In the forward region of the tracker, the cluster merging is now limited to few percent. The probability

that a reconstructed hit generated by a track with $P_t > 1.2$ GeV/c be merged is 0.66 %, to be compared with the value of 8.6 %, obtained without pile-up, and of 9.7 % with pile-up.

5.4 Cluster splitting

For the barrel silicon strip detectors, the effect of cluster splitting decrease by 8 %, while for the forward silicon detectors, it is reduce by 4 %. For the forward silicon region, cluster splitting is now limited to a few percent. For all MSGC detectors, the decrease is also about 4 % and the cluster splitting effect is more important than for silicon due to higher incident angle of tracks, and to the clustering algorithm.

In the appendix, figure 61 shows a comparison of the effect of cluster merging averaged over all barrel detectors from all types of event generation. Figure 62 gives such a comparison for the forward detectors. Figures 73 and 74 give the effect of cluster splitting averaged over all barrel and forward detectors, also for all types of generation.

6 Single 300 GeV $b\bar{b}$ jet events studies

6.1 Kinematics of $b\bar{b}$ jets

The following figures are obtained from primary vertex tracks from 500 $b\bar{b}$ jets with a transverse energy of 300 GeV per jet, generated by PYTHIA. The jets are in the acceptance of the CMS barrel tracker. Figure 9 shows the average number of primary charged and neutral tracks from the interaction point in a pseudorapidity bin $\Delta\eta = 0.1$, in the acceptance range of the CMS tracker ($|\eta| \leq 2.5$) without P_t cuts. The background gives about 5 primary tracks per bin; inside the jet, this number is about 14, amounting to approximately 450 primary tracks per event at the pp interaction point ($-2.5 \leq \eta \leq 2.5$). The primary tracks are generated with $|\eta| \leq 5$ which yields a mean number of 720 primary tracks per event, as shown in figure 10. Figure 11 shows the corresponding P_t distribution for these primaries with $|\eta| \leq 5$. The mean value is 0.80 GeV/c, to be compared to 0.60 GeV/c from single minimum bias events.

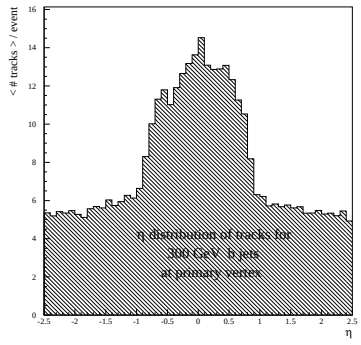

Figure 9: Pseudorapidity (η) distribution for 300 GeV $b\bar{b}$ jet events without P_t cuts. The bin size is 0.1.

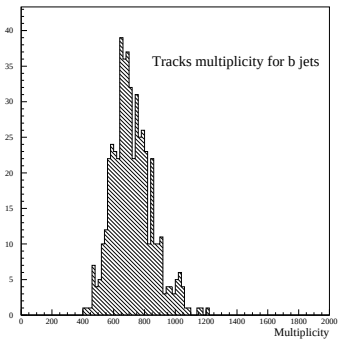

Figure 10: Primary tracks multiplicity distribution for 300 GeV $b\bar{b}$ jet events in the range $|\eta| \leq 5$ without P_t cuts.

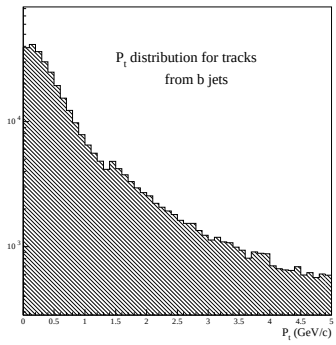

Figure 11: P_t distribution for primary tracks with $|\eta| \leq 5$ for 300 GeV $b\bar{b}$ jet events.

6.2 GEANT hits per detector in $b\bar{b}$ jet events

Primary and secondary charged tracks from $b\bar{b}$ jets at 300 GeV cross, per event, 1798 ± 6 silicon strip and MSGC detectors out of 17334. These tracks produce, on average, 2649 ± 7 GEANT hits per event. Table 9 shows the average number of GEANT hits per detector and per event for the different types of detectors (layers) obtained from 50 $b\bar{b}$ jets events.

As shown in figure 9, the cores of the jets are in the barrel acceptance. Therefore, the number of GEANT hits per detector in the barrel region is higher than in the forward region (table 9). All these numbers

Detectors type	Ghits/det		% of hit detectors	Tot # of det	pitch (μm)
	$< \# >$	RMS			
Barrel Si-1	2.34	1.90	28.5 %	440	67
Barrel Si-2	2.23	1.73	21.1 %	580	”
Barrel Si-3	2.17	1.70	16.2 %	716	100
Barrel Si-4	2.15	1.65	12.6 %	856	”
Barrel MSGC-1	2.08	1.60	12.1 %	756	200
Barrel MSGC-2	2.07	1.57	10.2 %	846	”
Barrel MSGC-3	2.05	1.45	8.4 %	936	”
Barrel MSGC-4	2.04	1.45	6.9 %	1026	”
Barrel MSGC-5	2.09	1.67	6.0 %	1116	”
Barrel MSGC-6	2.03	1.46	5.1 %	1206	”
Barrel MSGC-7	2.08	1.60	4.2 %	1296	”
Fwd Si-1-SS	1.81	0.84	17.9 %	216	100
Fwd Si-2-SS	1.88	0.83	24.9 %	360	”
Fwd Si-3-SS	1.75	0.68	14.5 %	480	”
Fwd Si-1-DS	1.79	0.66	19.4 %	288	67
Fwd Si-2-DS	1.89	0.87	24.1 %	360	”
Fwd Si-3-DS	1.78	0.71	14.6 %	576	”
Fwd MSGC-1	1.68	0.57	9.0 %	840	200
Fwd MSGC-2	1.72	0.65	9.8 %	960	”
Fwd MSGC-3	1.71	0.70	7.4 %	1080	”
Fwd MSGC-4	1.70	0.62	6.2 %	1200	”
Fwd MSGC-5	1.71	0.62	5.5 %	1200	”

Table 9: GEANT hits per hit detector in $b\bar{b}$ jets events.

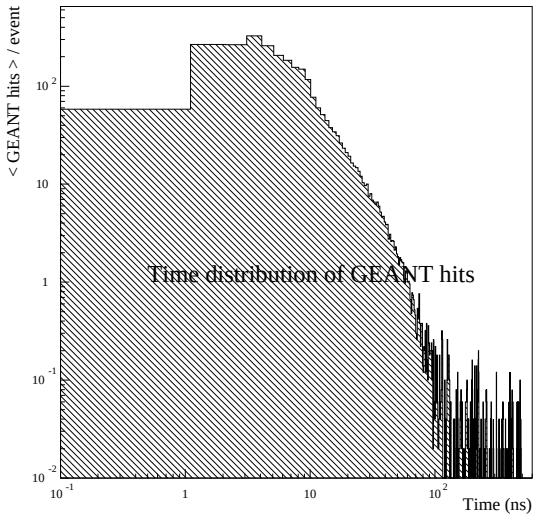

Figure 12: Time distribution of GEANT hits per event from $b\bar{b}$ jets. All silicon and MSGC detectors are included.

are higher than those obtained from single minimum bias events. However, the pile-up of minimum bias events gives a higher GEANT hit occupancy in the barrel silicon than $b\bar{b}$ jets, and a comparable number in the barrel MSGC region. In contrast to pile-up where the number of GEANT hits per detector decreases with radius, $b\bar{b}$ jet events give an occupancy independent of radius. This may be due to the mean P_t of 0.60 GeV/c for minimum bias and of 0.80 GeV/c for $b\bar{b}$ events.

6.3 Time distribution for $b\bar{b}$ GEANT hits

Figure 12 shows the average time distribution of GEANT hits per $b\bar{b}$ event for all strip detectors of the CMS tracker. In figure 21 (appendix), the number of GEANT hits per event is presented as function of arrival time at the barrel silicon detectors (hatched histogram). See also figure 22. Figures 23 and 24 are for the barrel MSGC detectors, figures 25 and 26 for the forward silicon detectors, and figures 27 and 28 for the forward MSGCs detectors.

6.4 Reconstructed hits per detector in $b\bar{b}$ jet events

Table 10 shows the analysis of reconstructed hits for the different detector types. On average, 1748 ± 6 silicon and MSGC detectors produced 3334 ± 8 reconstructed hits per event after the digitization and clusterization process. The "off-line" occupancy is always below 1.1 % and the average numbers of detectors producing at least one reconstructed hit per event are compatible with the corresponding numbers of GEANT hits, but always lower.

Detectors	Off-line occup		% of hit	Rhits/det		# of strips		Cluster
type	$< \# >$	RMS	detectors	$< \# >$	RMS	$< \# >$	RMS	size
Barrel Si-1	0.93 %	1.05	28.3 %	1.61	1.45	6.86	6.72	4.26
Barrel Si-2	0.91 %	1.00	20.9 %	1.55	1.41	6.70	6.63	4.32
Barrel Si-3	1.10 %	1.18	16.1 %	1.43	1.21	5.64	5.57	3.94
Barrel Si-4	1.07 %	1.17	12.5 %	1.41	1.16	5.44	5.07	3.86
Barrel MSGC-1	1.03 %	0.94	11.7 %	2.73	2.50	5.33	4.74	1.95
Barrel MSGC-2	1.01 %	0.91	9.9 %	2.67	2.34	5.21	4.56	1.95
Barrel MSGC-3	0.98 %	0.89	8.1 %	2.59	2.18	5.08	4.53	1.96
Barrel MSGC-4	0.98 %	0.92	6.6 %	2.62	2.31	5.13	4.61	1.96
Barrel MSGC-5	1.00 %	0.90	5.8 %	2.64	2.29	5.19	4.55	1.97
Barrel MSGC-6	0.96 %	0.82	4.9 %	2.57	2.27	4.97	4.14	1.93
Barrel MSGC-7	0.93 %	0.84	4.1 %	2.47	2.22	4.84	4.23	1.96
Fwd Si-1-SS	0.71 %	0.81	17.8 %	1.18	0.48	3.70	3.38	3.14
Fwd Si-2-SS	0.73 %	0.64	24.8 %	1.25	0.61	3.83	3.15	3.06
Fwd Si-3-SS	0.70 %	0.64	14.3 %	1.14	0.48	3.69	3.16	3.24
Fwd Si-1-DS	0.60 %	0.65	18.2 %	1.22	0.56	4.36	4.74	3.57
Fwd Si-2-DS	0.62 %	0.67	22.7 %	1.30	0.75	4.46	4.35	3.43
Fwd Si-3-DS	0.61 %	0.68	13.7 %	1.20	0.57	4.41	4.50	3.68
Fwd MSGC-1	0.79 %	0.69	8.7 %	2.05	1.63	4.14	3.47	2.02
Fwd MSGC-2	0.82 %	0.68	9.5 %	2.16	1.81	4.27	3.43	1.98
Fwd MSGC-3	0.84 %	0.75	7.2 %	2.18	1.75	4.34	3.55	1.99
Fwd MSGC-4	0.83 %	0.68	6.0 %	2.21	1.91	4.34	3.45	1.96
Fwd MSGC-5	0.81 %	0.77	5.4 %	2.12	1.65	4.19	3.60	1.98

Table 10: Reconstructed hits per detector in $b\bar{b}$ jets events.

In the appendix, figure 30 shows the "off-line" occupancy for the barrel detectors and figure 38 for the forward detectors. In figure 42 and 50, the corresponding cluster sizes are plotted.

6.5 Cluster merging in $b\bar{b}$ jet events

The effect of cluster merging (table 26) for tracks with $P_t < 0.3$ GeV/c is smaller than that obtained from single minimum bias events in the barrel silicon detectors. This is due to the fact that the mean P_t of primary particles from $b\bar{b}$ events is 0.80 GeV/c, compared to 0.60 GeV/c for MB events. There are therefore less low P_t tracks; such that the average cluster size is smaller (see tables 10 and 2) and the probability to merge them becomes also lower. In the barrel MSGCs, these low momentum tracks come

from secondaries produced by particles from the core of the jet. In such a high multiplicity environment, there is more local production of secondaries, then, the probability to merge a low P_t track increases. The effect of cluster merging from $b\bar{b}$ jet events in barrel MSGCs becomes comparable to MB events. In the forward region, where no jets have been generated, the effect of cluster merging is a little lower compared to one obtained from single MB events, due to the difference of the $< P_t >$ value. Cluster merging between high momentum tracks ($P_t > 1.2$ GeV/c) is more likely higher in the barrel region for jet events compared to MB events, as expected.

6.6 Cluster splitting in $b\bar{b}$ jet events

The cluster splitting effect (table 27) in $b\bar{b}$ events is comparable to that obtained from single MB at given P_t, but the global effect is lower due to the difference of the mean P_t values. A high momentum track gives a smaller splitting effect on the reconstructed hits than a low P_t track.

In the appendix, figure 56 shows the cluster merging effect for the barrel detectors in various P_t ranges and figure 64 for the forward detectors. In figures 68 and 76 the cluster splitting effect is given for various P_t ranges for the barrel and forward detectors, respectively.

7 Local studies inside single 300 GeV $b\bar{b}$ jet cores

After hadronization of the b quarks, each B mesons decays and produces at least, in the final state, one μ. The local studies concern only the barrel detectors crossed by these μ, which define the jet core directions.

7.1 GEANT hits per detector in $b\bar{b}$ jet cores

Table 11 shows the average number of GEANT hits per detector crossed by the μ and per event obtained from 50 $b\bar{b}$ jet events for the different barrel layers. This number of GEANT hits represents the local hits density inside the jet core.

Compared to the average barrel detector multiplicity (table 9) for the same events, the number of GEANT hits here increase by about 238 % in the silicon part, and between 167 % for the inner barrel MSGCs and 54 % for the outer ones.

Detectors type	Ghits/det		pitch (μm)
	$< \# >$	RMS	
Barrel Si-1	7.57	4.51	67
Barrel Si-2	8.05	4.80	”
Barrel Si-3	7.45	4.49	100
Barrel Si-4	6.97	4.40	”
Barrel MSGC-1	5.56	3.38	200
Barrel MSGC-2	5.15	3.17	”
Barrel MSGC-3	5.03	2.86	”
Barrel MSGC-4	4.68	2.61	”
Barrel MSGC-5	4.68	2.97	”
Barrel MSGC-6	3.99	2.94	”
Barrel MSGC-7	3.21	2.10	”

Table 11: GEANT hits per detector crossed by the μ in $b\bar{b}$ jet cores.

7.2 Reconstructed hits per detector in $b\bar{b}$ jet cores

Table 12 shows the average number of reconstructed hits per detector crossed by the μ and per event for the different barrel layers from 50 $b\bar{b}$ jet events. The local “off-line” occupancy and cluster size are also

given. The numbers of cluster are always below or comparable to the corresponding numbers of GEANT hits.

Detectors type	Off-line occup		Rhits/det		Cluster size
	$< \# >$	RMS	$< \# >$	RMS	
Barrel Si-1	1.87 %	1.21	6.70	3.90	2.09
Barrel Si-2	2.33 %	1.87	6.94	3.77	2.29
Barrel Si-3	3.18 %	2.15	6.29	3.30	2.45
Barrel Si-4	2.91 %	1.84	5.67	2.52	2.57
Barrel MSGC-1	2.06 %	1.32	5.31	3.18	2.00
Barrel MSGC-2	1.95 %	1.25	4.90	2.94	2.04
Barrel MSGC-3	1.92 %	1.14	4.92	2.56	2.02
Barrel MSGC-4	1.92 %	1.60	4.66	2.57	1.97
Barrel MSGC-5	1.77 %	1.25	4.70	2.96	1.95
Barrel MSGC-6	1.56 %	1.21	4.17	3.26	1.91
Barrel MSGC-7	1.22 %	0.76	3.04	1.65	2.05

Table 12: Reconstructed hits per detector crossed by the μ in $b\bar{b}$ jet cores.

In the appendix, figure 33 shows the "off-line" occupancy for the barrel detectors, and figure 45 gives the corresponding cluster sizes for detectors crossed by the μ.

Compared to the average barrel detector multiplicity (table 10) for the same events, we find for the local densities (jet core):

- The number of reconstructed hits per detector increases by about 327 % for the barrel silicon detectors.
- The corresponding increase is between 95 % for the inner and 23 % for the outer barrel MSGCs.
- The "off-line" occupancy increases by about 155 % for the barrel silicon detectors.
- It increases between 100 % and 31 % for the barrel MSGCs.
- The cluster size decreases by 42 % in average for the silicon detectors. This is due to the higher P_t of the particles present in the jet core.
- For the MSGCs, no differences are observed because the cluster size does not depend on the P_t of the incident track.

7.3 Cluster merging and splitting in $b\bar{b}$ jets core

In the appendix, figure 59 shows the average effect of cluster merging and figure 71 the average cluster splitting for detectors crossed by the μ. Compared to table 26 for global $b\bar{b}$ jets studies, the table 30 shows:

- Globally, a small decrease of the cluster merging effect in all detectors.
- A small decrease of the cluster splitting in the silicon detectors.
- A decrease of the cluster splitting of about -45 % in the MSGC detectors.

The merging and splitting effects are essentially due to the presence of low momentum tracks. In the jet core, the relative frequency of these tracks is lower and this explains the observed decrease.

8 MB pile-up events superimposed on 300 GeV $b\bar{b}$ jet studies

8.1 GEANT hits per detector in "$b\bar{b}$ jets + MB pile-up" events

Primary and secondary tracks from $b\bar{b}$ jets at 300 GeV (section 6) plus MB pile-up (section 4) cross per bunch crossing 9102 ± 21 silicon strip and MSGC detectors out of 17334. These tracks produce on average 18550 ± 30 GEANT hits per bunch crossing. Table 13 shows the average number of GEANT hits per detector and per bunch crossing for the different types of detectors obtained from 20 $b\bar{b}$ jet events superimposed on MB pile-up.

Detectors type	Ghits/det		% of hit detectors	Tot # of det	pitch (μm)
	$< \# >$	RMS			
Barrel Si-1	4.25	2.77	86.7 %	440	67
Barrel Si-2	3.21	2.14	76.5 %	580	”
Barrel Si-3	2.68	1.73	64.4 %	716	100
Barrel Si-4	2.44	1.64	51.2 %	856	”
Barrel MSGC-1	2.53	1.67	67.2 %	756	200
Barrel MSGC-2	2.33	1.55	57.1 %	846	”
Barrel MSGC-3	2.22	1.48	46.3 %	936	”
Barrel MSGC-4	2.12	1.37	36.1 %	1026	”
Barrel MSGC-5	2.09	1.43	30.5 %	1116	”
Barrel MSGC-6	2.04	1.42	24.8 %	1206	”
Barrel MSGC-7	2.06	1.58	20.3 %	1296	”
Fwd Si-1-SS	2.99	1.59	81.6 %	216	100
Fwd Si-2-SS	3.61	1.89	89.7 %	360	”
Fwd Si-3-SS	2.49	1.26	68.1 %	480	”
Fwd Si-1-DS	3.09	1.62	83.1 %	288	67
Fwd Si-2-DS	3.50	1.89	88.3 %	360	”
Fwd Si-3-DS	2.47	1.22	68.4 %	576	”
Fwd MSGC-1	2.35	1.10	67.3 %	840	200
Fwd MSGC-2	2.45	1.19	69.3 %	960	”
Fwd MSGC-3	2.16	0.99	56.4 %	1080	”
Fwd MSGC-4	2.03	0.86	47.8 %	1200	”
Fwd MSGC-5	1.94	0.78	41.0 %	1200	”

Table 13: GEANT hits per hit detector in "$b\bar{b}$ jet + MB pile-up" events.

Compared to MB pile-up events, the average number of GEANT hits per detector for "$b\bar{b}$ jets + MB pile-up" events increases by about:

- 11 % for the outermost and 17 % for the innermost barrel silicon layers.
- 4 % for the outermost and 8 % for the innermost barrel MSGC layers.
- Between 8 % and 15 % for the forward silicon detectors.
- Between 3 % and 7 % for the forward MSGC detectors.

The number of detectors crossed by a track in "$b\bar{b}$ jets + MB pile-up" also increases compared to MB pile-up events only, by about:

- 21 % for the outermost and 7 % for the innermost barrel silicon layers.
- 27 % for the outermost and 11 % for the innermost barrel MSGC layers.

- Between 8 % and 16 % for the forward silicon detectors.
- Between 10 % and 15 % for the forward MSGC detectors.

The comparison to single $b\bar{b}$ jet events gives an increase of the number of GEANT hits per detector by about:

- 82 % for the innermost and 13 % for the outermost barrel silicon layers.
- Around 0 % for the 3 outermost and 22 % for the innermost barrel MSGC layers.
- Between 39 % and 92 % for the forward silicon detectors.
- Between 13 % and 42 % for the forward MSGC detectors.

8.2 Reconstructed hits per detector in "$b\bar{b}$ jets + MB pile-up" events

Table 14 shows the analysis of reconstructed hits for the different detector types. On average, a total of 8888 ± 21 silicon and MSGC detectors produce 25030 ± 35 reconstructed hits per event after the digitization and clusterization process. The "off-line" occupancy is always higher then 0.9 % and the average number of detectors producing at least one reconstructed hit per event are compatible but always lower than the corresponding numbers for GEANT hits.

Detectors	Off-line occup		% of hit	Rhits/det		On-line occup		Cluster
type	$< \# >$	RMS	detectors	$< \# >$	RMS	$< \# >$	RMS	size
Barrel Si-1	2.08 %	1.85	86.6 %	3.20	2.16	1.81 %	1.63	4.77
Barrel Si-2	1.59 %	1.57	76.4 %	2.37	1.73	1.17 %	1.26	4.92
Barrel Si-3	1.56 %	1.52	64.2 %	1.86	1.29	1.06 %	1.04	4.25
Barrel Si-4	1.41 %	1.43	50.9 %	1.63	1.11	0.68 %	0.76	4.38
Barrel MSGC-1	1.46 %	1.20	66.0 %	3.89	3.14	1.00 %	0.79	1.94
Barrel MSGC-2	1.32 %	1.14	55.7 %	3.59	2.98	0.74 %	0.64	1.91
Barrel MSGC-3	1.24 %	1.11	45.1 %	3.33	2.79	0.57 %	0.50	1.92
Barrel MSGC-4	1.19 %	1.10	35.1 %	3.23	2.76	0.43 %	0.39	1.90
Barrel MSGC-5	1.13 %	1.01	29.4 %	3.10	2.61	0.37 %	0.28	1.88
Barrel MSGC-6	1.12 %	1.04	23.9 %	3.07	2.62	0.32 %	0.23	1.89
Barrel MSGC-7	1.05 %	0.92	19.4 %	2.90	2.49	0.28 %	0.15	1.87
Fwd Si-1-SS	1.28 %	1.13	76.9 %	2.22	1.28	1.00 %	0.88	2.99
Fwd Si-2-SS	1.58 %	1.16	89.6 %	2.77	1.56	1.44 %	1.02	2.95
Fwd Si-3-SS	1.07 %	0.95	67.9 %	1.79	1.01	0.75 %	0.67	3.11
Fwd Si-1-DS	1.08 %	0.98	81.3 %	2.41	1.44	0.88 %	0.87	3.10
Fwd Si-2-DS	1.18 %	1.00	81.4 %	2.70	1.54	0.96 %	0.82	3.31
Fwd Si-3-DS	0.87 %	0.79	65.8 %	1.84	1.02	0.59 %	0.52	3.53
Fwd MSGC-1	1.17 %	0.94	65.6 %	2.93	2.28	0.80 %	0.62	2.06
Fwd MSGC-2	1.28 %	1.06	67.8 %	3.24	2.58	0.88 %	0.71	2.03
Fwd MSGC-3	1.13 %	0.93	54.8 %	2.92	2.38	0.62 %	0.51	2.00
Fwd MSGC-4	1.05 %	0.87	46.3 %	2.75	2.22	0.48 %	0.40	1.97
Fwd MSGC-5	0.98 %	0.76	39.9 %	2.57	1.95	0.40 %	0.31	1.98

Table 14: Reconstructed hits per detector in "$b\bar{b}$ jets + MB pile-up" events.

In the appendix, figure 32 shows the "off-line" and "on-line" occupancy for the barrel detectors and figure 40 for the forward detectors. In figure 44 and 52 are plotted the corresponding cluster sizes.

Compared to MB pile-up events, the "off-line" occupancy for "$b\bar{b}$ jets + MB pile-up" increases by about (the jets are in the barrel region):

- 13 % to 17 % for the barrel silicon detectors.
- 3 % to 9 % for the barrel MSGC detectors.
- 9 % to 16 % for the forward silicon detectors.
- 4 % to 8 % for the forward MSGC detectors.

Except for the 2 inner barrel silicon layers and 1 forward silicon ring, the "on-line" occupancy is always lower or equal to 1 % on average. It reaches 1.8 % for the inner barrel silicon layer and 1.2 % for the second one. Compared to MB pile-up events, it increases by about:

- 24 % to 41 % for the barrel silicon detectors.
- 4 % to 28 % for the barrel MSGC detectors.
- 12 % to 34 % for the forward silicon detectors.
- 17 % to 25 % for the forward MSGC detectors.

8.3 Cluster merging in "$b\bar{b}$ jets + MB pile-up" events

Compared to single $b\bar{b}$ jet events, an increase of the order of 6 % is observed (see table 26 and 28) for the cluster merging effect with low P_t tracks ($P_t < 0.3$ GeV/c). The comparison with other P_t ranges gives comparables values. On average and without P_t cuts, this effect increases also by about 6 %. It is more pronounced in the barrel region and lower in the forward detectors because all jets are in the barrel acceptance and therefore, the local multiplicity is higher.

A comparison of cluster merging between "MB pile-up + $b\bar{b}$" jet events with MB pile-up events gives comparable results on values in all P_t ranges in all layers and rings. Cluster merging effect (outside the core of the jet) is driven by low P_t tracks coming from the minimum bias events.

8.4 Cluster splitting in "$b\bar{b}$ jets + MB pile-up" events

A comparison of cluster splitting with $b\bar{b}$ events gives a small increase of a few percent for all detectors in all P_t ranges except for the barrel MSGCs where the increase is about 10 % and even more in the range $P_t < 0.3$ GeV/c. A comparison with MB pile-up events gives similar values in all detectors and in all P_t ranges.

In the appendix, figure 58 shows the effect of cluster merging for the barrel detectors in various P_t ranges and figure 66 for the forward detectors. In figures 70 and 78 is illustrated the cluster splitting effect in various P_t ranges for the barrel and forward detectors.

9 Local studies inside $b\bar{b}$ jets core superimposed on MB pile-up events

For these studies, only detectors crossed by the μ coming from b quark decays are taken into account. They are based upon 20 bunch crossings. Due to this, the following results have a limited statistical significance.

9.1 GEANT hits per detector in $b\bar{b}$ jet core + MB pile-up events

Table 15 shows the average number of GEANT hits per detector and per event for the various barrel detectors crossed by μ. Compared to the results from $b\bar{b}$ jet cores (table 11), the number of GEANT hits per detector from $b\bar{b}$ jet core superimposed on MB pile-up events increases by a factor of about:

- 20 % for the silicon barrel detectors.
- 12 % for the barrel MSGCs except for the 2 outermost.

Compared to global $b\bar{b}$ jets + MB pile-up events (table 13), the number of GEANT hits per detector increases by a factor about:

- 200 % for the silicon barrel detectors.
- 150 % for the barrel MSGC except for the 2 outermost where it is 93 % and 24 %.

Detectors type	Ghits/det		pitch (μm)
	$< \# >$	RMS	
Barrel Si-1	10.8	5.38	67
Barrel Si-2	9.69	5.71	”
Barrel Si-3	8.56	4.56	100
Barrel Si-4	7.48	4.75	”
Barrel MSGC-1	6.20	2.97	200
Barrel MSGC-2	5.61	3.23	”
Barrel MSGC-3	5.97	3.39	”
Barrel MSGC-4	5.11	2.56	”
Barrel MSGC-5	5.16	3.17	”
Barrel MSGC-6	3.94	2.85	”
Barrel MSGC-7	2.56	1.94	”

Table 15: GEANT hits per detector crossed by a μ $b\bar{b}$ jet cores plus MB pile-up events.

9.2 Reconstructed hits per detector in $b\bar{b}$ jet cores + MB pile-up events

Table 16 shows the average number of reconstructed hits per detector and per event for the different barrel detectors crossed by the μ from b quarks. The local “off-line” occupancy and cluster size are also listed.

Detectors type	Off-line occup		Rhits/det		Cluster size
	$< \# >$	RMS	$< \# >$	RMS	
Barrel Si-1	3.55 %	1.78	9.22	4.34	2.77
Barrel Si-2	3.31 %	2.22	7.71	3.97	2.74
Barrel Si-3	4.01 %	2.49	7.21	3.45	2.58
Barrel Si-4	3.87 %	2.71	6.00	3.08	2.77
Barrel MSGC-1	2.60 %	1.44	6.59	3.60	2.02
Barrel MSGC-2	2.52 %	1.57	6.00	3.32	2.13
Barrel MSGC-3	2.93 %	2.72	6.64	3.55	1.92
Barrel MSGC-4	2.70 %	2.77	5.92	3.17	1.96
Barrel MSGC-5	2.26 %	1.48	5.87	3.68	1.97
Barrel MSGC-6	1.82 %	1.10	4.45	3.32	2.09
Barrel MSGC-7	1.16 %	1.00	2.59	1.90	2.32

Table 16: Reconstructed hits per detector crossed by a μ $b\bar{b}$ jet cores plus MB pile-up events.

Compared to $b\bar{b}$ jet core events (table 12), the number of clusters increase by about 20 % for all barrel detectors, except for the outermost MSGCs where it decreases by -15 %. The cluster size increases in the silicon detectors by 16 % on average due to the presence of low P_t tracks from minimum bias events. In the MSGCs, the cluster sizes are similar as they are independent of P_t. The “off-line” occupancy

increases by about 32 % in all detectors, except for the inner silicon (+90 %) and the outer MSGC (-5 %) detectors.

Compared to global $b\bar{b}$ jets events with minimum bias pile-up (table 14), the number of clusters per detector increases by about +242 % in the barrel silicon detectors and by +75 % in the MSGCs, except for the outer one where it decreases by -11 %. The cluster sizes decrease by 41 % in the silicon, because the fraction of low momentum tracks decreases inside the jet core. They stay constant for the MSGCs. The "off-line" occupancy increases by between 71 % for the inner silicon and 174 % for the outer silicon detectors. It also increases by 100 % in the MSGCs, except for the outer one where there is a reduction of -11 %.

In the appendix, figure 34 shows the "off-line" occupancy for the barrel detectors. In figure 46 are plotted the corresponding cluster sizes.

9.3 Cluster merging and splitting in $b\bar{b}$ jet cores + MB pile-up events

A comparison with $b\bar{b}$ jet cores studies (table 30) gives a small increase of cluster merging (6 % on average) without P_t cuts, comparable values for cluster splitting effect in the silicon detectors, and an increase of about 25 % in the MSGCs are found, except for the outermost layer. These increases are due to the presence of the low momentum tracks coming from minimum bias events. The effect of pile-up is to increase the fraction of low P_t tracks, which strongly affect cluster merging and cluster splitting effects.

Compared to global $b\bar{b}$ jets with minimum pile-up (table 28), an average decrease of 10 % is observed for the cluster merging effect. A comparison of cluster splitting (table 29) gives a decrease of 11 % for the silicon and 47 % for the MSGC detectors. This is also due to the fraction of low momentum tracks from minimum bias events which is larger for the global studies.

In the appendix, figure 60 shows the average effect on cluster merging and figure 72 the average effect on cluster splitting.

10 High P_t tracks and cluster merging effect

Table 17 reports a summary of results on cluster merging for $P_t > 1.2$ GeV/c for various detector types: single MB, MB pile-up, single MB without δ rays production, single MB with a 2 Tesla field, $b\bar{b}$ barrel jets at 300 GeV with and without MB pile-up events.

Detector type	Single MB	MB pile-up	Single MB no δ rays	$b\bar{b}$ jets	$b\bar{b}$ jets + MB pile-up	Single MB at 2 Tesla
Barrel Si	10.9 %	14.4 %	0.92 %	14.7 %	15.9 %	9.1 %
Barrel MSGC	4.3 %	5.6 %	0.38 %	2.8 %	5.6 %	1.7 %
Fwd Si	12.1 %	15.7 %	0.95 %	8.5 %	15.2 %	7.0 %
Fwd MSGC	8.4 %	9.3 %	0.48 %	2.5 %	9.2 %	1.9 %
All	8.6 %	9.7 %	0.66 %	6.9 %	9.9 %	4.9 %

Table 17: Cluster merging effect for high P_t tracks.

The cluster merging effect is always more important in silicon than in MSGC detectors. It is ranging on average between 0.66 % for single MB without δ rays production to 9.9 % for $b\bar{b}$ jet events with pile-up.

In case of local $b\bar{b}$ jet studies, the probability to merge 2 tracks with $P_t > 1.2$ GeV/c together may reach 8.7 % without pile-up and 14.6 % with for the barrel silicon layers. Anywhere else, it is negligible.

11 Conclusion

For single minimum bias events, the average "off-line" occupancy is always below 1 % for all the strip detectors of the CMS tracker hit by a track (table 2). With a 2 Tesla field, it does not exceed 0.91 % (table 4). It reaches 1.78 % in the inner barrel silicon layer with minimum bias pile-up (table 6). Without δ rays production, this occupancy is the same as that of single MB (table 8). In case of $b\bar{b}$ jets (table 10), it reaches 1.10 % in the barrel silicon detectors and 2.08 % with pile-up events (table 14). The maximum local "off-line" occupancy is ranging from 3.18 % in the silicon for single $b\bar{b}$ events to 4.01 % including pile-up events (tables 12 and 16).

Except for the inner barrel silicon layers, where it is 1.42 %, all layers have an "on-line" occupancy lower than 0.95 % per bunch crossing on average including pile-up. It reaches respectively 1.81 % and 1.17 % with $b\bar{b}$ jets superimposed on MB pile-up events.

One effect of pile-up is to increase the "off-line" occupancy by a factor less than 2. The most important effect is the increase of the number of detectors crossed by a track. For the inner barrel silicon layer, one has between 8.9 % hit detectors per bunch crossing with single MB events and 81.0 % including pile-up events and up to 86.6 % with $b\bar{b}$ jets superimposed on MB pile-up.

The effects of cluster merging and splitting do not depend on pile-up; this means that it is an inherent detector and momentum property. Usually, a low P_t track is merged with another one. In most cases, these tracks are secondaries. In case of cluster splitting, which is due to digitization, also low momentum tracks are the more important one due to the incident angle trajectory. In single MB events, 8.6 % of reconstructed hits generated by tracks with $P_t > 1.2$ GeV/c are merged. This number decreases to 4.9 % with a 2 Tesla field. Without δ rays, this number decreases to 0.66 % which is the most significant effect when including δ ray production.

From local $b\bar{b}$ jet studies with and without pile-up events, one find that cluster merging is always less important than in global studies. This is due to the lower fraction of low P_t tracks. Note that all jets are generated in the barrel acceptance. The probability to merge two tracks with $P_t > 1.2$ GeV/c together becomes non negligible. It may reach 14.6 % in the inner barrel silicon layer when pile-up events are included.

List of Tables

1 GEANT hits per hit detector in single MB events. 7

2 Reconstructed hits per detector in single MB events. 9

3 GEANT hits per hit detector in single MB events with a 2 Tesla field. 10

4 Reconstructed hits per detector in single MB events with a 2 Tesla field. 11

5 GEANT hits per detector in MB pile-up events. 12

6 Reconstructed hits per detector in MB pile-up events. 13

7 GEANT hits per detector in single MB events whitout δ rays production. 14

8 Reconstructed hits per detector in single MB events whitout δ rays production. 15

9 GEANT hits per hit detector in $b\bar{b}$ jets events. 17

10 Reconstructed hits per detector in $b\bar{b}$ jets events. 18

11 GEANT hits per detector crossed by the μ in $b\bar{b}$ jet cores. 19

12 Reconstructed hits per detector crossed by the μ in $b\bar{b}$ jet cores. 20

13 GEANT hits per hit detector in "$b\bar{b}$ jet + MB pile-up" events. 21

14 Reconstructed hits per detector in "$b\bar{b}$ jets + MB pile-up" events. 22

15 GEANT hits per detector crossed by a μ $b\bar{b}$ jet cores plus MB pile-up events. 24

16 Reconstructed hits per detector crossed by a μ $b\bar{b}$ jet cores plus MB pile-up events. . . . 24

17 Cluster merging effect for high P_t tracks. 25

18 Incident ϕ angle in degrees for primary tracks from single MB events (P_t in GeV/c). . . 28

19 Cluster merging for various P_t ranges in single MB events. 29

20 Cluster splitting for various P_t ranges in single MB events. 30

21 Cluster merging for various P_t ranges in single MB events with a 2 Tesla field. 31

22 Cluster splitting for various P_t ranges in single MB events with a 2 Tesla field. 32

23 Cluster merging for different P_t ranges in MB pile-up events. 33

24 Cluster splitting for different P_t ranges in MB pile-up events. 34

25 Cluster splitting and merging in single MB events without δ ray production. 35

26 Cluster merging for various P_t ranges in $b\bar{b}$ jet events. 36

27 Cluster splitting for various P_t ranges in $b\bar{b}$ jet events. 37

28 Cluster merging for various P_t ranges in $b\bar{b}$ jet + MB pile-up events. 38

29 Cluster splitting for various P_t ranges in $b\bar{b}$ jet + MB pile-up events. 39

30 Cluster splitting and merging in $b\bar{b}$ jet cores. 40

31 Cluster splitting and merging in $b\bar{b}$ jet cores + MB pile-up. 40

Appendix: tables

Detectors type	$0.0 < P_t < 0.3$ ϕ (∘)	$0.3 < P_t < 0.6$ ϕ (∘)	$0.6 < P_t < 0.9$ ϕ (∘)	$0.9 < P_t < 1.2$ ϕ (∘)	$1.2 < P_t$ ϕ (∘)
Barrel Si-1	30.0	18.5	11.4	7.9	4.8
Barrel Si-2	45.0	23.9	14.6	10.3	6.3
Barrel Si-3	55.0	30.2	18.0	13.0	8.0
Barrel Si-4	?	37.5	21.7	15.6	9.5
Barrel MSGC-1	?	45.0	30.9	22.3	13.4
Barrel MSGC-2	?	52.0	35.2	24.5	14.7
Barrel MSGC-3	?	60.0	40.0	27.5	16.1
Barrel MSGC-4	?	67.0	46.2	30.6	17.9
Barrel MSGC-5	?	80.0	51.8	32.8	19.6
Barrel MSGC-6	?	?	60.1	36.0	21.1
Barrel MSGC-7	?	?	63.5	40.0	22.9
Fwd Si-1-SS	10.0	5.0	3.3	2.3	1.1
Fwd Si-2-SS	12.0	7.0	5.7	2.9	1.7
Fwd Si-3-SS	16.0	12.0	9.1	4.7	3.0
Fwd Si-1-DS	9.0	5.0	3.7	2.2	1.2
Fwd Si-2-DS	12.0	8.0	6.6	3.4	2.0
Fwd Si-3-DS	17.0	12.0	10.0	5.2	3.1
Fwd MSGC-1	?	23.0	11.0	8.6	5.5
Fwd MSGC-2	?	27.0	16.0	10.5	6.5
Fwd MSGC-3	?	31.0	20.0	14.0	8.4
Fwd MSGC-4	?	34.0	26.0	17.4	10.3
Fwd MSGC-5	?	?	35.0	21.8	13.1

Table 18: Incident ϕ angle in degrees for primary tracks from single MB events (P_t in GeV/c).

Detectors type	$0.0 < P_t < 0.3$		$0.3 < P_t < 0.6$		$0.6 < P_t < 0.9$	
	Ghits/Rhit	RMS	Ghits/Rhit	RMS	Ghits/Rhit	RMS
Barrel Si-1	2.04	2.02	1.07	0.32	1.01	0.10
Barrel Si-2	2.03	2.01	1.07	0.36	1.01	0.13
Barrel Si-3	1.92	1.84	1.07	0.33	1.01	0.11
Barrel Si-4	2.33	2.48	1.08	0.34	1.01	0.11
Barrel MSGC-1	2.20	2.49	1.09	0.41	1.01	0.14
Barrel MSGC-2	2.28	2.52	1.09	0.41	1.01	0.12
Barrel MSGC-3	2.45	2.78	1.08	0.34	1.02	0.19
Barrel MSGC-4	2.46	2.51	1.08	0.35	1.02	0.19
Barrel MSGC-5	2.58	2.99	1.07	0.31	1.02	0.23
Barrel MSGC-6	2.67	3.10	1.07	0.32	1.03	0.18
Barrel MSGC-7	2.90	3.59	1.05	0.26	1.01	0.14
Fwd Si-1-SS	1.21	0.53	1.00	0.02	1.00	0.00
Fwd Si-2-SS	1.28	0.94	1.00	0.03	1.00	0.02
Fwd Si-3-SS	1.25	0.52	1.00	0.03	1.00	0.00
Fwd Si-1-DS	1.25	0.61	1.00	0.07	1.00	0.03
Fwd Si-2-DS	1.34	0.93	1.00	0.05	1.00	0.02
Fwd Si-3-DS	1.33	1.26	1.00	0.05	1.00	0.00
Fwd MSGC-1	1.27	0.60	1.00	0.04	1.00	0.00
Fwd MSGC-2	1.32	0.62	1.00	0.04	1.00	0.03
Fwd MSGC-3	1.30	0.61	1.00	0.03	1.00	0.02
Fwd MSGC-4	1.31	0.62	1.00	0.05	1.00	0.01
Fwd MSGC-5	1.29	0.58	1.00	0.05	1.00	0.02
	$0.9 < P_t < 1.2$		$1.2 < P_t$		all P_t	
	Ghits/Rhit	RMS	Ghits/Rhit	RMS	Ghits/Rhit	RMS
Barrel Si-1	1.00	0.00	1.00	0.04	1.64	1.65
Barrel Si-2	1.00	0.00	1.00	0.02	1.61	1.60
Barrel Si-3	1.00	0.03	1.00	0.02	1.48	1.38
Barrel Si-4	1.00	0.03	1.00	0.03	1.61	1.78
Barrel MSGC-1	1.00	0.00	1.00	0.03	1.45	1.56
Barrel MSGC-2	1.00	0.00	1.00	0.00	1.47	1.58
Barrel MSGC-3	1.00	0.03	1.00	0.00	1.50	1.72
Barrel MSGC-4	1.00	0.00	1.00	0.00	1.51	1.59
Barrel MSGC-5	1.00	0.00	1.00	0.00	1.57	1.91
Barrel MSGC-6	1.00	0.00	1.00	0.00	1.62	2.02
Barrel MSGC-7	1.00	0.00	1.00	0.00	1.70	2.35
Fwd Si-1-SS	1.00	0.00	1.00	0.00	1.14	0.45
Fwd Si-2-SS	1.00	0.03	1.00	0.03	1.17	0.76
Fwd Si-3-SS	1.00	0.00	1.00	0.00	1.12	0.39
Fwd Si-1-DS	1.00	0.05	1.00	0.00	1.16	0.50
Fwd Si-2-DS	1.00	0.00	1.00	0.00	1.22	0.76
Fwd Si-3-DS	1.00	0.00	1.00	0.04	1.16	0.90
Fwd MSGC-1	1.00	0.00	1.00	0.00	1.12	0.42
Fwd MSGC-2	1.00	0.00	1.00	0.03	1.14	0.45
Fwd MSGC-3	1.00	0.00	1.00	0.00	1.13	0.43
Fwd MSGC-4	1.00	0.06	1.00	0.00	1.14	0.45
Fwd MSGC-5	1.00	0.00	1.00	0.00	1.14	0.42

Table 19: Cluster merging for various P_t ranges in single MB events.

Detector Type	all P_t		$0.0 < P_t < 0.3$		$0.3 < P_t < 0.6$	
	Rhits/Ghit	RMS	Rhits/Ghit	RMS	Rhits/Ghit	RMS
Barrel Si-1	1.42	1.57	1.62	1.95	1.12	0.45
Barrel Si-2	1.42	1.72	1.66	2.22	1.12	0.45
Barrel Si-3	1.28	1.03	1.47	1.36	1.10	0.44
Barrel Si-4	1.37	1.58	1.71	2.19	1.12	0.65
Barrel MSGC-1	2.88	2.82	3.64	3.46	2.95	2.65
Barrel MSGC-2	2.97	2.93	3.79	3.63	3.08	2.80
Barrel MSGC-3	3.01	3.01	3.76	3.66	3.30	3.09
Barrel MSGC-4	3.09	3.00	3.85	3.57	3.51	3.32
Barrel MSGC-5	3.07	2.96	3.71	3.54	3.41	3.15
Barrel MSGC-6	3.26	3.22	3.79	3.79	3.07	2.86
Barrel MSGC-7	3.30	3.19	3.90	3.65	3.13	2.86
Fwd Si-1-SS	1.05	0.40	1.07	0.47	1.03	0.18
Fwd Si-2-SS	1.08	0.52	1.10	0.63	1.03	0.17
Fwd Si-3-SS	1.03	0.23	1.05	0.29	1.01	0.12
Fwd Si-1-DS	1.07	0.60	1.09	0.67	1.05	0.57
Fwd Si-2-DS	1.09	0.54	1.12	0.65	1.04	0.27
Fwd Si-3-DS	1.05	0.28	1.07	0.35	1.02	0.16
Fwd MSGC-1	1.80	1.62	1.96	1.92	1.90	1.50
Fwd MSGC-2	1.91	1.68	2.05	1.88	2.06	1.71
Fwd MSGC-3	1.95	1.70	2.05	1.87	2.18	1.79
Fwd MSGC-4	2.03	1.75	2.11	1.77	2.39	2.13
Fwd MSGC-5	1.96	1.49	2.02	1.54	2.48	2.23
	$0.6 < P_t < 0.9$		$0.9 < P_t < 1.2$		$1.2 < P_t$	
	Rhits/Ghit	RMS	Rhits/Ghit	RMS	Rhits/Ghit	RMS
Barrel Si-1	1.06	0.35	1.05	0.25	1.04	0.21
Barrel Si-2	1.04	0.24	1.04	0.22	1.04	0.26
Barrel Si-3	1.03	0.20	1.02	0.18	1.02	0.15
Barrel Si-4	1.03	0.20	1.02	0.17	1.02	0.14
Barrel MSGC-1	1.83	0.91	1.60	1.05	1.20	0.49
Barrel MSGC-2	1.95	1.05	1.67	0.91	1.30	0.69
Barrel MSGC-3	2.06	1.10	1.72	0.80	1.32	0.78
Barrel MSGC-4	2.28	1.26	1.76	0.91	1.35	0.59
Barrel MSGC-5	2.58	1.87	1.88	0.82	1.42	0.77
Barrel MSGC-6	3.16	2.85	1.84	0.80	1.50	0.69
Barrel MSGC-7	3.44	3.00	1.98	0.96	1.52	0.92
Fwd Si-1-SS	1.03	0.16	1.03	0.18	1.03	0.18
Fwd Si-2-SS	1.04	0.34	1.04	0.22	1.05	0.23
Fwd Si-3-SS	1.02	0.12	1.02	0.14	1.02	0.15
Fwd Si-1-DS	1.03	0.20	1.04	0.19	1.03	0.19
Fwd Si-2-DS	1.05	0.23	1.05	0.24	1.05	0.22
Fwd Si-3-DS	1.03	0.16	1.02	0.16	1.04	0.20
Fwd MSGC-1	1.39	1.04	1.08	0.41	1.05	0.26
Fwd MSGC-2	1.55	1.11	1.15	0.43	1.09	0.45
Fwd MSGC-3	1.72	1.30	1.27	0.59	1.11	0.41
Fwd MSGC-4	1.90	1.50	1.39	0.83	1.16	0.47
Fwd MSGC-5	1.99	1.22	1.46	0.68	1.18	0.56

Table 20: Cluster splitting for various P_t ranges in single MB events.

Detectors type	$0.0 < P_t < 0.3$		$0.3 < P_t < 0.6$		$0.6 < P_t < 0.9$	
	Ghits/Rhit	RMS	Ghits/Rhit	RMS	Ghits/Rhit	RMS
Barrel Si-1	1.74	1.73	1.00	0.06	1.00	0.03
Barrel Si-2	1.66	1.65	1.00	0.04	1.00	0.04
Barrel Si-3	1.67	1.72	1.00	0.05	1.00	0.07
Barrel Si-4	1.67	1.84	1.00	0.04	1.00	0.05
Barrel MSGC-1	1.42	1.37	1.00	0.05	1.00	0.00
Barrel MSGC-2	1.46	1.52	1.00	0.05	1.00	0.00
Barrel MSGC-3	1.48	1.41	1.01	0.07	1.00	0.00
Barrel MSGC-4	1.60	1.68	1.01	0.08	1.00	0.03
Barrel MSGC-5	1.74	1.99	1.00	0.04	1.00	0.03
Barrel MSGC-6	1.79	1.99	1.00	0.03	1.00	0.00
Barrel MSGC-7	2.14	2.63	1.00	0.05	1.00	0.03
Fwd Si-1-SS	1.17	0.45	1.01	0.07	1.00	0.00
Fwd Si-2-SS	1.20	0.75	1.00	0.04	1.00	0.04
Fwd Si-3-SS	1.16	0.44	1.00	0.00	1.00	0.00
Fwd Si-1-DS	1.23	0.79	1.00	0.05	1.00	0.04
Fwd Si-2-DS	1.19	0.47	1.00	0.05	1.00	0.06
Fwd Si-3-DS	1.21	0.61	1.00	0.05	1.00	0.00
Fwd MSGC-1	1.08	0.33	1.00	0.03	1.00	0.00
Fwd MSGC-2	1.09	0.35	1.00	0.03	1.00	0.00
Fwd MSGC-3	1.11	0.39	1.00	0.03	1.00	0.00
Fwd MSGC-4	1.12	0.40	1.00	0.03	1.00	0.03
Fwd MSGC-5	1.18	0.53	1.00	0.03	1.00	0.00
	$0.9 < P_t < 1.2$		$1.2 < P_t$		all P_t	
	Ghits/Rhit	RMS	Ghits/Rhit	RMS	Ghits/Rhit	RMS
Barrel Si-1	1.00	0.00	1.00	0.03	1.45	1.40
Barrel Si-2	1.00	0.06	1.00	0.00	1.41	1.34
Barrel Si-3	1.00	0.00	1.00	0.03	1.41	1.39
Barrel Si-4	1.00	0.00	1.00	0.00	1.41	1.47
Barrel MSGC-1	1.00	0.00	1.00	0.00	1.29	1.14
Barrel MSGC-2	1.00	0.00	1.00	0.00	1.30	1.24
Barrel MSGC-3	1.00	0.00	1.00	0.00	1.29	1.13
Barrel MSGC-4	1.00	0.00	1.00	0.00	1.34	1.29
Barrel MSGC-5	1.00	0.00	1.00	0.00	1.39	1.49
Barrel MSGC-6	1.00	0.00	1.00	0.00	1.35	1.37
Barrel MSGC-7	1.00	0.00	1.00	0.00	1.49	1.81
Fwd Si-1-SS	1.00	0.06	1.00	0.00	1.11	0.37
Fwd Si-2-SS	1.00	0.00	1.00	0.00	1.13	0.62
Fwd Si-3-SS	1.00	0.05	1.00	0.04	1.10	0.36
Fwd Si-1-DS	1.00	0.00	1.00	0.07	1.15	0.64
Fwd Si-2-DS	1.00	0.05	1.00	0.04	1.13	0.40
Fwd Si-3-DS	1.00	0.00	1.00	0.00	1.14	0.50
Fwd MSGC-1	1.00	0.00	1.00	0.00	1.06	0.29
Fwd MSGC-2	1.00	0.00	1.00	0.00	1.06	0.29
Fwd MSGC-3	1.00	0.00	1.00	0.00	1.07	0.33
Fwd MSGC-4	1.00	0.00	1.00	0.04	1.07	0.32
Fwd MSGC-5	1.00	0.00	1.00	0.00	1.10	0.39

Table 21: Cluster merging for various P_t ranges in single MB events with a 2 Tesla field.

Detector Type	all P_t		$0.0 < P_t < 0.3$		$0.3 < P_t < 0.6$	
	Rhits/Ghit	RMS	Rhits/Ghit	RMS	Rhits/Ghit	RMS
Barrel Si-1	1.28	1.43	1.43	1.79	1.03	0.18
Barrel Si-2	1.26	1.17	1.40	1.45	1.02	0.12
Barrel Si-3	1.24	1.01	1.38	1.25	1.00	0.06
Barrel Si-4	1.33	1.22	1.37	1.53	1.00	0.05
Barrel MSGC-1	2.36	2.44	3.03	2.94	1.66	1.00
Barrel MSGC-2	2.46	2.62	3.25	3.21	1.72	1.03
Barrel MSGC-3	2.38	2.31	3.09	2.86	1.82	0.99
Barrel MSGC-4	2.49	2.41	3.31	3.04	2.00	1.17
Barrel MSGC-5	2.62	2.65	3.59	3.35	2.11	1.50
Barrel MSGC-6	2.68	3.76	3.64	3.43	2.32	2.32
Barrel MSGC-7	2.87	3.02	3.91	3.80	2.62	2.25
Fwd Si-1-SS	1.03	0.16	1.04	0.20	1.01	0.08
Fwd Si-2-SS	1.04	0.56	1.06	0.68	1.00	0.05
Fwd Si-3-SS	1.02	0.22	1.03	0.27	1.00	0.03
Fwd Si-1-DS	1.05	0.46	1.07	0.57	1.01	0.09
Fwd Si-2-DS	1.04	0.24	1.06	0.28	1.01	0.09
Fwd Si-3-DS	1.05	0.76	1.08	0.95	1.01	0.10
Fwd MSGC-1	1.52	1.16	1.74	1.34	1.21	0.70
Fwd MSGC-2	1.58	1.23	1.80	1.42	1.32	0.84
Fwd MSGC-3	1.70	1.53	1.95	1.79	1.47	0.93
Fwd MSGC-4	1.70	1.30	1.94	1.49	1.59	1.03
Fwd MSGC-5	1.76	1.50	2.04	1.89	1.69	0.98
	$0.6 < P_t < 0.9$		$0.9 < P_t < 1.2$		$1.2 < P_t$	
	Rhits/Ghit	RMS	Rhits/Ghit	RMS	Rhits/Ghit	RMS
Barrel Si-1	1.03	0.17	1.02	0.14	1.03	0.18
Barrel Si-2	1.02	0.14	1.02	0.14	1.03	0.16
Barrel Si-3	1.00	0.05	1.00	0.06	1.00	0.06
Barrel Si-4	1.00	0.03	1.00	0.04	1.00	0.05
Barrel MSGC-1	1.25	0.49	1.18	0.44	1.07	0.26
Barrel MSGC-2	1.35	0.99	1.25	1.15	1.10	0.41
Barrel MSGC-3	1.36	0.79	1.26	0.53	1.09	0.30
Barrel MSGC-4	1.43	0.78	1.29	0.66	1.12	0.34
Barrel MSGC-5	1.48	0.72	1.27	0.53	1.14	0.37
Barrel MSGC-6	1.47	0.65	1.44	0.93	1.14	0.35
Barrel MSGC-7	1.60	1.03	1.39	0.72	1.16	0.39
Fwd Si-1-SS	1.00	0.04	1.00	0.06	1.01	0.08
Fwd Si-2-SS	1.00	0.06	1.01	0.07	1.00	0.06
Fwd Si-3-SS	1.00	0.00	1.01	0.07	1.00	0.06
Fwd Si-1-DS	1.01	0.07	1.01	0.12	1.02	0.12
Fwd Si-2-DS	1.01	0.10	1.01	0.12	1.02	0.12
Fwd Si-3-DS	1.01	0.08	1.01	0.08	1.01	0.09
Fwd MSGC-1	1.06	0.45	1.02	0.17	1.01	0.07
Fwd MSGC-2	1.08	0.47	1.04	0.29	1.01	0.13
Fwd MSGC-3	1.14	0.96	1.07	0.40	1.02	0.17
Fwd MSGC-4	1.20	0.89	1.07	0.45	1.03	0.18
Fwd MSGC-5	1.21	0.65	1.15	1.04	1.05	0.32

Table 22: Cluster splitting for various P_t ranges in single MB events with a 2 Tesla field.

Detectors type	$0.0 < P_t < 0.3$		$0.3 < P_t < 0.6$		$0.6 < P_t < 0.9$	
	Ghits/Rhit	RMS	Ghits/Rhit	RMS	Ghits/Rhit	RMS
Barrel Si-1	2.08	1.93	1.09	0.36	1.02	0.12
Barrel Si-2	2.11	2.18	1.08	0.38	1.01	0.11
Barrel Si-3	1.98	1.85	1.08	0.36	1.01	0.10
Barrel Si-4	2.25	2.45	1.10	0.42	1.02	0.14
Barrel MSGC-1	2.20	2.44	1.11	0.42	1.02	0.16
Barrel MSGC-2	2.39	2.68	1.11	0.44	1.02	0.17
Barrel MSGC-3	2.55	2.95	1.09	0.36	1.03	0.24
Barrel MSGC-4	2.48	2.50	1.11	0.40	1.02	0.18
Barrel MSGC-5	2.52	2.67	1.08	0.34	1.03	0.23
Barrel MSGC-6	2.87	3.42	1.08	0.37	1.04	0.22
Barrel MSGC-7	2.95	3.51	1.07	0.29	1.02	0.14
Fwd Si-1-SS	1.24	0.61	1.01	0.08	1.01	0.10
Fwd Si-2-SS	1.36	1.41	1.01	0.12	1.01	0.09
Fwd Si-3-SS	1.30	0.58	1.01	0.10	1.01	0.08
Fwd Si-1-DS	1.28	0.70	1.01	0.12	1.01	0.10
Fwd Si-2-DS	1.38	1.04	1.01	0.10	1.00	0.06
Fwd Si-3-DS	1.28	0.57	1.01	0.11	1.00	0.05
Fwd MSGC-1	1.28	0.61	1.01	0.10	1.00	0.05
Fwd MSGC-2	1.34	0.63	1.01	0.11	1.00	0.06
Fwd MSGC-3	1.31	0.61	1.01	0.10	1.00	0.06
Fwd MSGC-4	1.31	0.62	1.01	0.10	1.00	0.07
Fwd MSGC-5	1.28	0.56	1.01	0.07	1.00	0.07
	$0.9 < P_t < 1.2$		$1.2 < P_t$		all P_t	
	Ghits/Rhit	RMS	Ghits/Rhit	RMS	Ghits/Rhit	RMS
Barrel Si-1	1.00	0.04	1.00	0.06	1.68	1.60
Barrel Si-2	1.00	0.00	1.00	0.06	1.65	1.73
Barrel Si-3	1.00	0.00	1.00	0.04	1.52	1.40
Barrel Si-4	1.00	0.00	1.00	0.04	1.59	1.74
Barrel MSGC-1	1.00	0.06	1.00	0.04	1.47	1.56
Barrel MSGC-2	1.00	0.07	1.00	0.00	1.51	1.68
Barrel MSGC-3	1.00	0.04	1.00	0.00	1.55	1.85
Barrel MSGC-4	1.00	0.00	1.00	0.00	1.53	1.60
Barrel MSGC-5	1.00	0.03	1.00	0.00	1.57	1.76
Barrel MSGC-6	1.00	0.03	1.00	0.00	1.70	2.25
Barrel MSGC-7	1.00	0.03	1.00	0.00	1.76	2.36
Fwd Si-1-SS	1.00	0.07	1.00	0.00	1.17	0.52
Fwd Si-2-SS	1.01	0.11	1.00	0.00	1.23	1.14
Fwd Si-3-SS	1.00	0.00	1.00	0.00	1.15	0.44
Fwd Si-1-DS	1.01	0.08	1.00	0.00	1.19	0.58
Fwd Si-2-DS	1.00	0.05	1.00	0.07	1.25	0.85
Fwd Si-3-DS	1.00	0.00	1.00	0.00	1.15	0.43
Fwd MSGC-1	1.00	0.00	1.00	0.00	1.14	0.44
Fwd MSGC-2	1.00	0.05	1.00	0.04	1.16	0.46
Fwd MSGC-3	1.00	0.03	1.00	0.00	1.14	0.44
Fwd MSGC-4	1.00	0.05	1.00	0.00	1.15	0.45
Fwd MSGC-5	1.00	0.06	1.00	0.00	1.14	0.41

Table 23: Cluster merging for different P_t ranges in MB pile-up events.

Detector Type	all P_t		$0.0 < P_t < 0.3$		$0.3 < P_t < 0.6$	
	Rhits/Ghit	RMS	Rhits/Ghit	RMS	Rhits/Ghit	RMS
Barrel Si-1	1.41	1.46	1.60	1.79	1.15	0.58
Barrel Si-2	1.43	1.60	1.68	2.05	1.13	0.50
Barrel Si-3	1.31	1.23	1.53	1.64	1.11	0.45
Barrel Si-4	1.33	1.36	1.60	1.88	1.15	0.70
Barrel MSGC-1	2.85	2.74	3.58	3.38	2.92	2.55
Barrel MSGC-2	2.97	2.95	3.79	3.68	3.06	2.78
Barrel MSGC-3	3.05	3.00	3.89	3.67	3.24	2.98
Barrel MSGC-4	3.08	3.07	3.76	3.57	3.62	3.57
Barrel MSGC-5	3.02	2.79	3.59	3.24	3.45	3.12
Barrel MSGC-6	3.38	3.48	4.19	4.19	3.20	2.97
Barrel MSGC-7	3.26	3.17	3.86	3.61	3.19	3.00
Fwd Si-1-SS	1.07	0.50	1.09	0.60	1.03	0.19
Fwd Si-2-SS	1.11	0.80	1.14	0.97	1.05	0.22
Fwd Si-3-SS	1.04	0.26	1.06	0.34	1.02	0.13
Fwd Si-1-DS	1.08	0.67	1.10	0.71	1.07	0.76
Fwd Si-2-DS	1.11	0.84	1.14	0.99	1.05	0.22
Fwd Si-3-DS	1.05	0.27	1.08	0.34	1.03	0.17
Fwd MSGC-1	1.81	1.65	1.96	1.97	1.90	1.47
Fwd MSGC-2	1.92	1.82	2.07	2.02	2.07	1.87
Fwd MSGC-3	1.96	1.69	2.07	1.86	2.19	1.80
Fwd MSGC-4	2.03	1.73	2.09	1.74	2.36	2.05
Fwd MSGC-5	1.95	1.46	2.00	1.52	2.47	2.13
	$0.6 < P_t < 0.9$		$0.9 < P_t < 1.2$		$1.2 < P_t$	
	Rhits/Ghit	RMS	Rhits/Ghit	RMS	Rhits/Ghit	RMS
Barrel Si-1	1.07	0.45	1.06	0.26	1.06	0.25
Barrel Si-2	1.05	0.22	1.04	0.21	1.06	0.28
Barrel Si-3	1.03	0.19	1.03	0.19	1.03	0.19
Barrel Si-4	1.04	0.25	1.02	0.15	1.03	0.20
Barrel MSGC-1	1.84	0.92	1.61	1.11	1.20	0.53
Barrel MSGC-2	1.98	1.12	1.72	0.92	1.27	0.57
Barrel MSGC-3	2.09	1.21	1.70	0.73	1.34	0.74
Barrel MSGC-4	2.25	1.22	1.82	1.12	1.35	0.55
Barrel MSGC-5	2.56	1.86	1.77	0.79	1.45	0.69
Barrel MSGC-6	3.16	2.85	1.91	0.94	1.49	0.75
Barrel MSGC-7	3.26	2.92	2.05	1.07	1.51	0.93
Fwd Si-1-SS	1.05	0.21	1.03	0.16	1.07	0.26
Fwd Si-2-SS	1.07	0.55	1.05	0.24	1.06	0.25
Fwd Si-3-SS	1.03	0.19	1.02	0.14	1.03	0.17
Fwd Si-1-DS	1.04	0.22	1.03	0.18	1.05	0.24
Fwd Si-2-DS	1.10	1.03	1.04	0.20	1.06	0.25
Fwd Si-3-DS	1.03	0.17	1.04	0.20	1.04	0.19
Fwd MSGC-1	1.43	1.10	1.10	0.63	1.06	0.31
Fwd MSGC-2	1.53	1.15	1.15	0.42	1.08	0.43
Fwd MSGC-3	1.73	1.22	1.23	0.54	1.12	0.47
Fwd MSGC-4	1.94	1.54	1.41	0.94	1.19	0.71
Fwd MSGC-5	2.00	1.22	1.47	0.68	1.15	0.39

Table 24: Cluster splitting for different P_t ranges in MB pile-up events.

Detector type	Merging: all P_t		Splitting: all P_t	
	Ghits/Rhit	RMS	Rhits/Ghit	RMS
Barrel Si-1	1.26	0.95	1.28	1.10
Barrel Si-2	1.26	1.09	1.30	1.22
Barrel Si-3	1.26	1.07	1.25	0.99
Barrel Si-4	1.24	1.04	1.22	0.81
Barrel MSGC-1	1.31	1.30	2.79	2.67
Barrel MSGC-2	1.34	1.42	2.88	2.90
Barrel MSGC-3	1.32	1.31	2.83	2.68
Barrel MSGC-4	1.40	1.51	2.96	2.79
Barrel MSGC-5	1.39	1.64	2.90	2.87
Barrel MSGC-6	1.57	2.32	3.21	3.37
Barrel MSGC-7	1.62	2.33	3.27	3.11
Fwd Si-1-SS	1.01	0.10	1.01	0.15
Fwd Si-2-SS	1.02	0.13	1.01	0.13
Fwd Si-3-SS	1.01	0.11	1.01	0.08
Fwd Si-1-DS	1.01	0.10	1.03	0.46
Fwd Si-2-DS	1.02	0.13	1.02	0.31
Fwd Si-3-DS	1.01	0.12	1.02	0.47
Fwd MSGC-1	1.02	0.15	1.72	1.50
Fwd MSGC-2	1.03	0.20	1.80	1.58
Fwd MSGC-3	1.03	0.18	1.87	1.61
Fwd MSGC-4	1.04	0.21	1.89	1.59
Fwd MSGC-5	1.05	0.23	1.90	1.52

Table 25: Cluster splitting and merging in single MB events without δ ray production.

Detectors	$0.0 < P_t < 0.3$		$0.3 < P_t < 0.6$		$0.6 < P_t < 0.9$	
type	Ghits/Rhit	RMS	Ghits/Rhit	RMS	Ghits/Rhit	RMS
Barrel Si-1	1.97	1.96	1.10	0.40	1.02	0.14
Barrel Si-2	1.93	1.83	1.11	0.43	1.03	0.16
Barrel Si-3	1.97	1.97	1.11	0.43	1.02	0.14
Barrel Si-4	2.07	1.98	1.14	0.58	1.01	0.13
Barrel MSGC-1	2.14	2.31	1.12	0.49	1.01	0.13
Barrel MSGC-2	2.38	2.74	1.11	0.46	1.01	0.10
Barrel MSGC-3	2.43	2.93	1.07	0.39	1.01	0.11
Barrel MSGC-4	2.42	2.90	1.06	0.34	1.02	0.17
Barrel MSGC-5	2.84	3.72	1.08	0.32	1.03	0.19
Barrel MSGC-6	2.56	3.23	1.05	0.22	1.01	0.09
Barrel MSGC-7	3.16	3.71	1.01	0.12	1.01	0.10
Fwd Si-1-SS	1.18	0.51	1.00	0.00	1.00	0.00
Fwd Si-2-SS	1.20	0.48	1.01	0.09	1.00	0.00
Fwd Si-3-SS	1.21	0.50	1.00	0.03	1.00	0.06
Fwd Si-1-DS	1.18	0.47	1.00	0.00	1.00	0.00
Fwd Si-2-DS	1.23	0.60	1.01	0.09	1.00	0.06
Fwd Si-3-DS	1.23	0.51	1.00	0.05	1.00	0.00
Fwd MSGC-1	1.11	0.40	1.00	0.04	1.00	0.04
Fwd MSGC-2	1.14	0.43	1.00	0.03	1.00	0.03
Fwd MSGC-3	1.13	0.40	1.00	0.05	1.00	0.00
Fwd MSGC-4	1.18	0.49	1.00	0.04	1.00	0.00
Fwd MSGC-5	1.25	0.58	1.00	0.07	1.00	0.00
	$0.9 < P_t < 1.2$		$1.2 < P_t$		all P_t	
	Ghits/Rhit	RMS	Ghits/Rhit	RMS	Ghits/Rhit	RMS
Barrel Si-1	1.04	0.19	1.08	0.31	1.53	1.48
Barrel Si-2	1.02	0.14	1.07	0.28	1.48	1.35
Barrel Si-3	1.03	0.16	1.07	0.28	1.44	1.36
Barrel Si-4	1.01	0.10	1.05	0.23	1.46	1.35
Barrel MSGC-1	1.01	0.10	1.02	0.14	1.42	1.44
Barrel MSGC-2	1.00	0.00	1.02	0.13	1.47	1.65
Barrel MSGC-3	1.00	0.05	1.02	0.13	1.44	1.71
Barrel MSGC-4	1.00	0.00	1.01	0.11	1.45	1.72
Barrel MSGC-5	1.00	0.05	1.01	0.11	1.62	2.28
Barrel MSGC-6	1.00	0.00	1.01	0.08	1.47	1.89
Barrel MSGC-7	1.00	0.00	1.01	0.09	1.64	2.24
Fwd Si-1-SS	1.03	0.18	1.01	0.09	1.13	0.43
Fwd Si-2-SS	1.00	0.00	1.02	0.14	1.13	0.40
Fwd Si-3-SS	1.02	0.12	1.01	0.11	1.11	0.38
Fwd Si-1-DS	1.00	0.00	1.00	0.00	1.12	0.39
Fwd Si-2-DS	1.02	0.15	1.01	0.13	1.15	0.49
Fwd Si-3-DS	1.00	0.00	1.01	0.07	1.12	0.38
Fwd MSGC-1	1.00	0.00	1.00	0.00	1.05	0.27
Fwd MSGC-2	1.00	0.00	1.01	0.09	1.06	0.30
Fwd MSGC-3	1.00	0.00	1.00	0.04	1.06	0.27
Fwd MSGC-4	1.00	0.00	1.00	0.08	1.08	0.34
Fwd MSGC-5	1.00	0.00	1.00	0.04	1.12	0.42

Table 26: Cluster merging for various P_t ranges in $b\bar{b}$ jet events.

Detector Type	all P_t		$0.0 < P_t < 0.3$		$0.3 < P_t < 0.6$	
	Rhits/Ghit	RMS	Rhits/Ghit	RMS	Rhits/Ghit	RMS
Barrel Si-1	1.35	1.47	1.60	2.00	1.11	0.40
Barrel Si-2	1.29	1.06	1.51	1.45	1.11	0.46
Barrel Si-3	1.23	0.77	1.45	1.07	1.10	0.43
Barrel Si-4	1.26	0.92	1.53	1.32	1.13	0.57
Barrel MSGC-1	2.40	2.67	3.60	3.66	2.74	2.45
Barrel MSGC-2	2.42	2.57	3.63	3.34	2.85	2.66
Barrel MSGC-3	2.34	2.63	3.49	3.65	2.95	2.65
Barrel MSGC-4	2.40	2.71	3.59	3.64	3.24	3.06
Barrel MSGC-5	2.60	2.72	3.97	3.45	3.17	2.76
Barrel MSGC-6	2.39	2.61	3.65	3.39	3.03	3.00
Barrel MSGC-7	2.49	2.78	3.89	3.62	2.79	2.34
Fwd Si-1-SS	1.03	0.19	1.03	0.21	1.02	0.18
Fwd Si-2-SS	1.03	0.17	1.04	0.20	1.01	0.08
Fwd Si-3-SS	1.01	0.12	1.02	0.15	1.00	0.05
Fwd Si-1-DS	1.05	0.57	1.07	0.70	1.02	0.26
Fwd Si-2-DS	1.05	0.44	1.07	0.55	1.02	0.13
Fwd Si-3-DS	1.04	0.65	1.04	0.22	1.03	0.78
Fwd MSGC-1	1.77	1.57	1.89	1.56	1.93	1.71
Fwd MSGC-2	1.80	1.60	1.97	1.82	2.01	1.62
Fwd MSGC-3	1.84	1.66	1.97	1.88	2.20	1.85
Fwd MSGC-4	1.91	1.70	1.99	1.87	2.40	1.93
Fwd MSGC-5	1.88	1.70	2.01	2.01	2.38	1.85
	$0.6 < P_t < 0.9$		$0.9 < P_t < 1.2$		$1.2 < P_t$	
	Rhits/Ghit	RMS	Rhits/Ghit	RMS	Rhits/Ghit	RMS
Barrel Si-1	1.02	0.16	1.04	0.21	1.06	0.24
Barrel Si-2	1.04	0.22	1.04	0.20	1.06	0.26
Barrel Si-3	1.02	0.13	1.01	0.08	1.04	0.19
Barrel Si-4	1.01	0.10	1.00	0.06	1.03	0.17
Barrel MSGC-1	1.85	1.25	1.43	0.56	1.04	0.21
Barrel MSGC-2	1.95	1.06	1.52	0.62	1.06	0.25
Barrel MSGC-3	2.00	1.17	1.64	0.73	1.08	0.29
Barrel MSGC-4	2.23	1.40	1.62	0.65	1.09	0.30
Barrel MSGC-5	2.61	2.09	1.75	0.85	1.11	0.38
Barrel MSGC-6	3.00	2.61	1.67	0.82	1.14	0.42
Barrel MSGC-7	3.25	3.08	1.83	0.84	1.15	0.41
Fwd Si-1-SS	1.01	0.08	1.02	0.13	1.01	0.08
Fwd Si-2-SS	1.00	0.05	1.00	0.00	1.02	0.14
Fwd Si-3-SS	1.00	0.00	1.01	0.08	1.02	0.14
Fwd Si-1-DS	1.00	0.07	1.01	0.11	1.00	0.06
Fwd Si-2-DS	1.01	0.11	1.03	0.17	1.03	0.17
Fwd Si-3-DS	1.11	1.69	1.02	0.12	1.02	0.13
Fwd MSGC-1	1.60	1.80	1.12	0.71	1.01	0.07
Fwd MSGC-2	1.57	1.33	1.18	0.55	1.01	0.12
Fwd MSGC-3	1.67	0.95	1.17	0.40	1.03	0.30
Fwd MSGC-4	1.93	1.40	1.24	0.47	1.07	0.45
Fwd MSGC-5	1.97	1.27	1.42	0.61	1.10	0.49

Table 27: Cluster splitting for various P_t ranges in $b\bar{b}$ jet events.

Detectors type	$0.0 < P_t < 0.3$		$0.3 < P_t < 0.6$		$0.6 < P_t < 0.9$	
	Ghits/Rhit	RMS	Ghits/Rhit	RMS	Ghits/Rhit	RMS
Barrel Si-1	2.13	2.01	1.10	0.38	1.02	0.15
Barrel Si-2	2.11	2.03	1.11	0.44	1.02	0.16
Barrel Si-3	1.97	1.83	1.09	0.39	1.02	0.16
Barrel Si-4	2.21	2.07	1.11	0.45	1.02	0.14
Barrel MSGC-1	2.22	2.47	1.11	0.44	1.02	0.16
Barrel MSGC-2	2.40	2.67	1.11	0.47	1.02	0.16
Barrel MSGC-3	2.57	3.01	1.09	0.38	1.03	0.21
Barrel MSGC-4	2.49	2.48	1.09	0.37	1.02	0.22
Barrel MSGC-5	2.53	2.85	1.09	0.34	1.04	0.26
Barrel MSGC-6	2.71	3.26	1.10	0.37	1.04	0.22
Barrel MSGC-7	3.04	3.69	1.06	0.27	1.02	0.16
Fwd Si-1-SS	1.24	0.54	1.00	0.07	1.00	0.00
Fwd Si-2-SS	1.30	0.59	1.02	0.13	1.01	0.08
Fwd Si-3-SS	1.29	0.57	1.01	0.11	1.01	0.10
Fwd Si-1-DS	1.28	0.66	1.02	0.15	1.01	0.08
Fwd Si-2-DS	1.33	0.71	1.01	0.12	1.01	0.10
Fwd Si-3-DS	1.29	0.57	1.02	0.12	1.00	0.03
Fwd MSGC-1	1.27	0.60	1.01	0.10	1.00	0.06
Fwd MSGC-2	1.33	0.64	1.01	0.12	1.00	0.05
Fwd MSGC-3	1.30	0.60	1.01	0.10	1.00	0.06
Fwd MSGC-4	1.31	0.62	1.01	0.11	1.00	0.05
Fwd MSGC-5	1.28	0.57	1.01	0.10	1.00	0.06
	$0.9 < P_t < 1.2$		$1.2 < P_t$		all P_t	
	Ghits/Rhit	RMS	Ghits/Rhit	RMS	Ghits/Rhit	RMS
Barrel Si-1	1.02	0.14	1.03	0.18	1.70	1.65
Barrel Si-2	1.01	0.08	1.02	0.17	1.66	1.63
Barrel Si-3	1.01	0.08	1.03	0.17	1.51	1.38
Barrel Si-4	1.01	0.11	1.02	0.16	1.56	1.49
Barrel MSGC-1	1.00	0.05	1.01	0.09	1.47	1.57
Barrel MSGC-2	1.01	0.07	1.01	0.09	1.52	1.69
Barrel MSGC-3	1.00	0.06	1.01	0.08	1.55	1.87
Barrel MSGC-4	1.00	0.00	1.01	0.08	1.52	1.59
Barrel MSGC-5	1.00	0.03	1.01	0.08	1.56	1.82
Barrel MSGC-6	1.00	0.08	1.00	0.06	1.63	2.10
Barrel MSGC-7	1.00	0.05	1.00	0.07	1.76	2.44
Fwd Si-1-SS	1.02	0.12	1.00	0.06	1.16	0.46
Fwd Si-2-SS	1.01	0.11	1.01	0.10	1.20	0.50
Fwd Si-3-SS	1.00	0.00	1.00	0.04	1.15	0.43
Fwd Si-1-DS	1.00	0.00	1.01	0.08	1.18	0.55
Fwd Si-2-DS	1.00	0.00	1.00	0.06	1.21	0.59
Fwd Si-3-DS	1.00	0.05	1.00	0.06	1.15	0.44
Fwd MSGC-1	1.00	0.00	1.00	0.00	1.13	0.43
Fwd MSGC-2	1.00	0.03	1.00	0.05	1.16	0.47
Fwd MSGC-3	1.00	0.00	1.00	0.03	1.14	0.43
Fwd MSGC-4	1.00	0.04	1.00	0.06	1.14	0.45
Fwd MSGC-5	1.00	0.00	1.00	0.03	1.13	0.42

Table 28: Cluster merging for various P_t ranges in $b\bar{b}$ jet + MB pile-up events.

Detector Type	all P_t		$0.0 < P_t < 0.3$		$0.3 < P_t < 0.6$	
	Rhits/Ghit	RMS	Rhits/Ghit	RMS	Rhits/Ghit	RMS
Barrel Si-1	1.45	1.66	1.68	2.08	1.13	0.48
Barrel Si-2	1.44	1.67	1.69	2.15	1.14	0.52
Barrel Si-3	1.30	1.06	1.50	1.41	1.12	0.49
Barrel Si-4	1.30	0.97	1.56	1.31	1.13	0.54
Barrel MSGC-1	2.81	2.72	3.61	3.35	2.92	2.52
Barrel MSGC-2	2.95	2.99	3.91	3.74	2.81	2.81
Barrel MSGC-3	2.97	3.02	3.86	3.73	3.23	3.00
Barrel MSGC-4	3.00	2.97	3.85	3.56	3.52	3.35
Barrel MSGC-5	2.97	2.88	3.66	3.33	3.53	3.35
Barrel MSGC-6	3.17	3.31	4.06	3.98	3.15	3.11
Barrel MSGC-7	3.16	3.09	3.92	3.58	3.05	2.77
Fwd Si-1-SS	1.06	0.25	1.07	0.27	1.03	0.20
Fwd Si-2-SS	1.07	0.28	1.09	0.31	1.04	0.20
Fwd Si-3-SS	1.04	0.24	1.05	0.30	1.02	0.15
Fwd Si-1-DS	1.08	0.53	1.09	0.55	1.06	0.60
Fwd Si-2-DS	1.10	0.72	1.13	0.83	1.05	0.23
Fwd Si-3-DS	1.05	0.27	1.08	0.34	1.03	0.18
Fwd MSGC-1	1.79	1.58	1.93	1.83	1.90	1.48
Fwd MSGC-2	1.93	1.77	2.07	1.95	2.10	1.85
Fwd MSGC-3	1.97	1.71	2.07	1.84	2.23	1.84
Fwd MSGC-4	2.02	1.76	2.07	1.82	2.41	2.15
Fwd MSGC-5	1.96	1.51	2.01	1.61	2.50	2.07
	$0.6 < P_t < 0.9$		$0.9 < P_t < 1.2$		$1.2 < P_t$	
	Rhits/Ghit	RMS	Rhits/Ghit	RMS	Rhits/Ghit	RMS
Barrel Si-1	1.07	0.38	1.06	0.25	1.07	0.27
Barrel Si-2	1.05	0.25	1.05	0.22	1.06	0.28
Barrel Si-3	1.05	0.24	1.02	0.20	1.03	0.17
Barrel Si-4	1.04	0.21	1.03	0.22	1.03	0.19
Barrel MSGC-1	1.86	1.15	1.58	1.11	1.15	0.44
Barrel MSGC-2	1.93	1.10	1.66	0.90	1.18	0.46
Barrel MSGC-3	2.08	1.26	1.76	0.76	1.20	0.60
Barrel MSGC-4	2.25	1.25	1.79	0.92	1.24	0.49
Barrel MSGC-5	2.61	2.02	1.79	0.79	1.28	0.57
Barrel MSGC-6	3.19	2.84	1.85	0.89	1.31	0.56
Barrel MSGC-7	3.39	2.91	1.99	0.99	1.35	0.69
Fwd Si-1-SS	1.04	0.21	1.02	0.15	1.04	0.19
Fwd Si-2-SS	1.05	0.23	1.05	0.23	1.06	0.24
Fwd Si-3-SS	1.02	0.16	1.02	0.15	1.03	0.17
Fwd Si-1-DS	1.05	0.24	1.04	0.22	1.05	0.25
Fwd Si-2-DS	1.09	0.96	1.04	0.21	1.05	0.23
Fwd Si-3-DS	1.03	0.19	1.02	0.13	1.04	0.21
Fwd MSGC-1	1.42	1.13	1.08	0.60	1.04	0.25
Fwd MSGC-2	1.55	1.11	1.14	0.41	1.08	0.43
Fwd MSGC-3	1.72	1.34	1.25	0.59	1.10	0.45
Fwd MSGC-4	1.92	1.33	1.38	0.91	1.13	0.43
Fwd MSGC-5	2.03	1.25	1.41	0.66	1.16	0.44

Table 29: Cluster splitting for various P_t ranges in $b\bar{b}$ jet + MB pile-up events.

Detector type	Merging: all P_t		Splitting: all P_t	
	Ghits/Rhit	RMS	Rhits/Ghit	RMS
Barrel Si-1	1.24	0.58	1.11	0.31
Barrel Si-2	1.46	1.49	1.24	1.05
Barrel Si-3	1.37	1.08	1.14	0.39
Barrel Si-4	1.57	1.73	1.30	0.79
Barrel MSGC-1	1.23	0.94	1.19	0.75
Barrel MSGC-2	1.21	0.94	1.18	0.70
Barrel MSGC-3	1.32	1.34	1.29	1.20
Barrel MSGC-4	1.07	0.36	1.15	1.45
Barrel MSGC-5	1.51	1.95	1.53	2.06
Barrel MSGC-6	1.86	2.75	1.93	3.17
Barrel MSGC-7	1.16	0.73	1.09	0.48

Table 30: Cluster splitting and merging in $b\bar{b}$ jet cores.

Detector type	Merging: all P_t		Splitting: all P_t	
	Ghits/Rhit	RMS	Rhits/Ghit	RMS
Barrel Si-1	1.48	0.98	1.31	0.76
Barrel Si-2	1.41	1.01	1.16	0.39
Barrel Si-3	1.38	0.85	1.12	0.35
Barrel Si-4	1.65	1.81	1.27	0.69
Barrel MSGC-1	1.38	1.06	1.49	0.75
Barrel MSGC-2	1.31	1.11	1.39	0.70
Barrel MSGC-3	1.50	1.62	1.76	1.20
Barrel MSGC-4	1.22	0.70	1.58	1.45
Barrel MSGC-5	1.40	1.73	1.61	2.06
Barrel MSGC-6	2.09	3.26	2.43	3.17
Barrel MSGC-7	1.07	0.41	1.07	0.41

Table 31: Cluster splitting and merging in $b\bar{b}$ jet cores + MB pile-up.

List of Figures

1 MSGC cluster size for π at 3 GeV/c (S/N = 20) vs incident angle. 5

2 Number of clusters for π at 3 GeV/c vs incident angle for MSGCs. 5

3 MSGC efficiency for π at 3 GeV/c vs incident angle. 5

4 Number of primary plus secondary e^- before amplification in the MSGC. 5

5 Pseudorapidity (η) distribution for single minimun bias events without P_t cuts. The bin size in η is 0.1. 6

6 Primary track multiplicity distribution for single minimum bias events in the range $|\eta| \leq 5$ without P_t cuts. 6

7 P_t distribution for primary tracks of $|\eta| \leq 5$ in single minimum bias events. 6

8 Time distribution of GEANT hits per event from single MB. The bin size is 1 ns. All silicon and MSGC detectors are included. 8

9 Pseudorapidity (η) distribution for 300 GeV $b\bar{b}$ jet events without P_t cuts. The bin size is 0.1. 16

10 Primary tracks multiplicity distribution for 300 GeV $b\bar{b}$ jet events in the range $|\eta| \leq 5$ without P_t cuts. 16

11 P_t distribution for primary tracks with $|\eta| \leq 5$ for 300 GeV $b\bar{b}$ jet events. 16

12 Time distribution of GEANT hits per event from $b\bar{b}$ jets. All silicon and MSGC detectors are included. 17

13 Time distribution for GEANT hits per event from single MB for barrel silicon detectors (hatched histogram). The other histogram is for all silicon plus MSGC detectors. 44

14 Same as figure 13, but on a logarithmic scale. 44

15 Time distribution for GEANT hits per event from single MB for barrel MSGC detectors (hatched histogram). The other histogram is for all detectors. 44

16 Same as figure 15, but on a logarithmic scale. 44

17 Time distribution for GEANT hits per event from single MB for forward silicon detectors (hatched histogram). The other histogram is for all detectors. 45

18 Same as figure 17, but on a logarithmic scale. 45

19 Time distribution for GEANT hits per event from single MB for forward MSGC detectors (hatched histogram). The other histogram is for all detectors. 45

20 Same as figure 19, but on a logarithmic scale. 45

21 Time distribution per event for GEANT hits from $b\bar{b}$ jets for barrel silicon detectors (hatched histogram). The other histogram is for all detectors. 46

22 Same as figure 21, but on a logarithmic scale. 46

23 Time distribution per event for GEANT hits from $b\bar{b}$ jets for barrel MSGC detectors (hatched histogram). The other histogram is for all detectors. 46

24 Same as figure 23, but on a logarithmic scale. 46

25 Time distribution per event for GEANT hits from $b\bar{b}$ jets for forward silicon detectors (hatched histogram). The other histogram is for all detectors. 47

26 Same as figure 25, but on a logarithmic scale. 47

27 Time distribution per event for GEANT hits from $b\bar{b}$ jets for forward MSGC detectors (hatched histogram). The other histogram is for all detectors. 47

28 Same as figure 27, but on a logarithmic scale. 47

29 Barrel "off-line" occupancy for single minimun bias events vs radius. 48

30 Barrel "off-line" occupancy for $b\bar{b}$ jets events at 300 GeV vs radius. 48

31 Barrel occupancy for MB pile-up events vs radius. 48

32 Barrel occupancy for $b\bar{b}$ jets + MB pile-up events vs radius. 48

33 Local barrel occupancy for single $b\bar{b}$ jets events vs radius. 49

34 Local barrel occupancy for $b\bar{b}$ jets events with MB pile-up vs radius. 49

35 Barrel "off-line" occupancy for single MB, MB pile-up, single MB without δ rays, single MB at 2 Tesla and $b\bar{b}$ jets with and without MB pile-up vs radius. 49

36 Forward "off-line" occupancy for single MB, MB pile-up, single MB without δ rays, single MB at 2 Tesla and $b\bar{b}$ jets with and without MB pile-up vs radius. The occupancy for the 67 μm pitch silicon is always below the one for the 100 μm pitch. 49

37 Forward "off-line" occupancy for single minimun bias events vs radius. 50

38 Forward "off-line" occupancy for $b\bar{b}$ jets events at 300 GeV vs radius. 50

39 Forward occupancy for MB pile-up events vs radius. 50

40 Forward occupancy for $b\bar{b}$ jets + MB pile-up events vs radius. 50

41 Average cluster size for barrel detectors for single minimun bias events vs radius. 51

42 Average cluster size for barrel detectors for $b\bar{b}$ jets events at 300 GeV vs radius. 51

43 Average cluster size for barrel detectors for MB pile-up events vs radius. 51

44 Average cluster size for barrel detectors for $b\bar{b}$ jets + MB pile-up events vs radius. 51

45 Average cluster size for barrel detectors for local $b\bar{b}$ jets events vs radius. 52

46 Average cluster size for barrel detectors for local $b\bar{b}$ jets events + MB pile-up vs radius. . 52

47 Average cluster size for barrel detectors for single minimun bias events without δ rays vs radius. 52

48 Average cluster size for barrel detectors for single minimun bias events with a 2 Tesla field vs radius. 52

49 Average cluster size for forward detectors for single minimun bias events vs radius. . . . 53

50 Average cluster size for forward detectors for $b\bar{b}$ jets events at 300 GeV vs radius. 53

51 Average cluster size for forward detectors for MB pile-up events vs radius. 53

52 Average cluster size for forward detectors for $b\bar{b}$ jets + MB pile-up events vs radius. . . . 53

53 Average cluster size for forward detectors for single minimun bias events without δ rays vs radius. 54

54 Average cluster size for forward detectors for single minimun bias events with a 2 Tesla field vs radius. 54

55 Cluster merging effect for barrel detectors vs radius in various P_t ranges for single MB. . 55

56 Cluster merging effect for barrel detectors vs radius in various P_t ranges for $b\bar{b}$ jets at 300 GeV. 55

57 Cluster merging effect for barrel detectors vs radius in various P_t ranges for MB pile-up. 55

58 Cluster merging effect for barrel detectors vs radius in various P_t ranges for $b\bar{b}$ + MB pile-up. 55

59 Average cluster merging effect for barrel detectors vs radius for local $b\bar{b}$ jets. 56

60 Average cluster merging effect for barrel detectors vs radius for local $b\bar{b}$ jets + MB pile-up. 56

61 Average cluster merging effect for barrel detectors vs radius for single MB, MB pile-up, single MB without δ rays, single MB at 2 Tesla, $b\bar{b}$ jets with and without MB pile-up. . . 56

62 Average cluster merging effect for forward detectors vs radius for single MB, MB pile-up, single MB without δ rays, single MB at 2 Tesla, $b\bar{b}$ jets with and without MB pile-up. 56

63 Cluster merging effect for forward detectors vs radius in various P_t ranges for single MB. 57

64 Cluster merging effect for forward detectors vs radius in various P_t ranges for $b\bar{b}$ jets at 300 GeV. 57

65 Cluster merging effect for forward detectors vs radius in various P_t ranges for MB pile-up. 57

66 Cluster merging effect for forward detectors vs radius in various P_t ranges for $b\bar{b}$ + MB pile-up. 57

67 Cluster splitting effect for barrel detectors vs radius in various P_t ranges for single MB. . 58

68 Cluster splitting effect for barrel detectors vs radius in various P_t ranges for $b\bar{b}$ jets at 300 GeV. 58

69 Cluster splitting effect for barrel detectors vs radius in various P_t ranges for MB pile-up. 58

70 Cluster splitting effect for barrel detectors vs radius in various P_t ranges for $b\bar{b}$ + MB pile-up. 58

71 Average cluster splitting effect for barrel detectors vs radius for local $b\bar{b}$ jets. 59

72 Average cluster splitting effect for barrel detectors vs radius for local $b\bar{b}$ jets + MB pile-up. 59

73 Average cluster splitting effect for barrel detectors vs radius for single MB, MB pile-up, single MB without δ rays, single MB at 2 Tesla, $b\bar{b}$ jets with and without MB pile-up. . . 59

74 Average cluster splitting effect for forward detectors vs radius for single MB, MB pile-up, single MB without δ rays, single MB at 2 Tesla, $b\bar{b}$ jets with and without MB pile-up. 59

75 Cluster splitting effect for forward detectors vs radius in various P_t ranges for single MB. 60

76 Cluster splitting effect for forward detectors vs radius in various P_t ranges for $b\bar{b}$ jets at 300 GeV. 60

77 Cluster splitting effect for forward detectors vs radius in various P_t ranges for MB pile-up. 60

78 Cluster splitting effect for forward detectors vs radius in various P_t ranges for $b\bar{b}$ + MB pile-up. 60

Appendix: figures

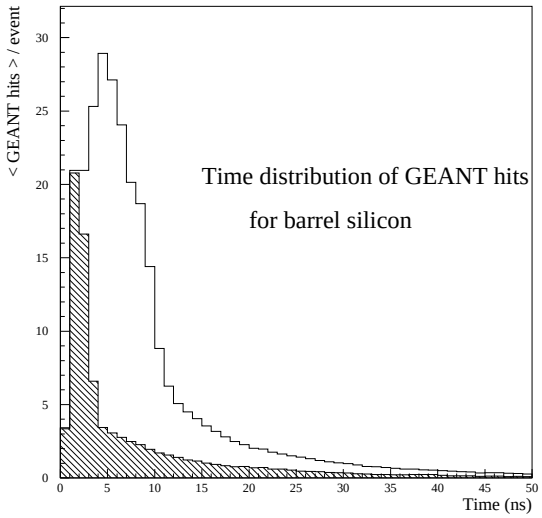

Figure 13: Time distribution for GEANT hits per event from single MB for barrel silicon detectors (hatched histogram). The other histogram is for all silicon plus MSGC detectors.

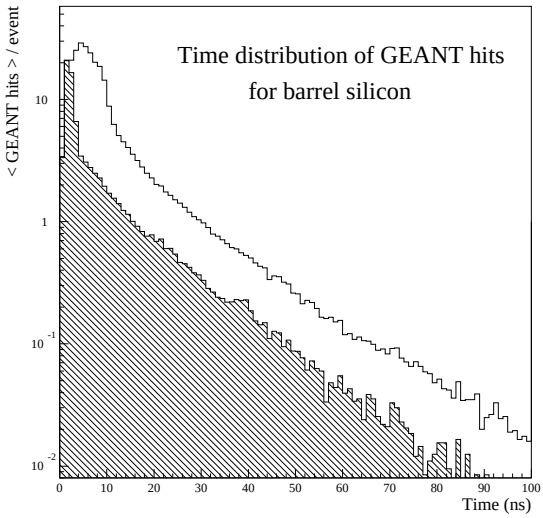

Figure 14: Same as figure 13, but on a logarithmic scale.

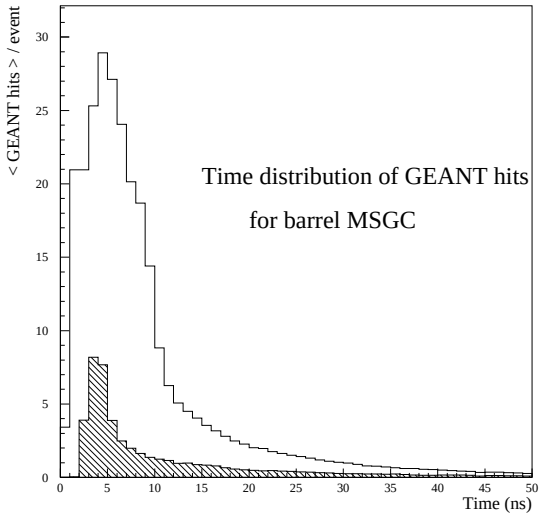

Figure 15: Time distribution for GEANT hits per event from single MB for barrel MSGC detectors (hatched histogram). The other histogram is for all detectors.

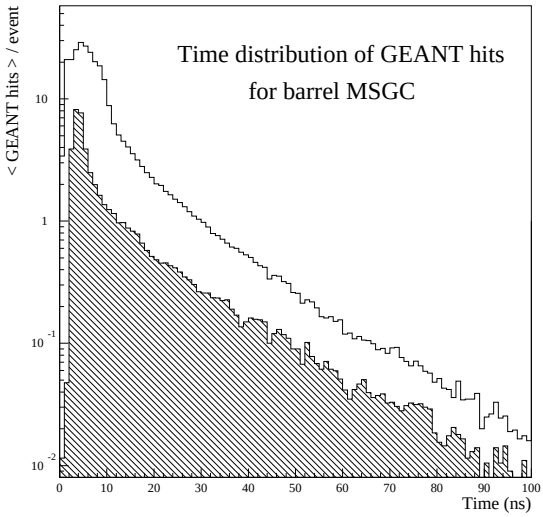

Figure 16: Same as figure 15, but on a logarithmic scale.

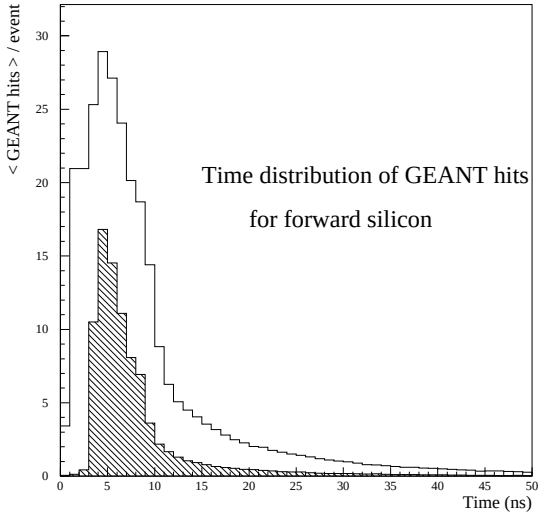

Figure 17: Time distribution for GEANT hits per event from single MB for forward silicon detectors (hatched histogram). The other histogram is for all detectors.

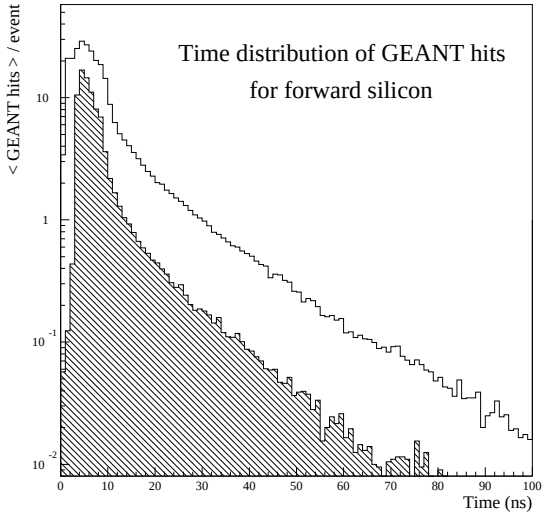

Figure 18: Same as figure 17, but on a logarithmic scale.

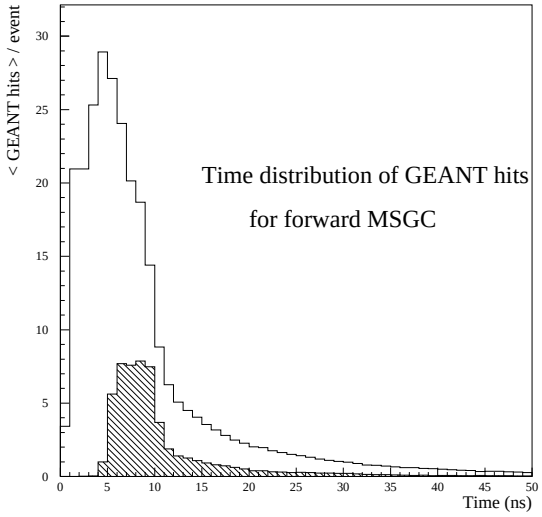

Figure 19: Time distribution for GEANT hits per event from single MB for forward MSGC detectors (hatched histogram). The other histogram is for all detectors.

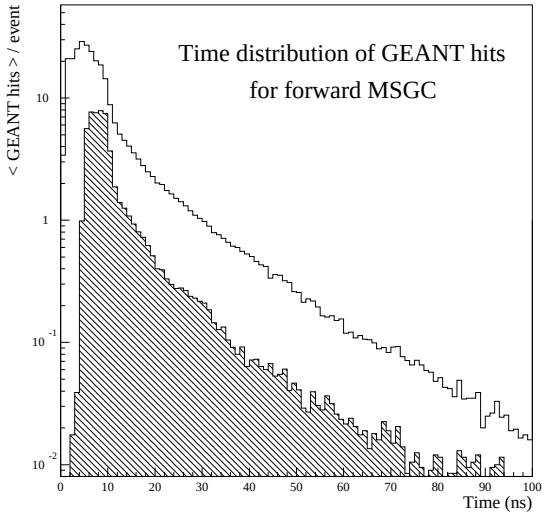

Figure 20: Same as figure 19, but on a logarithmic scale.

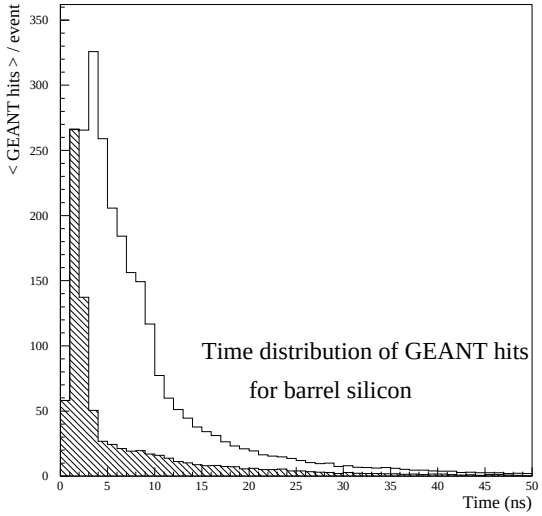

Figure 21: Time distribution per event for GEANT hits from $b\bar{b}$ jets for barrel silicon detectors (hatched histogram). The other histogram is for all detectors.

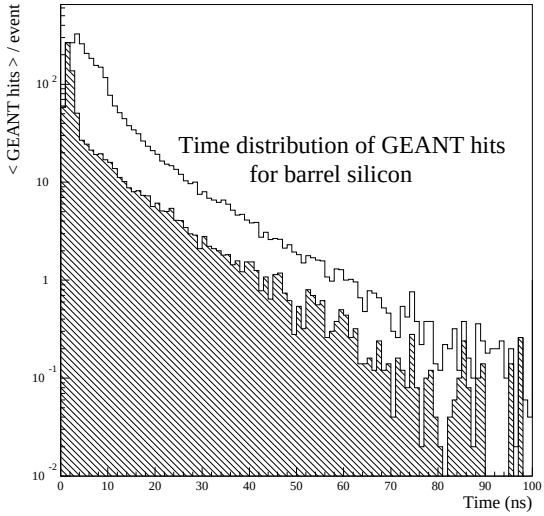

Figure 22: Same as figure 21, but on a logarithmic scale.

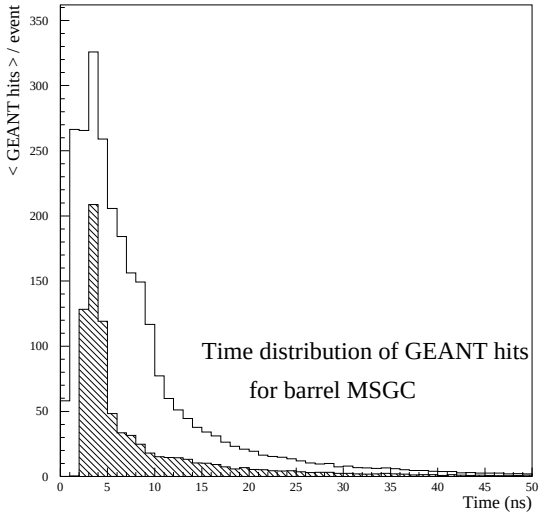

Figure 23: Time distribution per event for GEANT hits from $b\bar{b}$ jets for barrel MSGC detectors (hatched histogram). The other histogram is for all detectors.

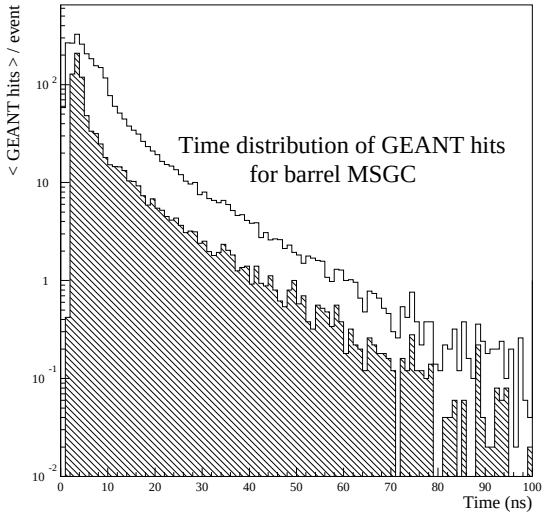

Figure 24: Same as figure 23, but on a logarithmic scale.

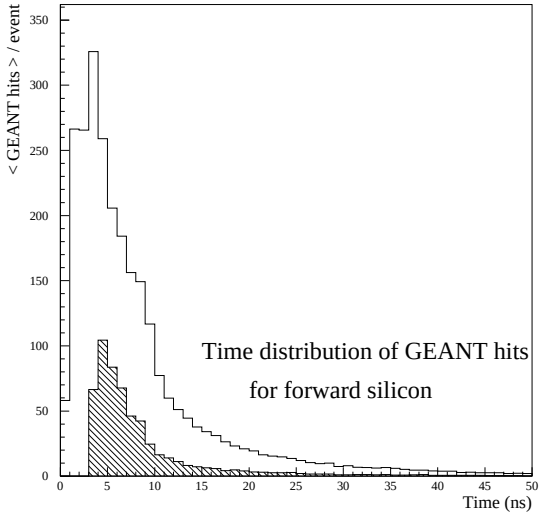

Figure 25: Time distribution per event for GEANT hits from $b\bar{b}$ jets for forward silicon detectors (hatched histogram). The other histogram is for all detectors.

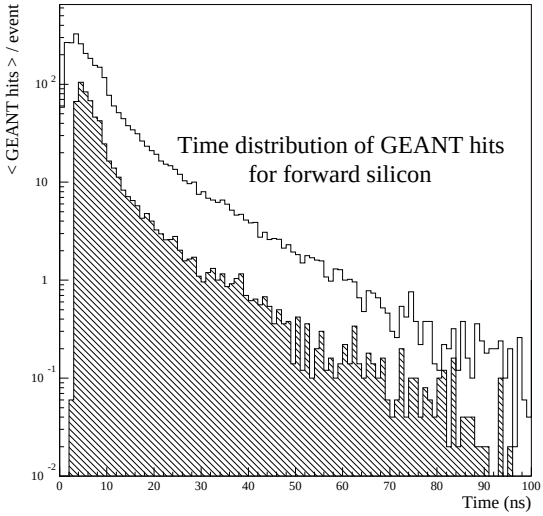

Figure 26: Same as figure 25, but on a logarithmic scale.

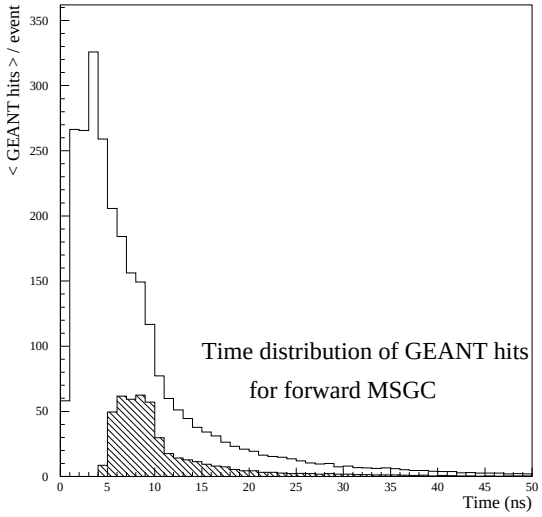

Figure 27: Time distribution per event for GEANT hits from $b\bar{b}$ jets for forward MSGC detectors (hatched histogram). The other histogram is for all detectors.

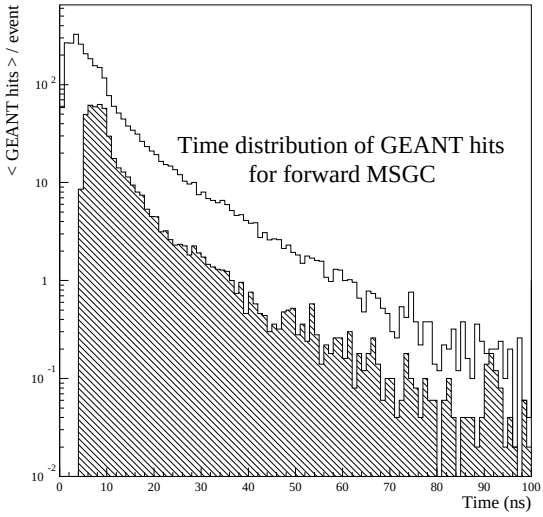

Figure 28: Same as figure 27, but on a logarithmic scale.

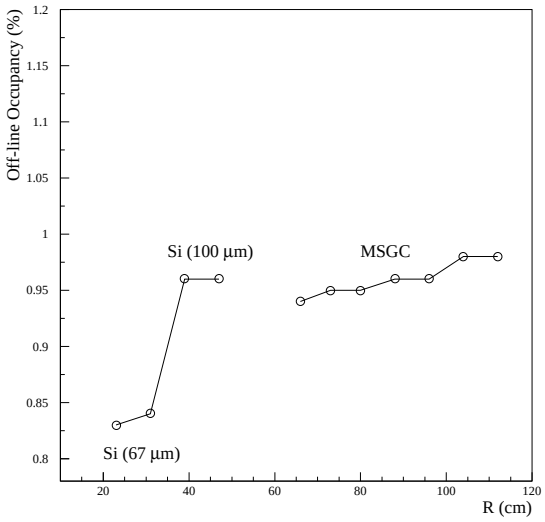

Figure 29: Barrel “off-line” occupancy for single minimun bias events vs radius.

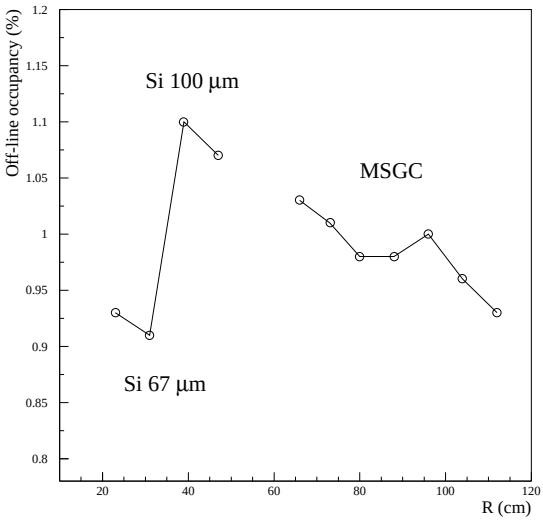

Figure 30: Barrel “off-line” occupancy for $b\bar{b}$ jets events at 300 GeV vs radius.

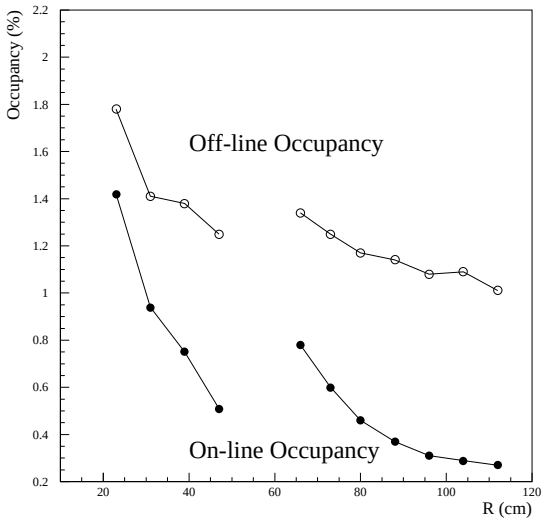

Figure 31: Barrel occupancy for MB pile-up events vs radius.

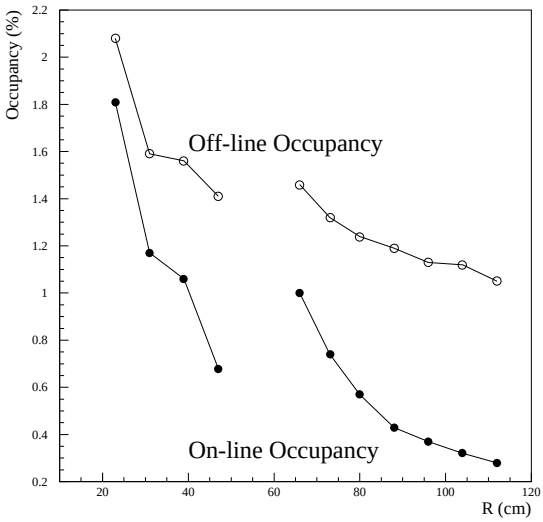

Figure 32: Barrel occupancy for $b\bar{b}$ jets + MB pile-up events vs radius.

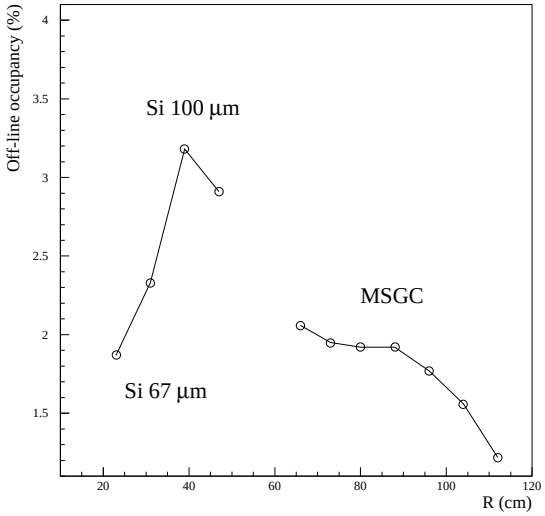

Figure 33: Local barrel occupancy for single $b\bar{b}$ jets events vs radius.

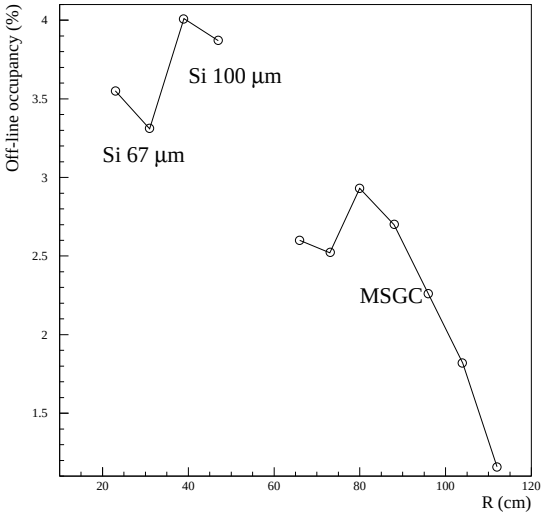

Figure 34: Local barrel occupancy for $b\bar{b}$ jets events with MB pile-up vs radius.

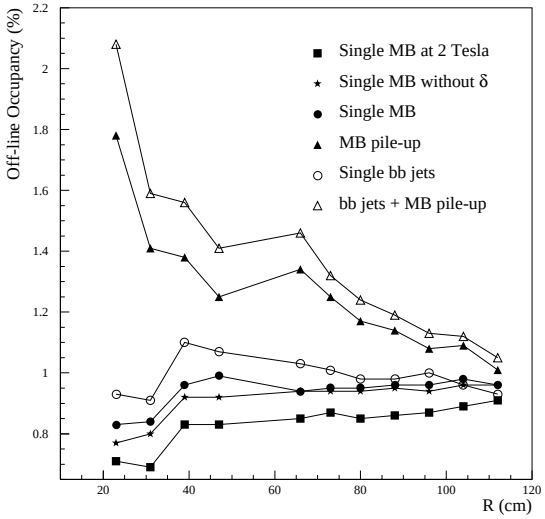

Figure 35: Barrel "off-line" occupancy for single MB, MB pile-up, single MB without δ rays, single MB at 2 Tesla and $b\bar{b}$ jets with and without MB pile-up vs radius.

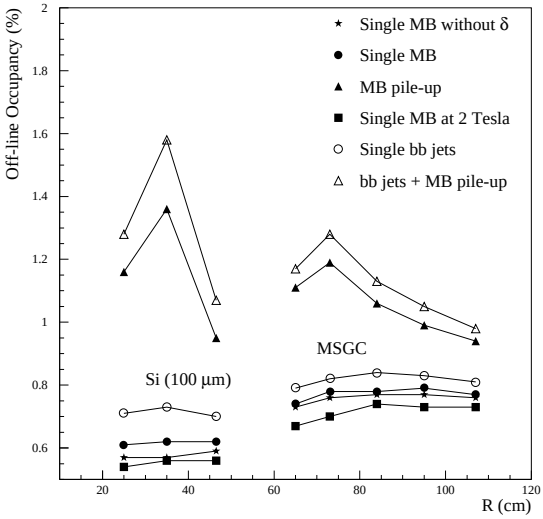

Figure 36: Forward "off-line" occupancy for single MB, MB pile-up, single MB without δ rays, single MB at 2 Tesla and $b\bar{b}$ jets with and without MB pile-up vs radius. The occupancy for the 67 μm pitch silicon is always below the one for the 100 μm pitch.

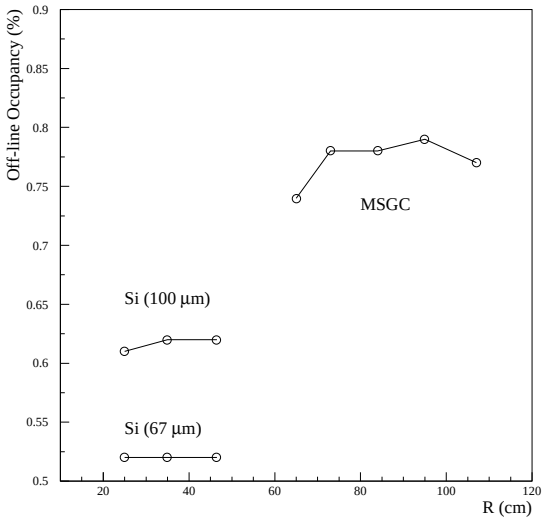

Figure 37: Forward "off-line" occupancy for single minimun bias events vs radius.

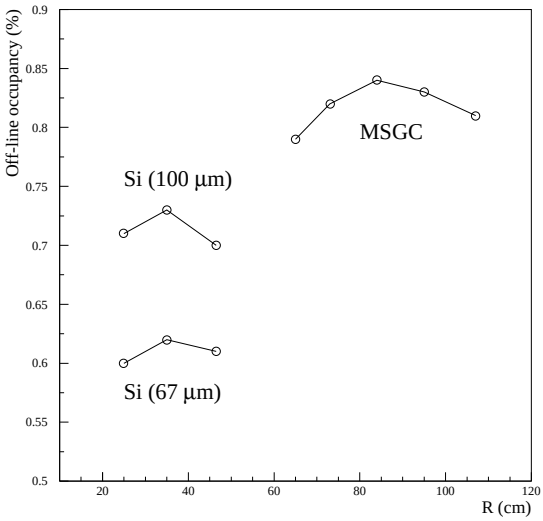

Figure 38: Forward "off-line" occupancy for $b\bar{b}$ jets events at 300 GeV vs radius.

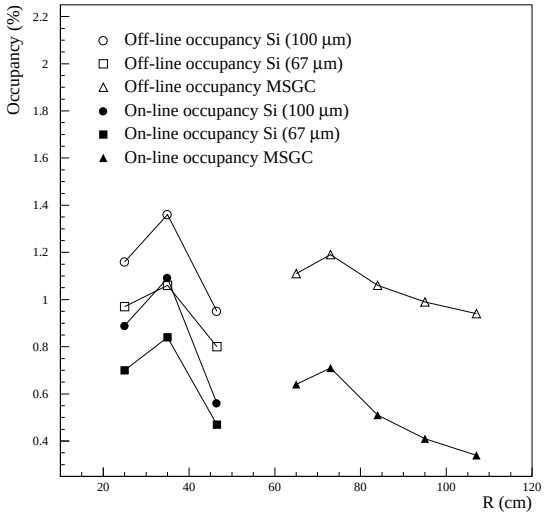

Figure 39: Forward occupancy for MB pile-up events vs radius.

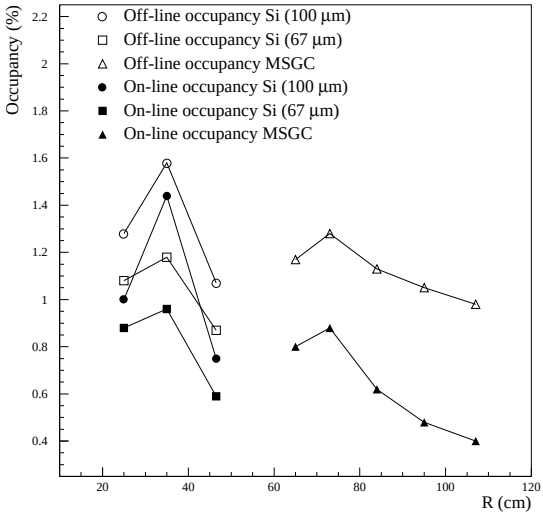

Figure 40: Forward occupancy for $b\bar{b}$ jets + MB pile-up events vs radius.

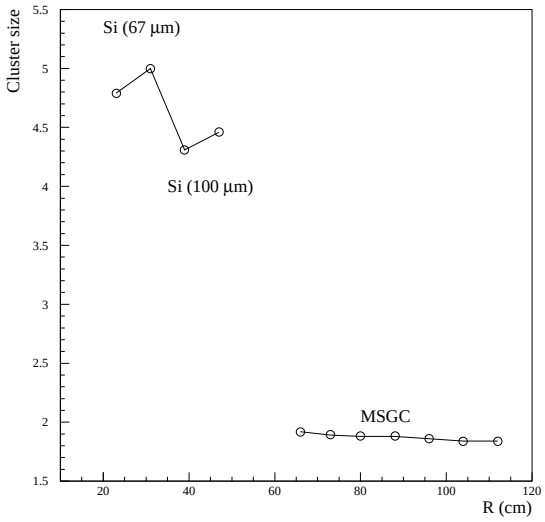

Figure 41: Average cluster size for barrel detectors for single minimun bias events vs radius.

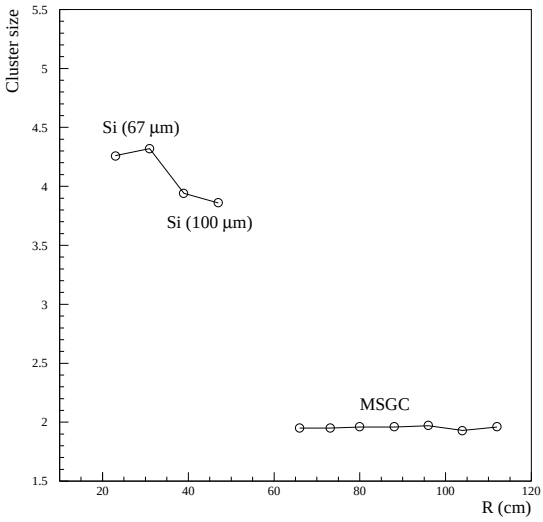

Figure 42: Average cluster size for barrel detectors for $b\bar{b}$ jets events at 300 GeV vs radius.

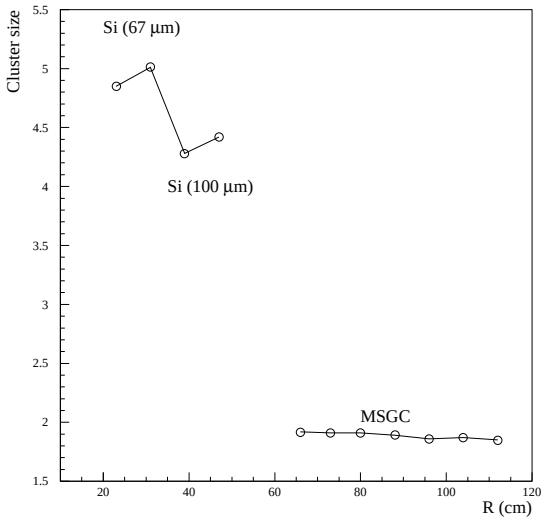

Figure 43: Average cluster size for barrel detectors for MB pile-up events vs radius.

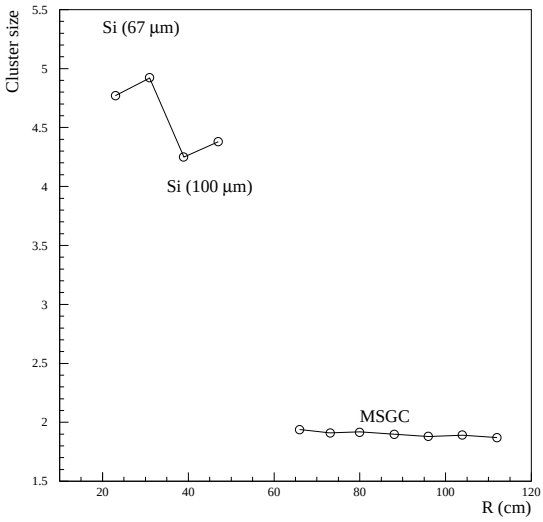

Figure 44: Average cluster size for barrel detectors for $b\bar{b}$ jets + MB pile-up events vs radius.

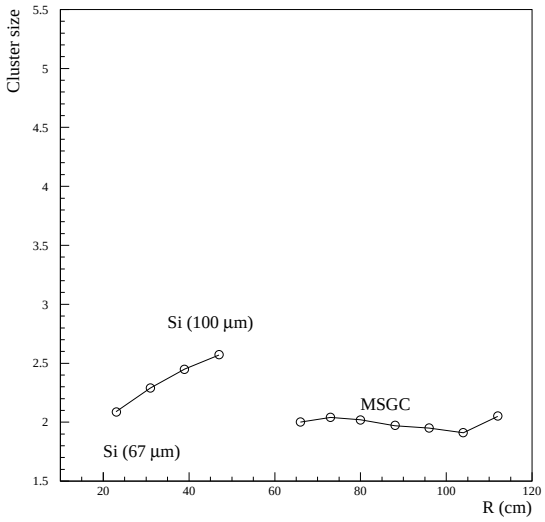

Figure 45: Average cluster size for barrel detectors for local $b\bar{b}$ jets events vs radius.

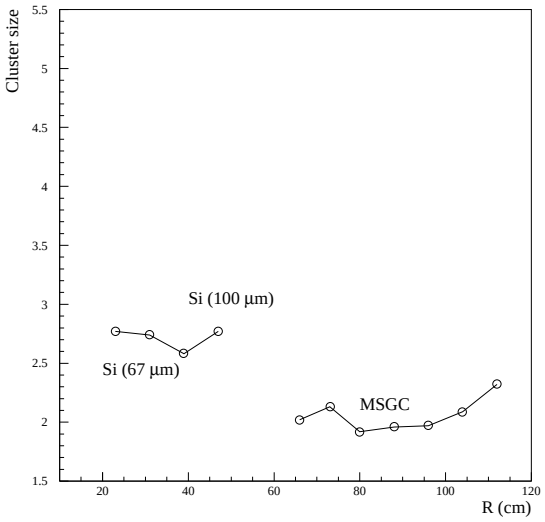

Figure 46: Average cluster size for barrel detectors for local $b\bar{b}$ jets events + MB pile-up vs radius.

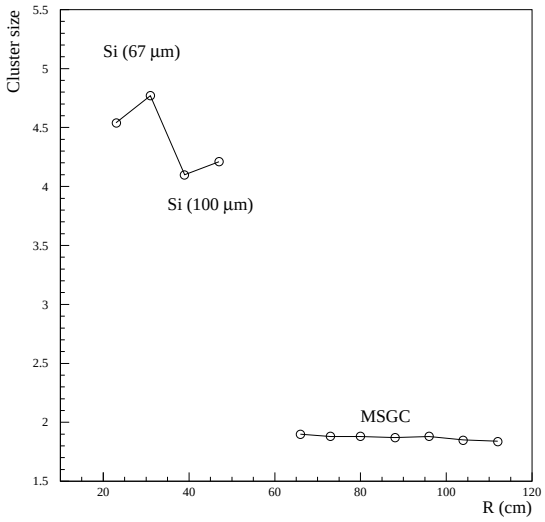

Figure 47: Average cluster size for barrel detectors for single minimun bias events without δ rays vs radius.

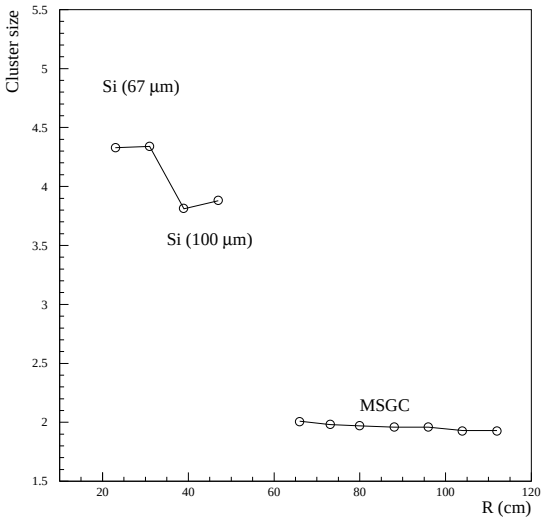

Figure 48: Average cluster size for barrel detectors for single minimun bias events with a 2 Tesla field vs radius.

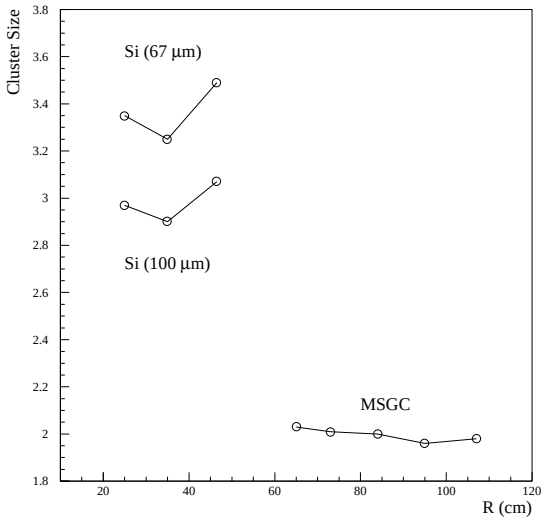

Figure 49: Average cluster size for forward detectors for single minimun bias events vs radius.

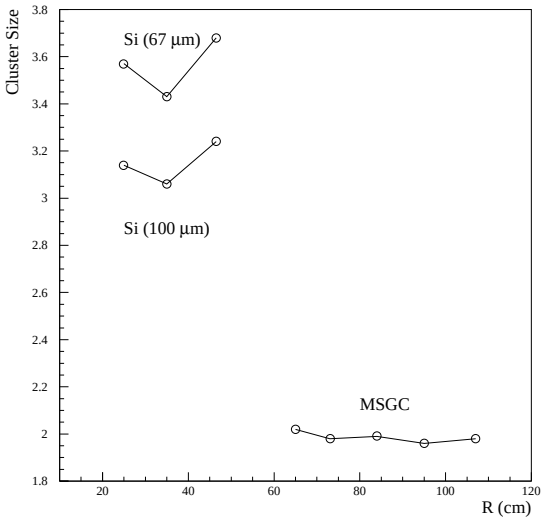

Figure 50: Average cluster size for forward detectors for $b\bar{b}$ jets events at 300 GeV vs radius.

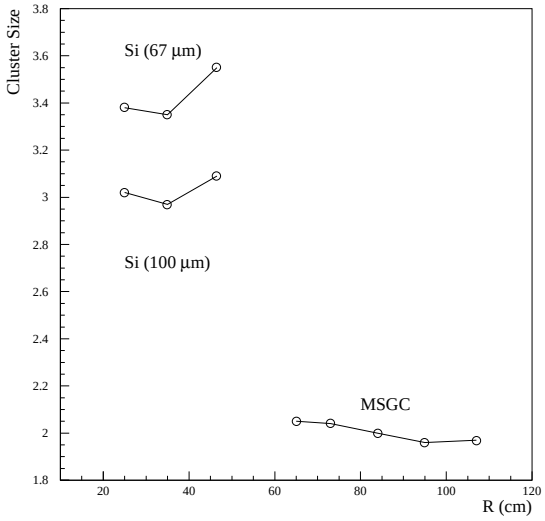

Figure 51: Average cluster size for forward detectors for MB pile-up events vs radius.

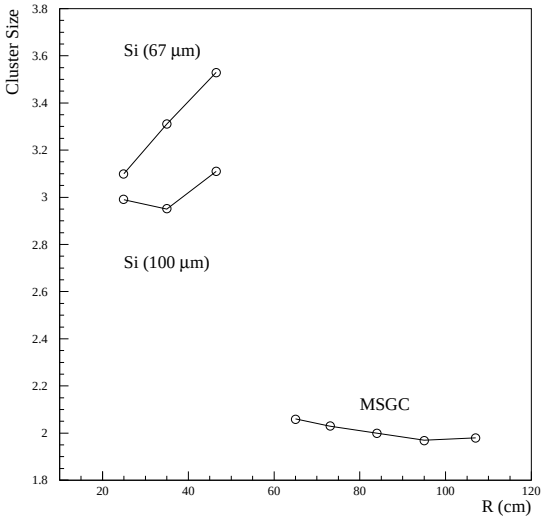

Figure 52: Average cluster size for forward detectors for $b\bar{b}$ jets + MB pile-up events vs radius.

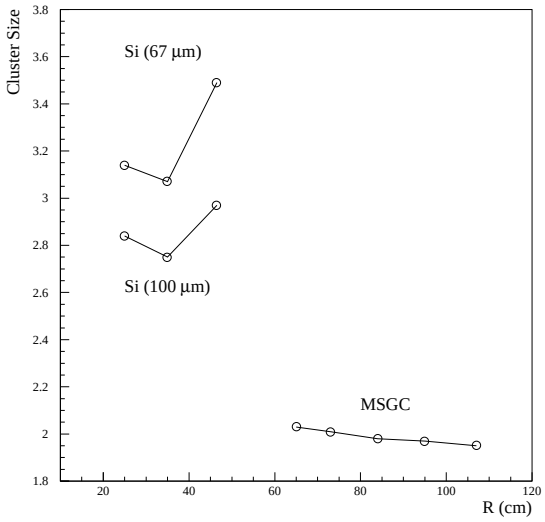

Figure 53: Average cluster size for forward detectors for single minimun bias events without δ rays vs radius.

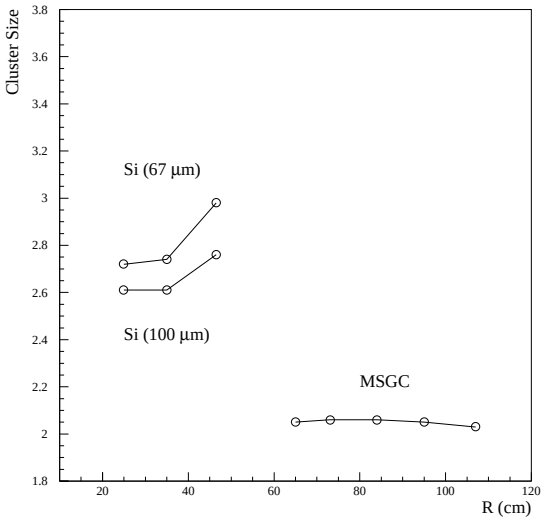

Figure 54: Average cluster size for forward detectors for single minimun bias events with a 2 Tesla field vs radius.

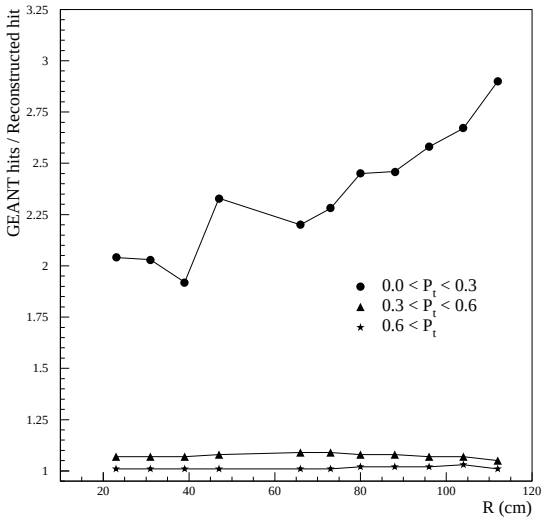

Figure 55: Cluster merging effect for barrel detectors vs radius in various P_t ranges for single MB.

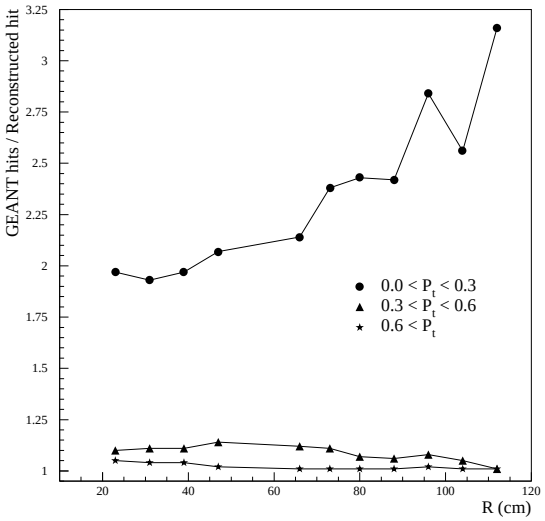

Figure 56: Cluster merging effect for barrel detectors vs radius in various P_t ranges for $b\bar{b}$ jets at 300 GeV.

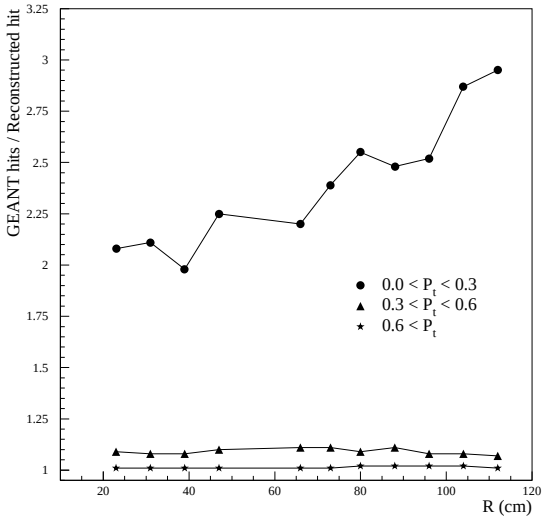

Figure 57: Cluster merging effect for barrel detectors vs radius in various P_t ranges for MB pile-up.

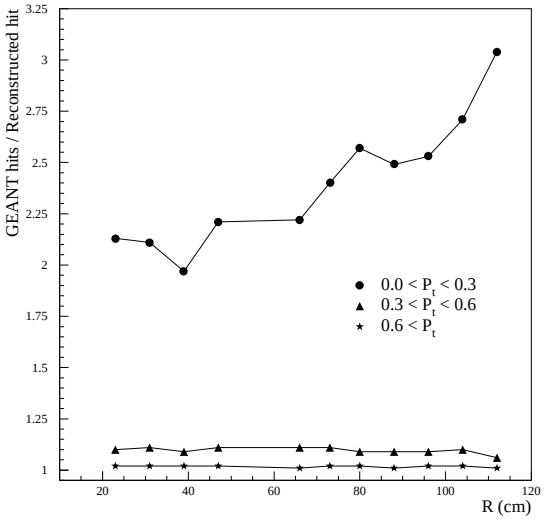

Figure 58: Cluster merging effect for barrel detectors vs radius in various P_t ranges for $b\bar{b}$ + MB pile-up.

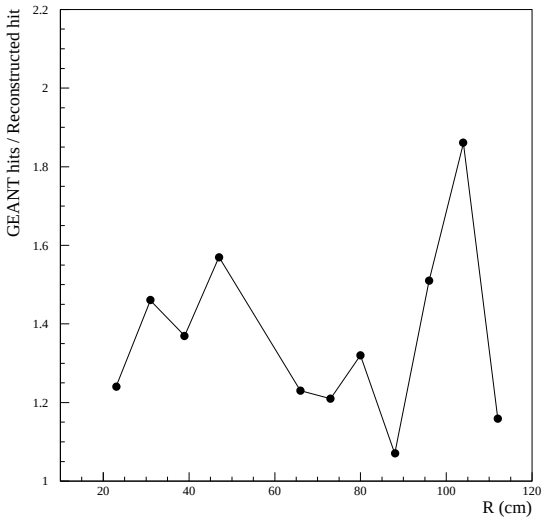

Figure 59: Average cluster merging effect for barrel detectors vs radius for local $b\bar{b}$ jets.

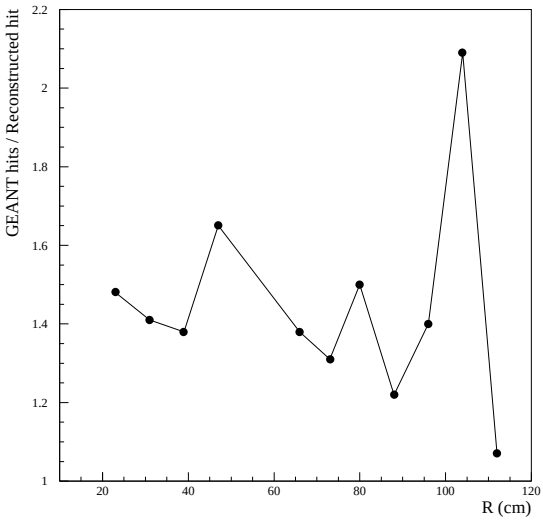

Figure 60: Average cluster merging effect for barrel detectors vs radius for local $b\bar{b}$ jets + MB pile-up.

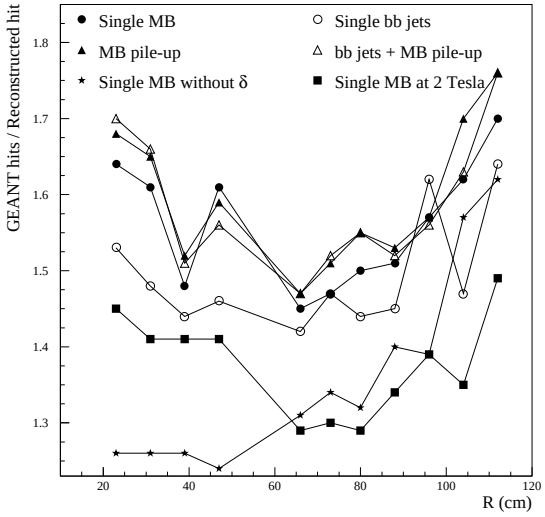

Figure 61: Average cluster merging effect for barrel detectors vs radius for single MB, MB pile-up, single MB without δ rays, single MB at 2 Tesla, $b\bar{b}$ jets with and without MB pile-up.

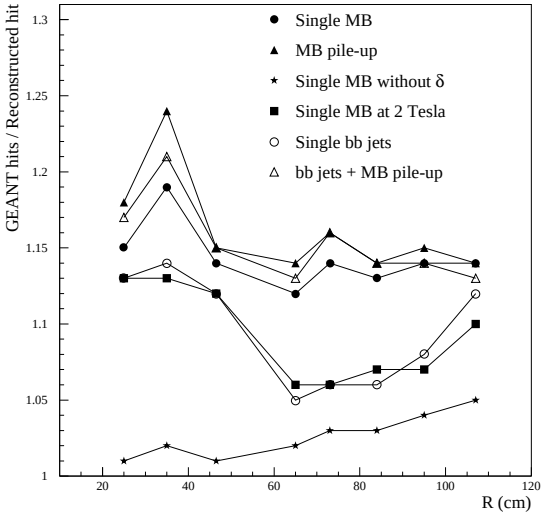

Figure 62: Average cluster merging effect for forward detectors vs radius for single MB, MB pile-up, single MB without δ rays, single MB at 2 Tesla, $b\bar{b}$ jets with and without MB pile-up.

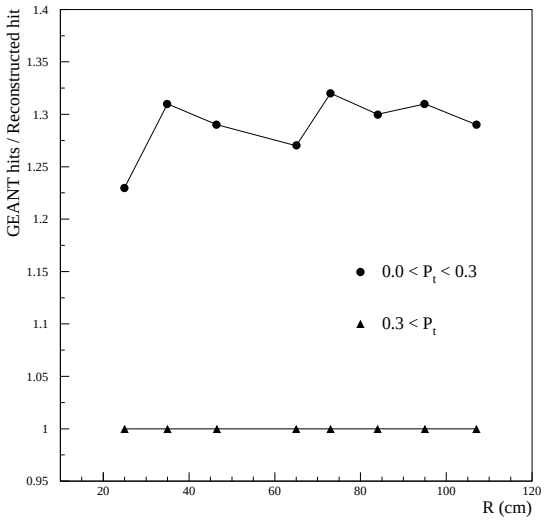

Figure 63: Cluster merging effect for forward detectors vs radius in various P_t ranges for single MB.

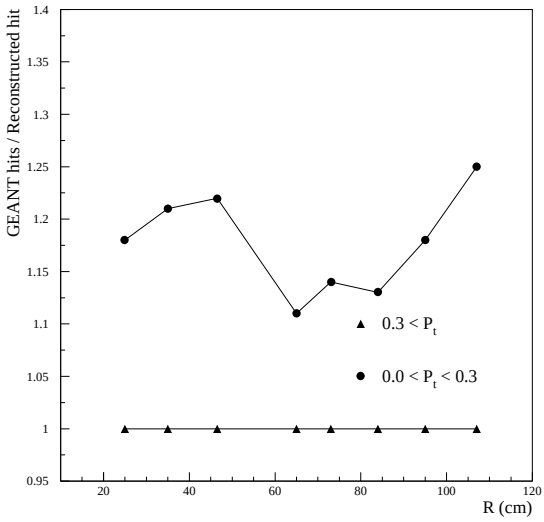

Figure 64: Cluster merging effect for forward detectors vs radius in various P_t ranges for $b\bar{b}$ jets at 300 GeV.

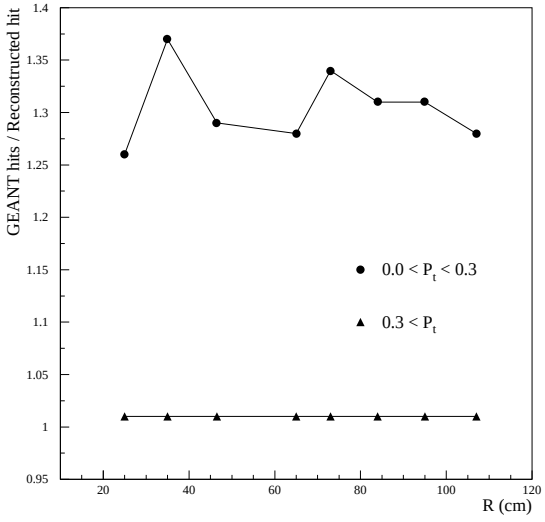

Figure 65: Cluster merging effect for forward detectors vs radius in various P_t ranges for MB pile-up.

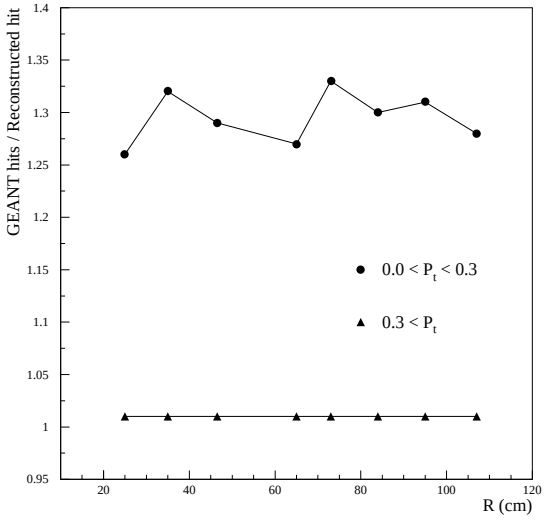

Figure 66: Cluster merging effect for forward detectors vs radius in various P_t ranges for $b\bar{b}$ + MB pile-up.

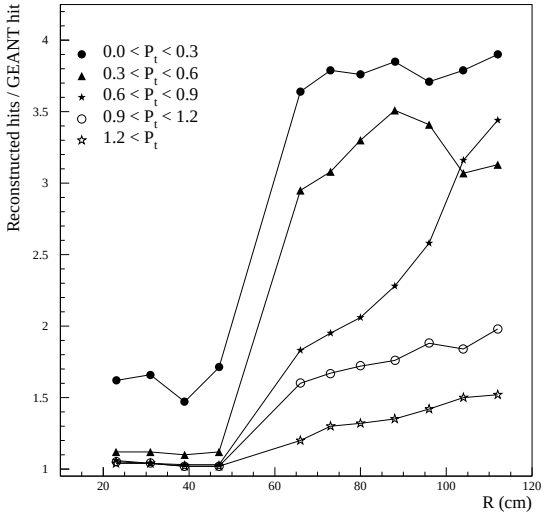

Figure 67: Cluster splitting effect for barrel detectors vs radius in various P_t ranges for single MB.

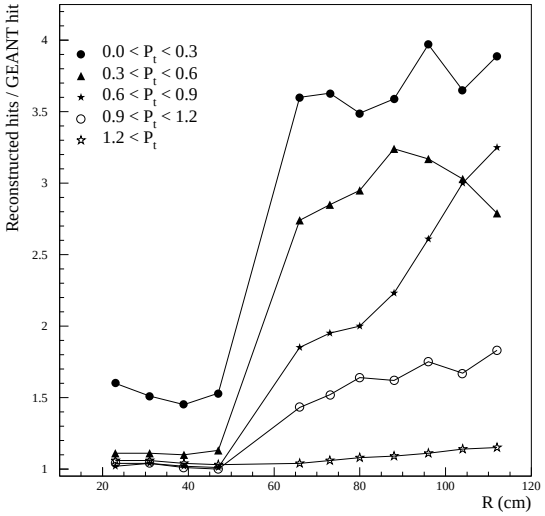

Figure 68: Cluster splitting effect for barrel detectors vs radius in various P_t ranges for $b\bar{b}$ jets at 300 GeV.

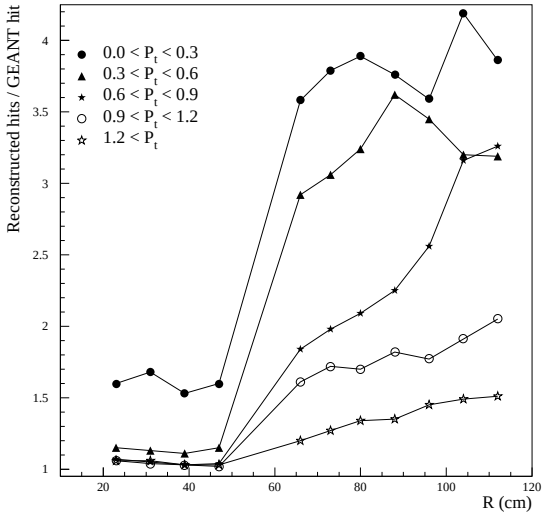

Figure 69: Cluster splitting effect for barrel detectors vs radius in various P_t ranges for MB pile-up.

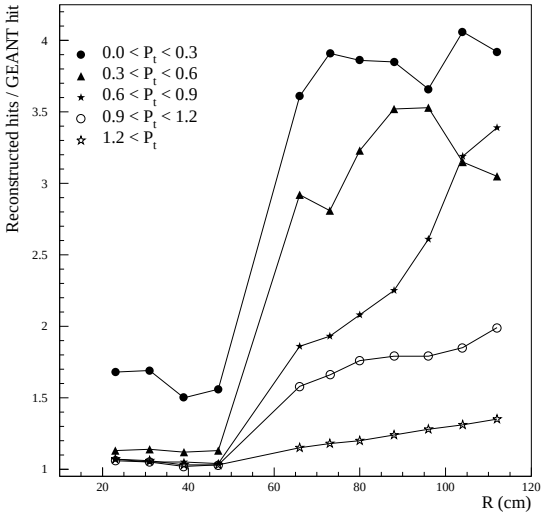

Figure 70: Cluster splitting effect for barrel detectors vs radius in various P_t ranges for $b\bar{b}$ + MB pile-up.

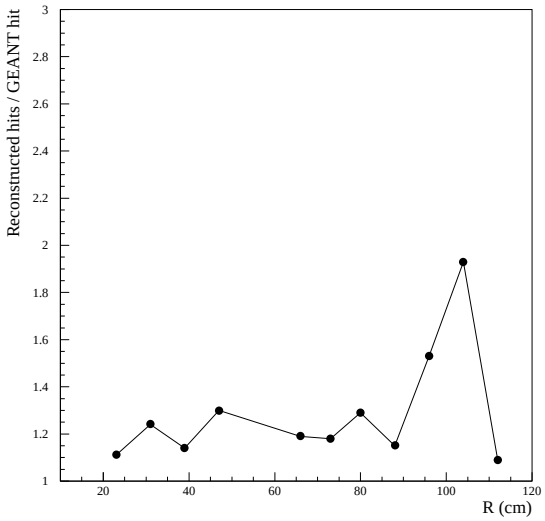

Figure 71: Average cluster splitting effect for barrel detectors vs radius for local $b\bar{b}$ jets.

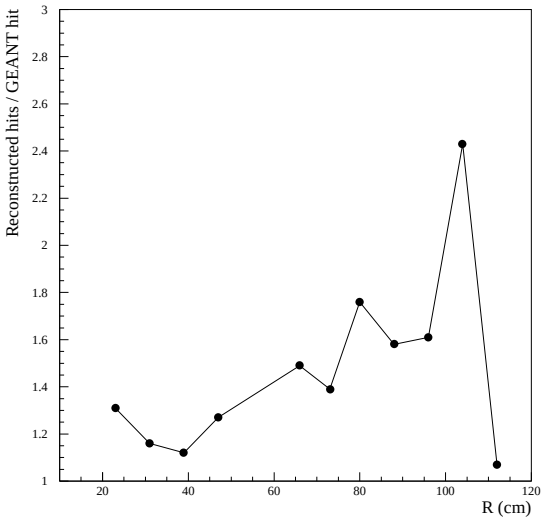

Figure 72: Average cluster splitting effect for barrel detectors vs radius for local $b\bar{b}$ jets + MB pile-up.

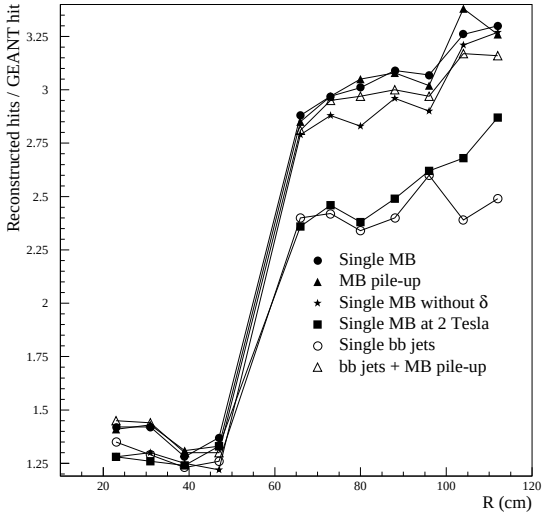

Figure 73: Average cluster splitting effect for barrel detectors vs radius for single MB, MB pile-up, single MB without δ rays, single MB at 2 Tesla, $b\bar{b}$ jets with and without MB pile-up.

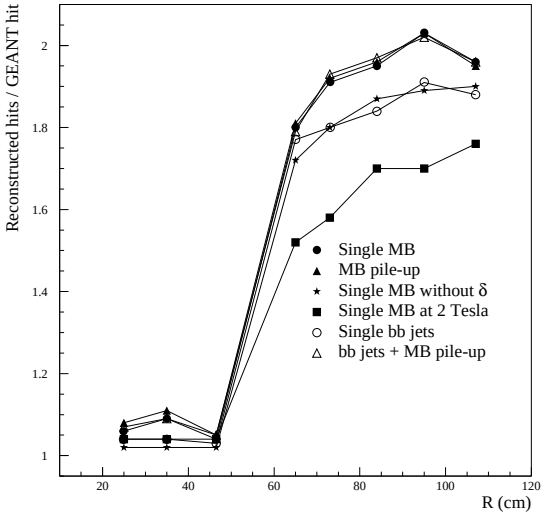

Figure 74: Average cluster splitting effect for forward detectors vs radius for single MB, MB pile-up, single MB without δ rays, single MB at 2 Tesla, $b\bar{b}$ jets with and without MB pile-up.

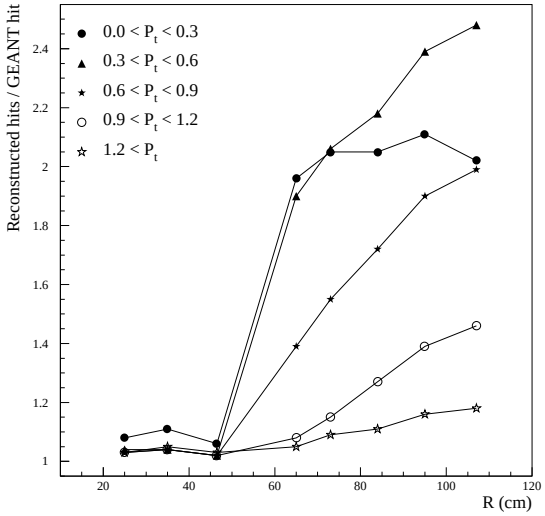

Figure 75: Cluster splitting effect for forward detectors vs radius in various P_t ranges for single MB.

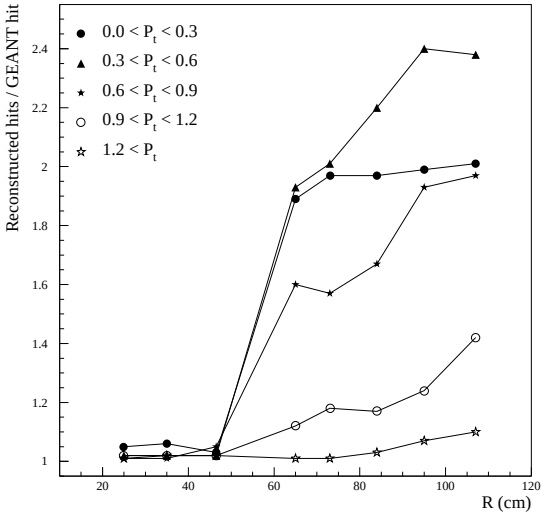

Figure 76: Cluster splitting effect for forward detectors vs radius in various P_t ranges for $b\bar{b}$ jets at 300 GeV.

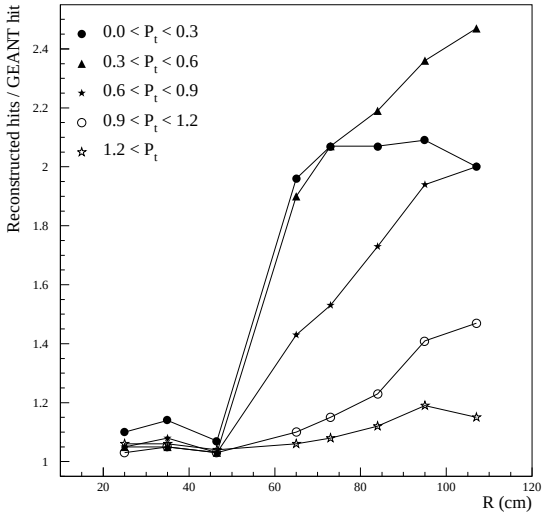

Figure 77: Cluster splitting effect for forward detectors vs radius in various P_t ranges for MB pile-up.

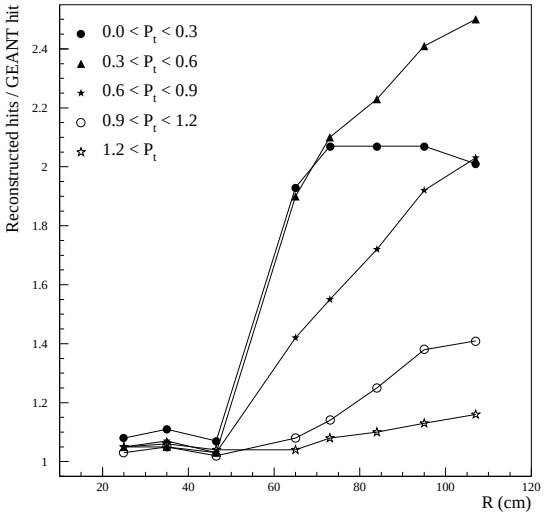

Figure 78: Cluster splitting effect for forward detectors vs radius in various P_t ranges for $b\bar{b}$ + MB pile-up.